ACCELERATOR AND INSTRUMENTATION R&D AND CONSTRUCTION

MAGNETIC FIELD MAPPING OF THE K800 CYCLOTRON

D. Johnson, T. Kuo, F. Marti, J. A. Nolen Jr., B. Sherrill, and A. Zeller

A new cycle of magnetic field measurements of the K800 cyclotron was performed in the last few months of 1987. This set of measurements was supposed to be the final one from which the data base for the trim coil fitting code would be created. The results of the previous mapping cycles have been described elsewhere.[1]

The hardware utilized in the measurement has been described in previous reports[2] and only minor mechanical changes were performed to accommodate a new RF support structure. Unfortunately, these changes created major problems due to misalignments in the mounting gear. The stress on the angular encoder, which determines the angle of the search coil bar, generated a false reading which seemed to indicate a large imperfection in the magnet, which was field dependent. The difficulties in diagnosing and correcting this problem delayed the mapping process substantially.

Main Grid

A set of 16 maps were measured in a grid of the Iα,Iβ plane, where Iα and Iβ are the currents in the two sections of the superconducting coil. The grid covers the operating region of the cyclotron. Figure 1 shows the measured points. The grid spacing is approximately twice the originally planned spacing. We decided to accelerate the mapping process in this way and postpone the finer grid measurements until the internal beam tests had been performed and the extraction elements installed. The field was measured every 0.1 inches in radius and every degree in azimuth.

As some of the iron pieces had been machined and the magnet reassembled, it was necessary to center the cryostat and coil with respect to the pole tips. The first harmonic in the extraction region was used to position the cryostat. The final position of the coil was determined by the forces on the radial links and the effect on the first harmonic.

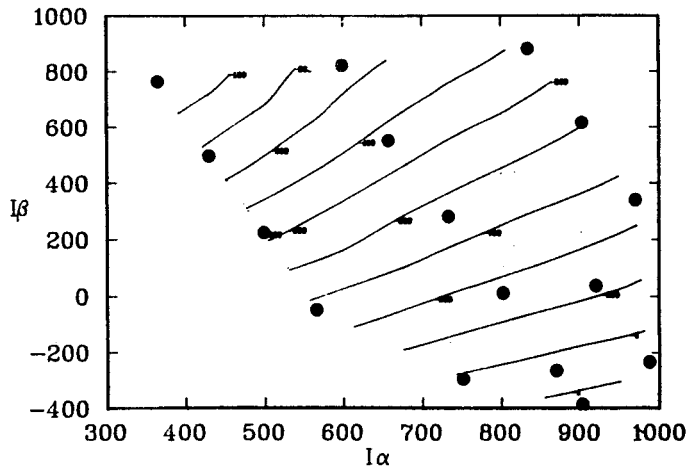

Fig. 1: The median plane magnetic field was measured at 16 points (filled circles) with currents Iα and Iβ in the main superconducting coils. The contour lines indicate points with equal third harmonic phase at r=33 inches.

We show in Fig. 2 the average field and first three harmonics for two of our extreme running conditions, the so called +/+ mode (Iα=833, Iβ=884 A) and the +/- mode (Iα=903, Iβ=-394 A). A polar plot of the three sector difference for those two maps is shown in Fig. 3. At each point we subtracted the average of the magnetic field at that location and the corresponding points 120 degrees apart. Ideally the cyclotron should have perfect 3-fold symmetry, and the three fold difference should be zero. These plots show the error fields and their location with respect to the pole tips.

An interesting feature is the variation of of the phase of the third harmonic (main contribution to the flutter) with excitation. Figure 4 shows the phase as a function of radius for the 16 maps in the main grid. We can see that the major spread occurs at a radius of

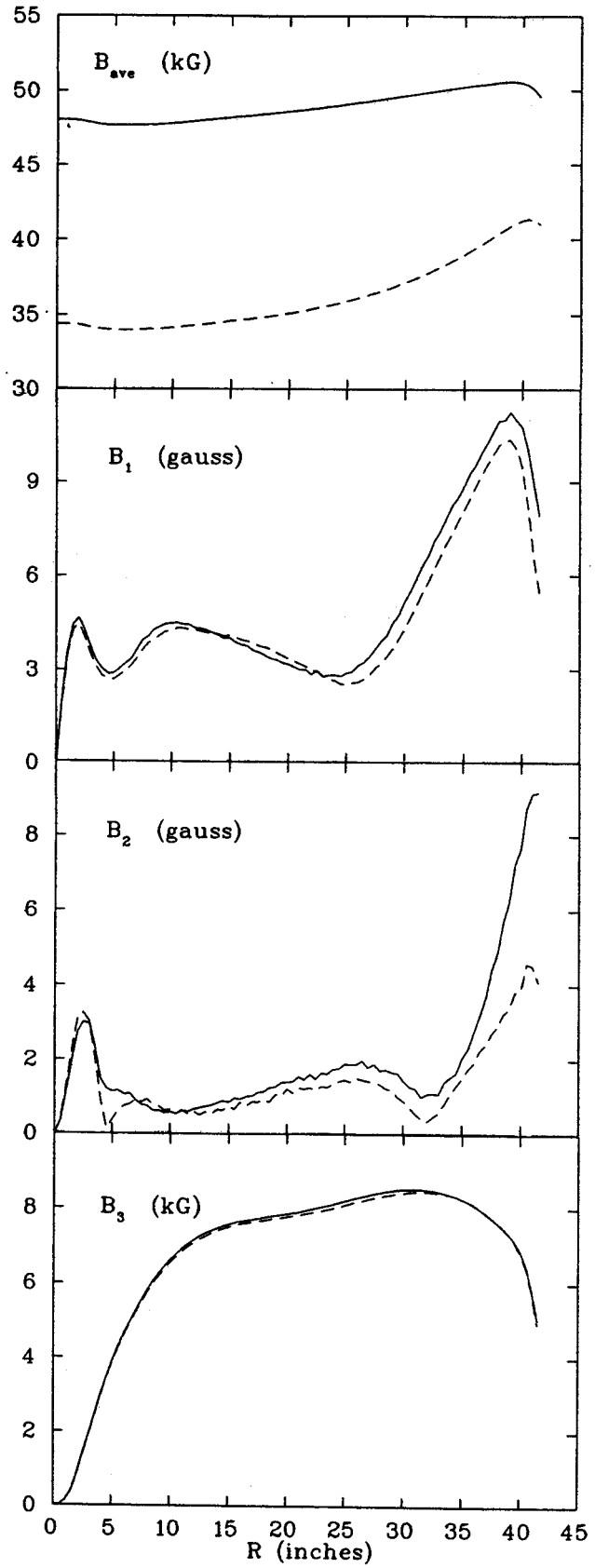

Fig. 2: Average field and first three harmonics of two measured points +/+ (833/884 A solid line) and +/- (903/-394 A dashed).

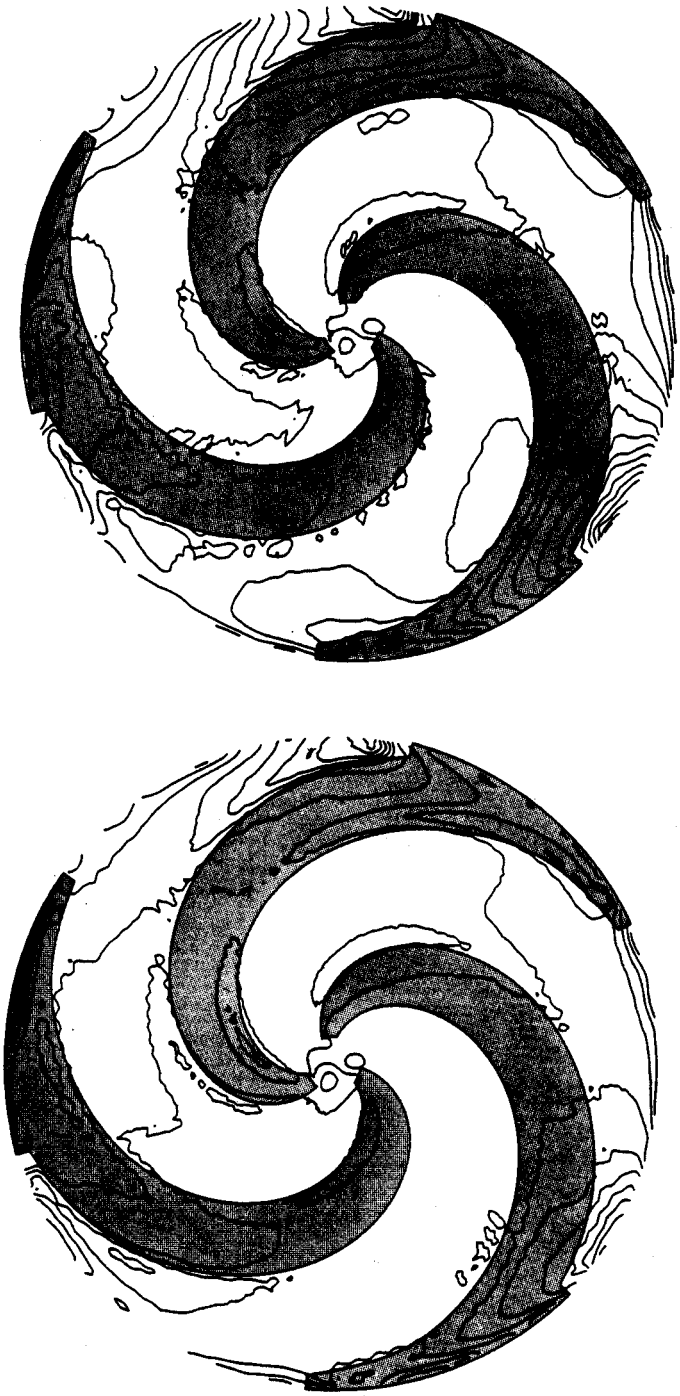

Fig. 3: Contour lines (every 5 gauss) indicating the errors in the magnetic field with respect to the three sector average. Top +/+ (833/884 A) and bottom +/- (903/-394 A).

approximately 33 inches. At this radius we have found the equi-phase contour lines in the Iα,Iβ plane, and plotted them in Fig. 1. It is a smooth and continuous mapping of the excitation plane.

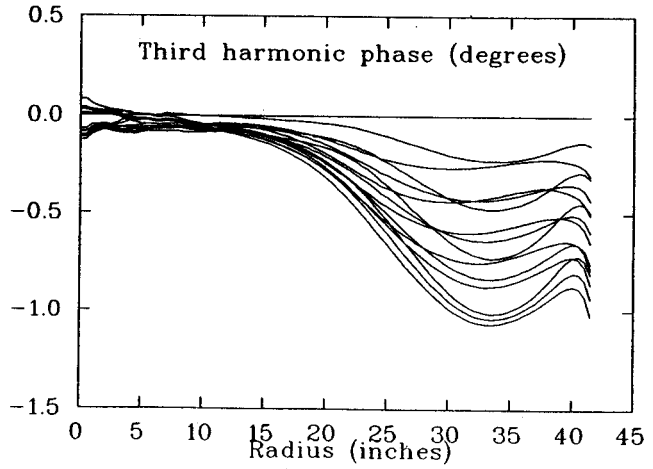

Fig. 4: Phase of the third harmonic with respect to the upper left corner point in Fig. 1 as a function of radius for all 16 measurements.

Trim coil fields

The magnetic fields of the 21 (per hill) trim coils have been measured at four different Iα, Iβ excitations. The four points are on the boundaries of the operating diagram and intermediate excitations are obtained by linear interpolation in these four. Figure 5 shows the average fields for all 21 trim coils for one of these measurements. The comparison with the theoretical (air core) calculation is shown in Fig. 6. In general, the trim coil fields are stronger than the air core calculation by peak percentage deviations ranging from 32 % at the least saturated field to 17 % for the full +/+ field.

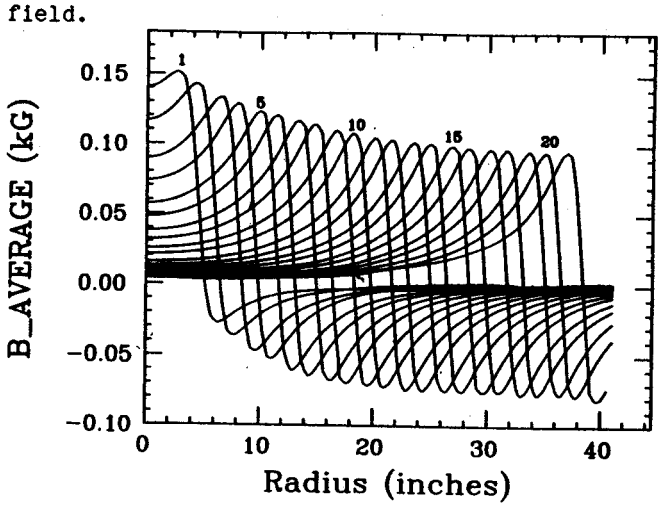

Fig. 5: Average field of the trim coils for 300 A for one of the four measured sets (Iα= 633.9, Iβ= -317.5).

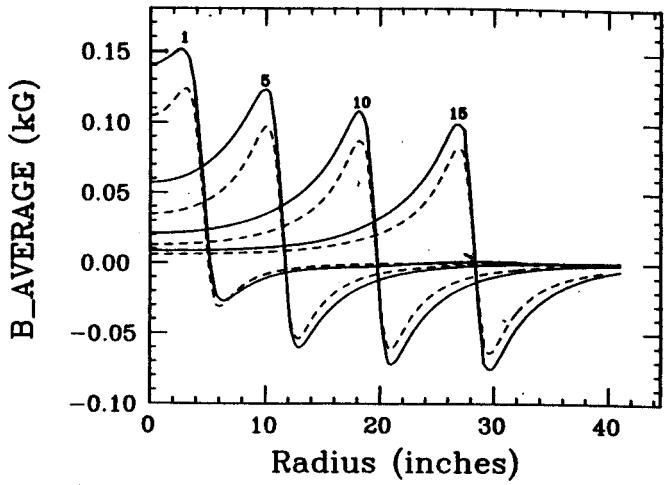

Fig. 6: Comparison of measured (solid line) and calculated (dashed line) trim coil fields for the set shown in Fig. 5.

Axial fields

The magnetic field along the vertical injection line on the cyclotron axis has been measured at four different excitations. A search coil with the same electronics used in the median plane measurements was employed, but without computer control. These fields are used in the axial injection calculations. Figure 7 shows the four measured fields and Fig. 8 a comparison with a POISSON calculation. The data and calculation agree well, except for details at the entrance of the yoke, z≈ 60 inches, due to the support structure.

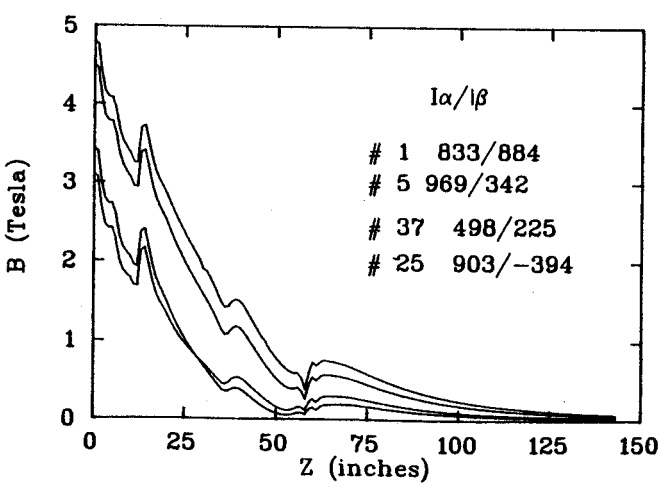

Fig. 7: Axial fields as a function of distance to the median plane.

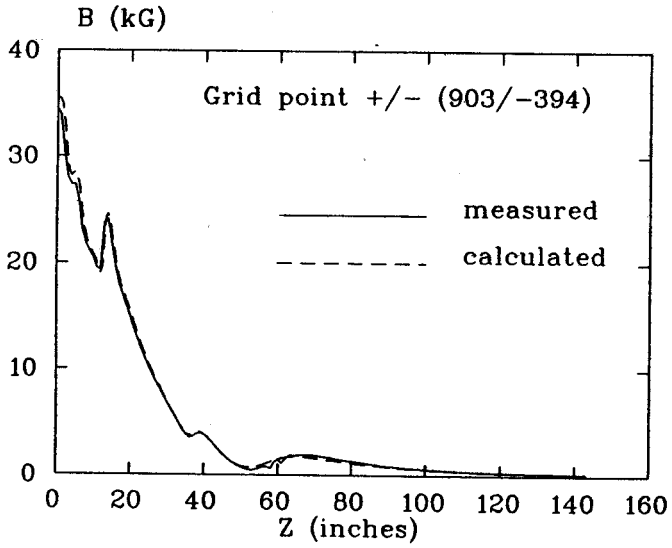

Fig. 8: Comparison of measurements with the Poisson calculation of the axial field.

References

1. Harwood, L. H., J. A. Nolen and A. F. Zeller, Proc. 11th Int. Conf. on Cyclotrons, (Ionics, Tokyo) 1987, 315.
2. Harwood, L. H., J. A. Nolen, Proc. 10th Int. Conf. on Cyclotrons, (IEEE, East Lansing) 1984, 101.

CURRENT STATUS OF THE K800 RF

J. Vincent, J. Brandon, T. Jones, J. Ottarson, and D. Scott

Introduction

Previous annual report papers have described the basic structure of the K800 rf system in some detail. This paper shall give a brief status of the project.

Initial Testing

Final assembly of the cyclotron resonators was completed Friday, Jan 8, 1987, at 4:40 pm. In air, low power measurements began at 5:00 pm that Friday and were completed on Saturday. For each resonator, the resonant frequency was measured as a function of tuning stem length. The structure was excited through the input coupler at levels below 50 Watts and matched. We found the coupler matched the structure very well throughout the frequency band, and that the necessary tuning stem lengths very closely matched calculations. Q measurements were also made in various ways during these tests. The Q of the structure appeared to be lower than we expected. The worst discrepancy of the Q occurred at the high-frequency end of the band where the tuning stem is shortest, and the skin depth smallest. Various data indicate that current levels in the structure are very close to calculations for a given dee voltage; therefore, if a problem exists, it must be due to lower rf conductivity somewhere. During the next week, while the cyclotron cavities were being prepared for high power operation, we phase matched the forward and reflected power signal cables from the directional coupler to the cyclotron resonator signal cables. This relative phase is nominally 0 degrees when the input coupling is matched and is used to generate the error signal which actuates the dee fine tuners.

High Power Testing

On Friday, January 15, at 4:40 pm (everything seems to come together - or come apart - on late Friday afternoons!) we initially attempted to excite the B cyclotron resonator with high power. In the few minutes we were able to operate, we noticed the final stage of the rf amplifier would phase shift at Kilohertz frequencies about the nominal phase. The frequency modulation induced drove it back and forth about the cyclotron cavity resonant frequency where the impedance is 50 Ohms when matched properly. This led to unstable and uncontrollable operation. However, the cyclotron cavity appeared to be coming on well - breaking through multipactoring and ramping with each rf pulse. It was clear that the final amplifier would need to be stabilized in order to operate favorably. About this time a 1/2 inch polyflow water connection came loose, and the cyclotron had its first bath. We found this was not to be due to the rf, it was simply a coincidence. We shut down and cleaned the cyclotron. Since this time a few more of these connections have come loose, without rf operation. We have changed the connector used, since it appears the original ones were unreliable.

On Saturday morning, we modified the B amplifier in an attempt to stabilize it. The transmission line side of the transmitter output coupler had a highpass load inserted in shunt with the transmission line. This consisted of a 12 pF capacitor in series with a 400 Ohm water cooled load. We replaced the 12 pF capacitor with a short, leaving a pure 400 Ohm load in shunt with the line. This effectively placed a small broadband load in shunt with the

transmitter output. It was hoped that this would be enough of a broadband load to hold the transmitter stable. Some cryogenic work was going on at the same time, so we were not able to come on again until later that afternoon.

On Saturday afternoon we again came up in pulse mode at 17.4 Mhz into the B resonator. This time the rf amplifier was stable and well behaved. We were able to fine tune the rf cavity, amplifier, and input coupling while in pulse mode. About 2:30 pm we switched to cw mode, and the cavity immediately popped on at somewhere around 50 kV. Everything seemed very stable, with reflected power at about zero. X-ray calibrations were made, and we then operated at 75 to 100 kV levels confirmed. We began closing the various loops and found them to all work acceptably for the first try. These loops consist of amplitude, phase, and input coupling regulators. However, since the broadband load was on the transmission line side of the coupler, the overall transmitter stability was a strong function of how heavily we were coupled to the line. The coupling capacitor value, along with the DC plate potential, has a strong influence on the overall transmitter efficiency. We decided to design a system in which the broadband load would be connected to the transmitter side of the output coupler. Then the output coupler setting would have a much weaker effect on the minimum load the final tube anode sees.

Also two screen bias regulator circuits failed during this period, indicating we would have to protect them against anode to screen sparks and plate crowbar conditions.

The following week we designed, fabricated, and procured the anode to load coupling apparatus, proper valued resistor elements, and spark gaps to protect the various bias regulators.

This week the A and C cyclotron resonators were also prepared for high power operation, and the A and C transmitter high pass transmission line loads were modified as was mentioned for B, since parts for the anode load would not be in until the following Monday.

On Saturday the 23rd, we brought all three systems on in open loop and adjusted them for three phase operation. We noted very little coupling from system to system, and it behaved very well. We obtained X-rays on all three systems to calibrate the dee voltage monitors, and muddled with the loops for a while. It became apparent that the 300kW power supply from the K50 days would not be able to stably supply enough power for the first beam test at 17.4 MHz.

The following week we received the parts necessary for the transmitter modifications and installed them. We also decided to go for a different beam energy at 15.59 MHz, where the necessary dee voltage would require less power. All sorts of mechanical and electrical tests were going on for other systems at the same time, so here comes Friday at 4:30 again before systems appeared to be ready for rf operation again.

On Saturday, January 30th, we again brought all three systems on line. This time everything was much more stable. We got all loops working very well and began driving up to higher voltages on all three dees together. We noted that we were having trouble with the anode supply. It uses a saturable reactor voltage regulator. When the rf sparks off the anode bias would increase from 16 kV to about 21 kV, then the mag amp would bring it back to about 17kV. The rf would start back up dragging the voltage to about 13kV, where the mag amp would slowly bring it back to 16kV. Of course while this is going on we are drawing screen current, and then it would settle back down as the plate voltage came back. As a consequence of this behavior we had to adjust all of our limiting circuits so they were operating properly or we would trip off for one reason or another. Also, when we were finally up to 95 kV on all three

dees, the breaker which feeds the anode power supply would trip after a couple minutes. We further noted that these surges of power would significantly affect the rest of the equipment in that area of the building. Since the equipment affected includes the ECR, injection line supplies, vacuum meters, and cyclotron trim coils, it became apparent that achieving internal beam under these conditions would not be possible. We would need our high power anode supply back in service. Fortunately, its newly designed transformer was due on Monday.

On Monday the transformer arrived and was installed and operational by Wednesday. We had trouble with the controls for this supply, but by Friday we were again in business. With the 1.2 MVA supply we had no trouble achieving the necessary power levels what so ever. However, now we began having problems with water leaks in the resonators, and with the input coupler vacuum to air insulators plating on the vacuum side eventually breaking down and cracking the insulator.

Conclusion

It is now Wednesday, February 17. We are almost done modifying the input coupler insulator shield rings to prevent them from plating. We have no water leaks currently, and in the last couple of weeks, until the recent coupler failures, we have been running the rf as requested. The system is virtually out of development mode and almost ready to be turned over as a normally operated system. When internal beam tests are complete, we will tune the rf system to the standard 10 frequencies over our band of 9 to 27 MHz to obtain calibration data. These data are then fed to a program which yields settings and calibrations for any desired frequency by cubic spline interpolation. We will also begin to condition the dee voltage up to as high as we can get it.

The couplers should be re-installed this afternoon, and we should be back on line tonight or tomorrow. We are very pleased with this entire system at this point. All of the system tuning parameters vary very smoothly, are repeatable, and are virtually identical from one system to another. It initially appears to be much easier to tune and operate than the K500 rf system. The system will most likely be turned over to operations in the next couple months. Remote controls for the system are already operational and used in beam tests.

This paper will end with the only upgrades that we feel would make the system easier to operate and more reliable.

1. Titanium plate the coupler insulators and guard rings to reduce the secondary emission of electrons from the copper and alumina surfaces.

2. Redesign, and rebuild the controls for the 1.2 MVA anode supply, including the crowbar circuits.

3. Finish the design, construction, and programming of the rf local control computer.

4. Work on making the final amplifier stable without the need of a broadband load in shunt.

None of the proposed upgrades are very costly, and since the system is working very well without them at this time, they may be scheduled as time for them becomes available. However, it should be made clear that we do not consider these upgrades as "extras", but as items which should be done as quickly as is convenient.

K800 VACUUM SYSTEMS

R. Blue, J. Kuchar and N. Friedman

The beam chamber of the K800 cyclotron is maintained at high vacuum by two types of pumping systems, cryogenic and turbomolecular. Cryopanels located in the lower dees provide the primary pumping but are supplemented by three external turbo pumps. The external pumps are installed 10 feet above the upper cap of the cyclotron to place them in a region of reduced magnetic field. Still it is necessary to enclose each pump in a shielding box having double walls of 1/4-inch steel. At maximum excitation of the cyclotron magnet this shield reduces the field at the pump from about 200 gauss to 15 gauss, a level suitable for turbopump operation. Each pump connects to the cyclotron through a 10-inch diameter tube, referred to as a "silo". Although these pumps have a rated pumping speed of 550 liters/second the conductance of the yoke penetration (5-inch dia.) and the silo limit the effective pumping speed for air to about 110 liters/sec. each. The external pumps serve primarily for initial pump down and to pump away gases released when the cryopanels are warmed up.

The helium-cooled cryopanel in each of the dees has about 900 square centimeters of pumping surface which, taking account of the transmission to the panel, should provide net pumping speed for nitrogen of about 2500 liters per second. The cryopanel is enclosed in a shroud cooled by liquid nitrogen, to shield the panel from high-temperature sources of radiant energy. A small reservoir for each of the cryogens is housed in the dee stem just below the dee, and heavy copper buses conduct heat from the cryopanel and its shroud to these reservoirs. A continuous supply of liquid helium and liquid nitrogen is delivered to the cryopanels via vacuum-jacketed cryolines interior to each lower dee stem.

Backing pumps for the turbomolecular pumps are located at the vacuum control station external to the K800 shielding vault. At this station each pump connects through a U-tube trap cooled in liquid nitrogen to prevent backstreaming. In addition to the three turbo backing pumps, the station has three other mechanical pumps for auxiliary vacuum systems associated with the K800. Each of the six mechanical pumps is rated at 190 liters per minute and connects to the K800 via about 100 feet of 1.5-inch diameter copper pipe. The auxiliary systems provide pumping of the beam chamber liner, the main coil cryostat vacuum jacket, and the guard system for a variety of rough vacuum requirements. Controls and gauging for the entire vacuum system are also located at the pumping station.

The liner vacuum system pumps the space exterior to the copper liner that separates the pole tips, trim coils, and valleys from the beam space. Since this liner cannot support more than a fraction of an atmosphere of differential pressure the liner must be pumped whenever the beam chamber is under vacuum. Although vacuum interlocks based on pressure gauges are provided, the ultimate protection against pressurization of the liner is a rupture disc assembly between the liner and the beam chamber.

If the main coil cryostat remains leak tight the vacuum insulation space of the cryostat is selfpumping once it has been evacuated and the coil is at operating temperature. However, provisions are made for pumping the cryostat whenever that is necessary. Originally the 6-inch diffusion pump for this purpose was mounted just below the cryostat on the flange of a butterfly valve valve that could be closed to isolate the cryostat vacuum. The pump could then be removed to allow the lower

cap of the magnet yoke to pass over the valve whenever bottom-side access to the cyclotron was needed. However the butterfly valve proved to be unreliable and has been replaced by a gate valve. The valve and diffusion pump are now on a 10-foot extension of 6-inch diameter tubing so that the larger valve does not obstruct the lowering of the lower cap. Backing for the diffusion pump is provided by one of the mechanical pumps at the station external to the vault.

The guard vacuum system serves a variety of needs relating to K800 systems. These include the rough pumping of air locks for beam probes and the inflecter, devices than can be installed into the beam chamber vacuum space or withdrawn to atmosphere for maintenance without requiring the venting of the cyclotron. The guard system also provides differential pumping as backup to seals for the beam chamber vacuum. This primarily involves the main gasket rings which seal between the upper and lower caps of the magnet yoke and the inner wall of the cryostat. Provisions are also made for pumping vacuum spaces in the dee stems should that become necessary.

The majority of the nearly 100 valves associated with the vacuum systems are air actuated via solenoid operated control valves mounted at strategic locations on each level of the vault and at the vacuum control station. The control valves are mounted on standardized manifold blocks of eight valves each so that maintenance when required can be handled by exchanging easily replaced assemblies. The control valves, in turn, are energized via 24 VDC outputs from a Gould programmable logic controller which provides the interlock logic to assure safe operation of this complex system of valves. The operator interface for control of the vacuum system is made by a PanelMate programmable CRT switch and indicator panel located at the vacuum control station.

The vacuum gauging requirements for the K800 are meet by four ion gauge tubes sensing high vacuum in the beam chamber and in each of the three turbopump silos. Due to the magnetic field external to the yoke, each of these tubes must be shielded and located as far as is practical from the yoke. In particular the tube sensing the beam chamber vacuum is mounted on a 6-foot stem of 1.5-inch diameter tubing which branches from one of the turbo pumping ports just outside the yoke. Its reading can thus be expected to differ somewhat from actual beam chamber vacuum. The rough vacuum portions of the system are monitored by 20 thermocouple gauges, most equipped with set points employed in the interlock logic. The beam chamber is also monitored by a broad-range Pirani gauge so that continuous metering is available through pump down from atmosphere to normal operating pressure. Other vacuum sensors include a capacitance manometer sensing the pressure differential between the beam chamber and the liner and a pressure switch to determine when venting has returned the beam chamber to atmospheric pressure.

The main vacuum system is further instrumented with a residual gas analyzer to provide vacuum diagnostic information. The analyzer head and power supply are mounted near one of the turbopumps at the top of a silo while the control and readout are at the vacuum control station. The silo where the RGA head is installed is specially equipped with a needle valve in parallel with the main gate valve so that the turbo can provide differential pumping to keep the RGA pressure in its operating range even when the beam chamber vacuum is much worse.

The vacuum system as described has been in use for about two months to pump the K800 even though many features relating to vacuum controls are not yet operational. Any assessment of the vacuum system performance is, therefore, preliminary. Under present conditions the three

turbo pumps alone can reduce the pressure at the ion gauge to about 2 X 10^{-5} after 4 hours of pumping. Correction for the the pumping conductance would indicate that the beam chamber pressure would be roughly a factor of two higher under these conditions. When two cryopanels are cooled the ion gauge pressure drops by about a decade. Although the available data is not yet sufficient to make firm conclusions the pressure readings are consistent with design expectations of about 2500 liters per second pumping for each panel. The third panel has not been placed into service due to a leak from the nitrogen volume into the beam space vacuum.

Operating experience with the K500 indicates that operating vacuum conditions can be expected to improve significantly as various leaks are tracked down and corrected. Even at present a small number of known leaks are making major contributions to the total gas load. It is quite reasonable to assume that beam chamber vacuums approaching 1 X 10^{-7} will be achieved. In addition to work involving the finding and fixing of leaks there is work to be done on vacuum gauges and the vacuum control logic before the vacuum systems will be fully operational.

K800 TRIM COILS INITIAL OPERATION

P. Miller, J. Easley, H. Hilbert, P. Koblas

The trim coils for the K800 cyclotron are constructed like those of the K500: the water-cooled copper conductor is wrapped around the iron hill pole piece such that the axis of the trim coil is horizontal.[1] There are six such pole pieces in the magnet. Figure 1 is a top view of the K800 showing their locations (Hill 1-3). Each trim coil consists of 10 turns of 0.25 inch square cross section copper conductor with a round center hole for water cooling, and operates at 400 A max. There are 21 such coils on each pole piece, labeled TC 1 to TC 21. Except for TC 1 and TC 21, one power supply is used for one TC number, that is, all six identical coils are wired in series. Three power supplies are provided for TC 1, one for each sector of the magnet (2 coils), to control the azimuthal averaged field and the magnetic first harmonic contributions separately for centering the beam. TC 21 is wired similarly to give a bump control for beam extraction.

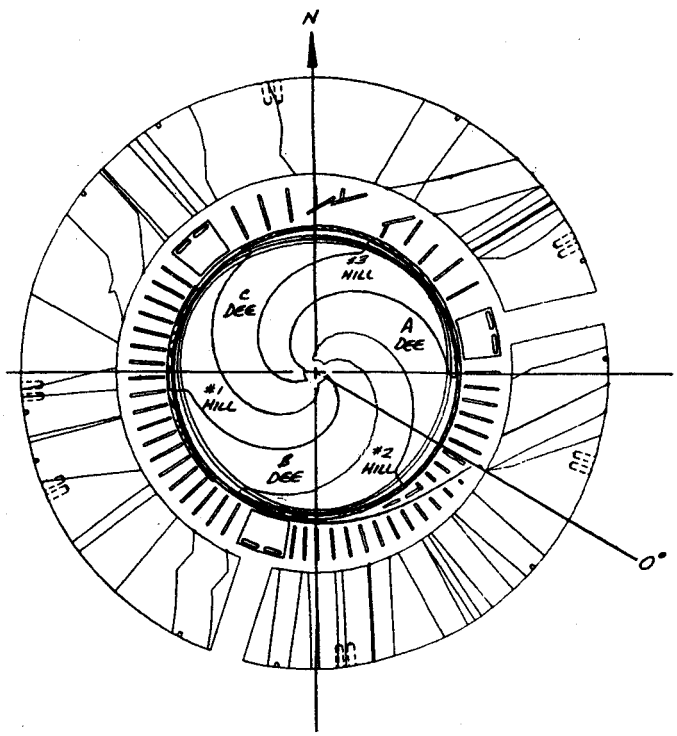

Fig. 1: Plan view showing pole tip locations.

Due to mechanical defects in the conductor procured for the trim coils it was necessary to wind some of the coils from spare conductor with a different size hole for water cooling (0.142 inch used on TC1-11, 0.188 inch used on TC 12-21). The resistance and water flow were verified to be compatible with the design goals before the coils were wound.

There is also a single circular trim coil, TC 0, in the upper and lower center plugs of the magnet excited by one power supply. To avoid deflection of the beam in the axial injection line the current leads for the lower coil were paired and repeated with 120 degree symmetry in their run along the beam pipe. This coil has a current limit of 250 A set by the available water flow. The coil and its compensating leads are made from 0.187 inch square conductor with a 0.125 inch diameter water cooling passage. The leads are flattened slightly to fit the available space in the center plug. The measured water flow rate was 0.16 GPM with approximately 40 psid. The calculated temperature rise at 250 A is 83° F, using the resistance 0.031 ohm for the K500 coil.

Overtemperature protection is provided by a thermal switch (160° F) on each coil (21 x 6 + 2 = 128 switches) read into the Modicon PLC for interlocking the power supplies through a diode matrix multiplexer that is scanned continuously by the PLC to allow immediate identification of the coil where overtemperature is detected. Six water flow switches (one per sector, top and bottom) interlock the power supplies if the total flow rate is too low. All power supplies are automatically turned off if any one temperature switch or flow switch detects a fault.

A special water temperature regulating loop maintains the average temperature of the trim

coil water, $(T_{outlet} + T_{inlet})/2$, equal to the temperature of the steel magnet core to prevent differential expansion of the pole tips relative to the core. Temperature differences of more than 10° F might cause misalignments. Note that this regulator is required whenever water is flowing to the coils, whether the power supplies are on or off. The temperature difference is monitored and the water flow is shut off (and power supplies are shut off) if the temperature gets out of bounds for more than 120 seconds. If this happens the water can be valved manually around the trim coils (to keep them isolated from the water when it is flowing again) until the temperature regulation has been restored.

Trim Coil Water and Electrical Connections

The water and electrical connections for TC 2 and TC 20 are shown schematically in Fig. 2. The water manifolds are represented by boxes labeled with abbreviations of the following: Main Manifold, Satellite Manifold 1, Satellite Manifold 2. Each of these contains LCW Supply (S) and Return (R). The numbers refer to pole tip number 1,2 or 3 (see Fig. 1). The main manifold is used for pole tip 3; it contains all of the electrical terminals.

In Fig. 2 water flows horizontally; electrical connections are lines with a vertical segment. The power supplies for TC 2 and TC 20 are the rectangles at the bottom. Wherever water must flow between the two electrical circuits an insulating water tube is used. Also, two electrically insulating water links are built into the main manifold. These are shown as small boxes labelled "MM L". Each coil has a temperature switch on its outlet side, indicated as a circle on the figure.

Except for TC 0, 1, 11 and 21, all other trim coils are connected in pairs as shown in Fig. 2. The exceptions will be discussed next. The direction of water flow is alternated to get a more uniform pole tip temperature as shown by the following table:

1 <-- 21	5 <-- 17	9 <-- 13
2 --> 20	6 --> 16	10 --> 12
3 <-- 19	7 <-- 15	11 <-- dummy
4 --> 18	8 -->14	

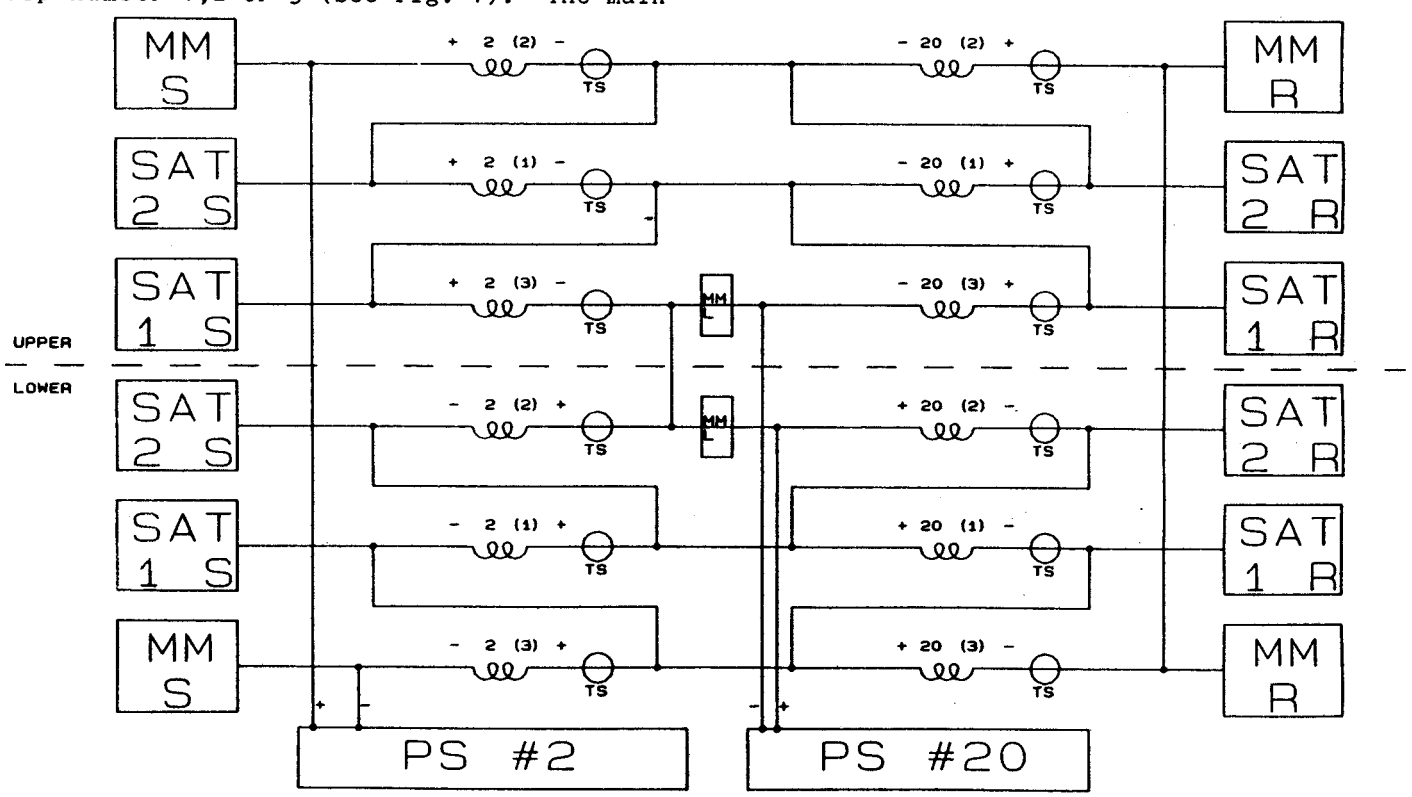

Fig. 2: Water and electrical schematic diagram, Trim coil 2 and Trim coil 20.

Figure 3 shows a schematic diagram like Fig. 2 for TC1 and TC 21, the trim coils used for centering and bump control. All of the water is provided by the main manifold.

Figure 4 is the diagram showing the water and electrical connections for TC 0 and TC 11. There are extra water lines for TC 0 in order to make the full pressure available for this coil. If TC 11 were connected in a similar way it would take more water than the others. Flow restricting tubes are therefore connected to simulate another trim coil (compare Fig. 2). The main manifold connections for TC 0 power supply are attached as shown to the water circuit for TC 11 (3 upper) and TC 11 (2 lower) because, originally, TC 0 was intended to be in these water circuits. However, this was not possible due to the extra restriction of water flow for TC 0 described above. In Fig. 4 the leads for TC 0 (on the magnet yoke surface), the "flow restrictor" and TC 11 comprise one water path; the coil TC 0 itself and the compensating leads in the center plug is another. The jumpers marked "X" in Fig. 4 separate the two water circuits.

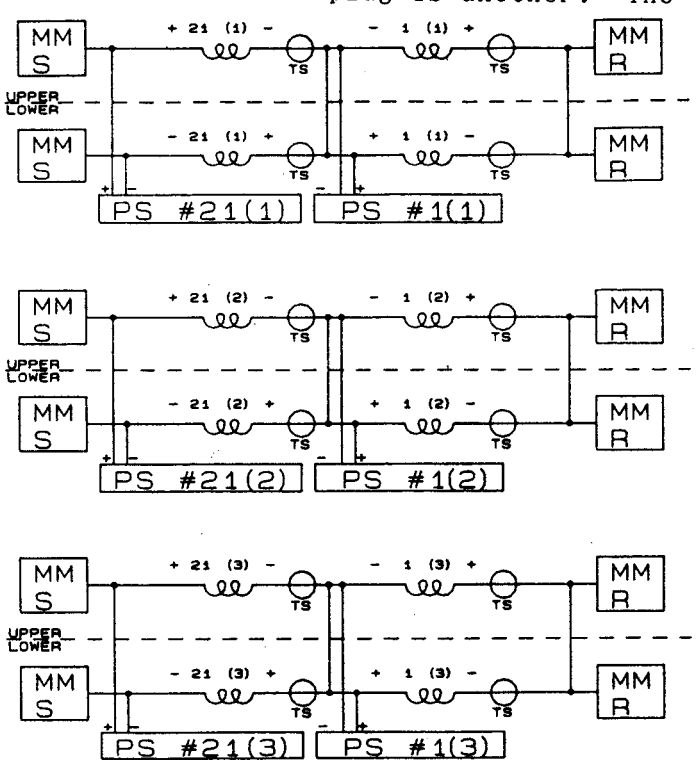

Fig. 3: Water and electrical schematic diagram, Trim coil 1 and Trim coil 21.

Table I gives the calculated load resistance on each trim coil power supply. The estimate includes .006 ohm for external leads. There are three power supplies each for TC 1 and TC 21; all three have the load resistance given in the table. Water flow and maximum temperature rise (at 400 A) are given for each coil, assuming that 70 psi is the pressure differential across each pair of coils.

Flow switches for the main and satellite manifolds were set to trip at 2.3 GPM. Harwil type Q-1 flow switches were equipped with 0.27" dia. orifices, which allow setting the trip point between 2 and 4 GPM. The flow data in Table II were measured with the Bell and Gosset calibrated meter valves (setting 0-50) and a portable differential pressure gauge (graduated in ft. of water).

Table I

Trim coil resistance and water flow estimate

Coil no.	Rload [ohm]	Flow [GPM]	Dia. [inch]	DeltaT [deg F]	DeltaP [psid]	Connect coil
1	0.02180	0.461	0.142	18.7	38.3	21
2	0.05467	0.462	0.142	19.2	40.3	20
3	0.06205	0.429	0.142	23.8	44.6	19
4	0.06430	0.422	0.142	25.2	46.2	18
5	0.06721	0.412	0.142	27.1	47.7	17
6	0.06984	0.405	0.142	28.7	49.2	16
7	0.07318	0.394	0.142	31.0	50.7	15
8	0.07592	0.388	0.142	32.8	52.1	14
9	0.07853	0.381	0.142	34.7	53.2	13
10	0.08071	0.376	0.142	36.2	54.3	12
11	0.08332	0.424	0.142	33.2	70.0	--
12	0.10581	0.376	0.188	48.3	15.7	10
13	0.10931	0.381	0.188	49.3	16.8	9
14	0.11244	0.387	0.188	50.1	17.9	8
15	0.11595	0.395	0.188	50.7	19.3	7
16	0.11888	0.405	0.188	50.7	20.8	6
17	0.12239	0.413	0.188	51.3	22.3	5
18	0.12533	0.422	0.188	51.5	23.8	4
19	0.12883	0.428	0.188	52.2	25.4	3
20	0.13177	0.461	0.188	49.6	29.7	2
21	0.05028	0.462	0.188	52.4	31.7	1

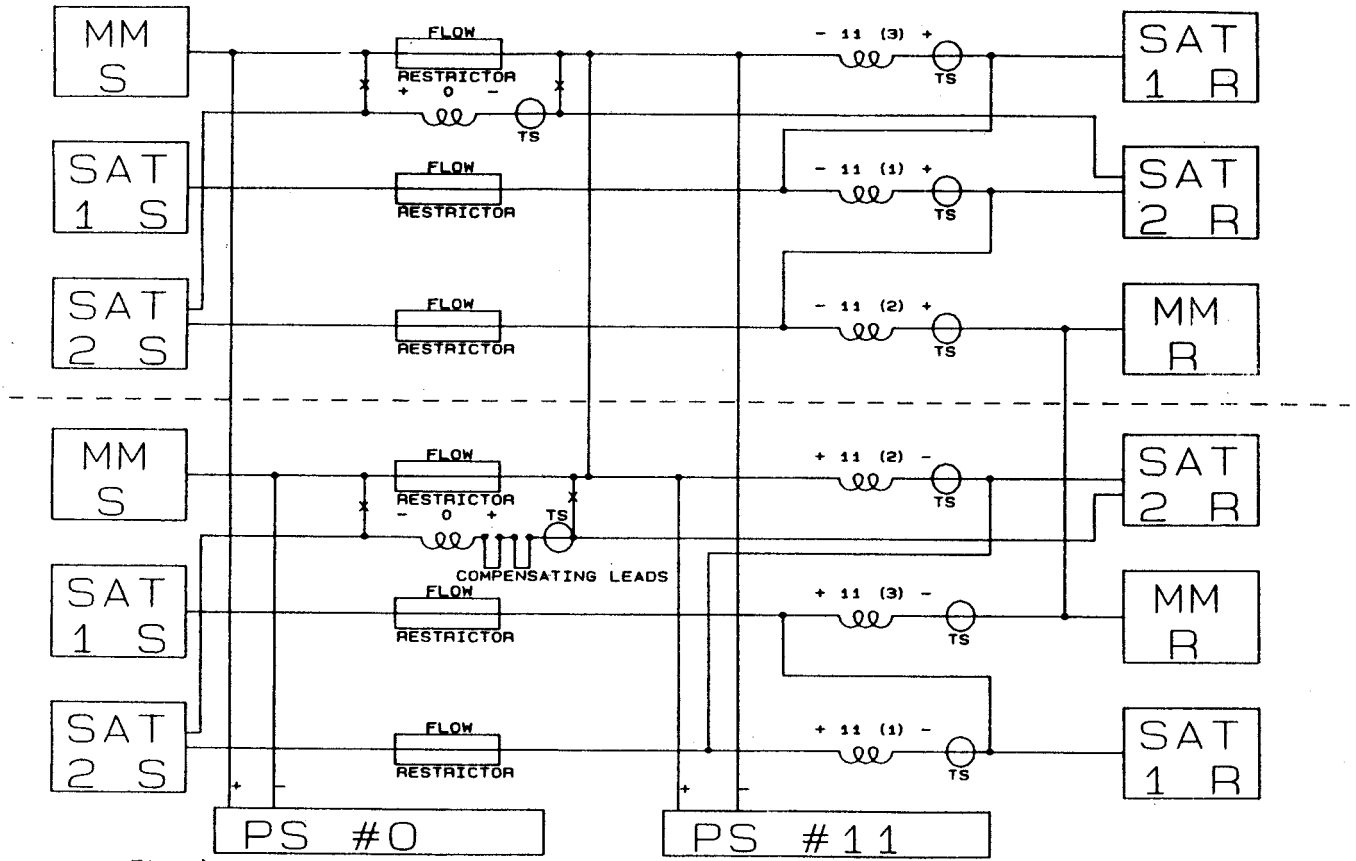

Fig. 4: Water and electrical schematic diagram, Trim coil 11 and Trim coil 0.

Method for Testing Polarity of Coil/Power Supply Connections

Correct polarity of the magnetic field was determined by using a Magnaprobe gimballed compass needle held near each hill while one power supply was turned on at a time. The direction of the magnetic field was noted as the probe was moved along the center of the hill.

The red end of the Magnaprobe points in the direction of the magnetic field. This was determined by observing the probe when held near an isolated power supply cable carrying current in a known direction. The total field of our cyclotrons points downward in the beam chamber during operation. The sign convention for trim coil current is related to that as follows. When a trim coil current is positive, the magnetic field it produces at the center of the cyclotron, on the median plane, points downward.

Therefore, the field in the gap adjacent to the coil points radially inward for lower coils, outward for upper coils, which is the test criterion.

Power Supply Water Flow

The power supplies are all the same: 55 V at 400 A maximum output, current regulated with 0.25 A stability. (mfg. by Alpha Scientific Co.)

The flow switches in the power supplies were set to trip at 1.5 GPM. One flow switch was defective and was replaced (coil 14 power supply).

We found debris in the water lines of the trim coil power supplies, which reduced the water flow. We believe that dirt entered through the supply manifold and lodged in orifices in the Hansen quick- disconnects at the back of each power supply. We noticed an

Table II

Trim Coil Water Flow Data

Meter valve set	Pin [psi]	Pout [psi]	deltaP [psi]	T [oF]	Gauge [ft. of water]	Flow [GPM]	Cv	
Lower hill #1 (West)								
20	88	18	70	76	9.4	4.0	0.48	
20	102	22	80	76.5	7.0	3.0	0.34	
40	102	74	28	76.5	16.1	2.3	0.43	RVT*
Lower hill #2 (East)								
20	85	13	72	77	10.5	4.2	0.49	
20	96	18	78	76.5	10.0	4.1	0.46	
40	95	65	30	76.5	16.0	2.3	0.42	RVT*
Lower hill #3 (North)								
20	88	16	72	76	11.0	4.3	0.51	
20	99	20	79	76	15.0	5.0	0.56	
40	101	72	29	76	16.1	2.3	0.43	RVT*
Upper hill #1 (West)								
20	74	3	71	76	8.0	3.65	0.43	
Upper hill #2 (East)								
20	73	4	69	76	9.0	3.9	0.47	
Upper hill #3 (North)								
20	72	4	68	77	14.0	4.8	0.58	

*RVT--Return valve was throttled to obtain the desired flow.

increase in flow in several supplies after the quick disconnects were operated once. Some of the water circuits were flushed by depressing the self-sealing valve in the Hansen fitting to let water flow out of the system. We have installed a filter in the water supply to prevent further contamination.

Normal flow during testing was 2 GPM through two power supplies in series (supply pressure 111 psi, return pressure 29 psi). There were 28 power supplies, including 2 spares in the group, requiring a total flow of 28 GPM. Flow was measured with a 0-3.5 GPM glass tube/float type flow meter, fitted with rubber hoses and #3 Hansen quick disconnects to match those on the power supplies. A few supplies were connected (one at a time) directly to the water supply and return manifolds. The water flow ranged from 2.5 to 3.34 GPM under those conditions, as expected.

References

1. T. Antaya et al. Annual Report 1986, p. 133.

K800 EXIT CHANNEL FIELD MAPS

A.F. Zeller, T. Kuo, J. Nolen, and R. Swanson

During the recent K800 magnetic field mapping, measurements were obtained of the field profile out to a radius near the outer cryostat wall from the inside, and in the exit channel from a point outside the tank wall to outside the yoke. There existed a gap in the measurements from 55" radius to the edge of the inner yoke. Beam optics calculations for the external beamline are begun at 55", so knowledge of this region was needed to finish the external beamline layout. Additionally, measurements of the external fringe fields along the beam path were needed to correctly position the external elements.

A search coil mounted on the end of a long rod was used to map the exit channel from the outer edge of the yoke to a position past the middle of the coil package. Data were recorded along three tracks nearly parallel to the extracted beam trajectories, separated by 1/4", allowing determination of the edge angle produced by the inner edge of the yoke and the tank wall. A previously calibrated search coil connected to the Voltage-to-Frequency Converter allowed measurements every 1/2 to 1" along the path. Maps for three fields were obtained: field #38 which corresponds to a rigidity of 1 GeV/c, field #25 which is 200 MeV/u and field #1 the peak field at 1.6 GeV/c. At point #1 an NMR signal was obtained in the exit channel and was used to provide the absolute field. At the two lower fields the NMR signal was below the working level of the probes, so Hall probe readings were used for absolute field levels. Finally the Hall probe was used to measure the external fringe fields from the edge of the yoke to about 3 meters along the beam trajectory. However, the beam transport system requires a quadrupole to be placed 2' from the yoke, so only that part is used in the optics calculations. The total field maps are composed of the search coil measurements and the Hall probe measurements. The results are shown in Fig. 1 for the three fields, from the middle of the coil package out to the first quad. Some of the magnetic elements are also shown. Figure 2 shows an enlarged portion, from 55" to the quad. Note that the zero point is the outside edge of the yoke and that the field has the opposite sign from the main cyclotron field.

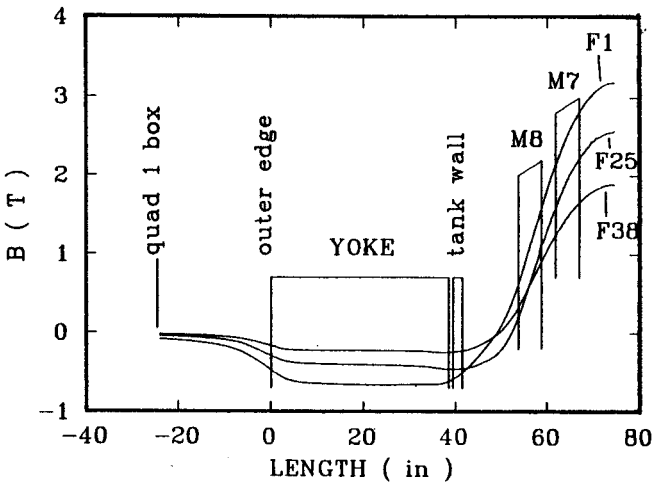

Fig. 1: Total maps for three cyclotron field settings from the middle of the coil package to the first quad in the external beamline. Data are plotted for only one of the three tracks at each field.

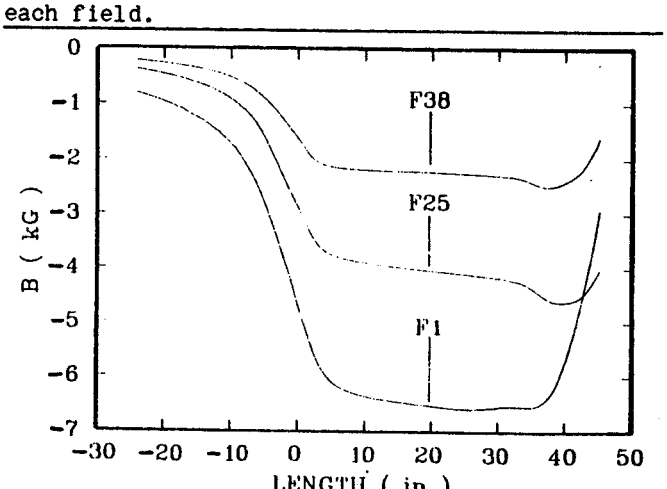

Fig. 2: Field maps from a 55" radius to the first quad. Note the field is negative with respect to the central field.

THE K800 EXIT CHANNEL DESIGN USING RESISTIVE COILS

A.F. Zeller, J.A. Nolen, and R.T. Swanson

Because of the problems associated with the use of permanent magnets in the K800 exit channel, discussed elsewhere in this Report, a dipole coil system was designed which makes the different rigidity beams follow the same trajectory. Without correction, the trajectory of the most rigid beam, 1.6 GeV/c, follows a sagitta corresponding to a 7 degree bend out to the first quadrupole. The least rigid beam, 1 GeV/c, makes only a 3 degree bend, so a correction is necessary. The required additional field is about 3 kG. The solution of making a small correction (1 degree) to the most rigid beams helps reduce the contamination of the interior with new first harmonics since the largest corrections have to be applied at fields where the yoke is least saturated. A calculation by D. Johnson and F. Marti for the case where the most saturation occurs, i.e. at full field, for a coil producing 3 kG yields 1.5 G of new first harmonic at a 40" radius. This represents an upper limit to the first harmonic since the field needed at high fields is significently less than this.

The simplest possible coil configuration which would permit a large beam tube in the 7" square exit channel is a racetrack (flat) coil. However, this configuration produces a very inhomogeneous field, which adds to the intrinsic sextupole shape of the exit channel. (It always adds since the corrections have the same sign as the exit channel field.) Therefore, the coil is composed of two sections: an upper racetrack coil consisting of 6 x 6 turns of 1/4" square copper conductor, and a lower saddle coil consisting of 4 x 4 turns. A POISSON calculation of the coil cross sections is shown if Fig. 1. The calculations were done in the two limits of air core and unsaturated iron surrounding the coils to demonstrate that the coils produced uniform fields in either case. The calculation shown in Fig. 1 is an intermediate case, where a layer of infinite permeability iron surrounds the coils several feet away. Running the coils with separate power supplies would provide a method of making the field more homogeneous, however, initial running will be with a single supply until the need for two supplies has been evaluated.

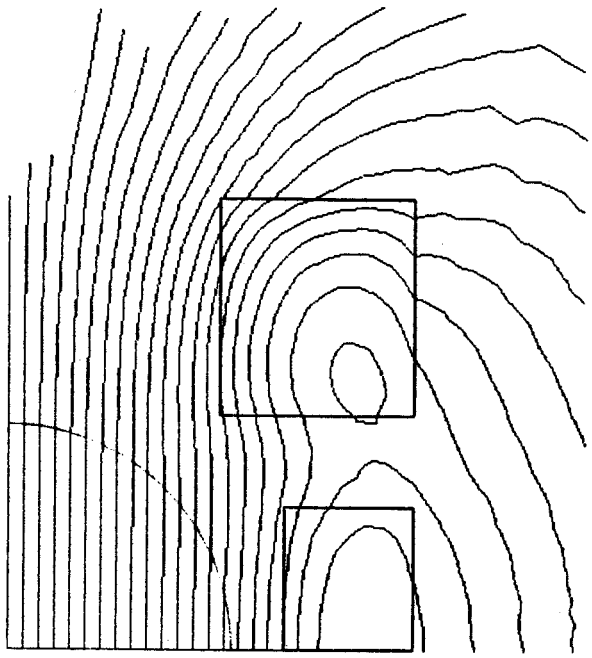

Fig. 1: POISSON calculation showing the two coil configuration of the upper quadrant of the system. This illustration is for a modified air core calculation: assuming that infinite permeability iron is located several feet away. The upper coils have 36 turns, while the lower coils have 16. The beam tube has a 3" diameter.

The overall layout of the coils in the exit channel is shown in Fig. 2. This arrangement allows the use of a 3" diameter beam tube, reducing the possibility of beam hitting the tube and reducing the pumping impedance for this section of the beamline.

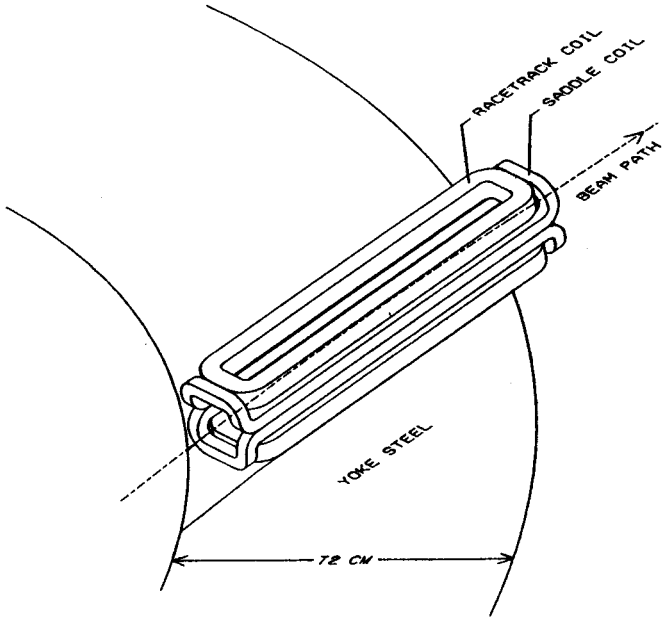

Fig. 2: Isometric view of the coils in the exit channel. The channel is 7 x 7 in^2.

PERMANENT DIPOLE MAGNET TESTS

A.F. Zeller, J.A. Nolen, S. Tanaka, and N. Bhattacharya

The K800 permanent magnet exit channel design discussed in last year's Annual Report[1] depended on the use of SmCo to produce dipoles and quadrupoles. Before placing an order for the complete set of magnets a prototype dipole ring segment was ordered from the low bidder. The dipole magnet, a 1" thick twelve segment piece, was glued into the brass retaining ring, and is shown in Fig. 1. The original specifications called for a remanent magnetization of 10 kG and a straight line coercivity out to 16 kG, however, these specifications could not be met. A remanence of 8 kG was then specified, with the expectation that a higher remanence would be achieved and that the individual pieces would then be exposed to a magnetic field to "knock down" the remanence to 8 kG. This was designed to reduce the possibilities of "holes" in the assembled magnet, i.e. places in the assembly which are subjected to more demagnetization and hence are more demagnetized in the 6.6 kG yoke field. Because the initial remanence of the pieces was found to be only 8 kG, the individual pieces were not knocked down. The individual segments are seen to consist of 3 to 4 individual pieces glued together to produce the required shapes. Several defects were found in the magnet: There are large glue gaps between segments, many chips; missing pieces replaced with epoxy, and a very eccentric center hole. The hole would not fit on a 1.5" diameter pipe.

The magnetic field was measured with a Hall probe, both in the radial direction and in the beam direction. The field integral found by multiplying the field level calculated by PANDIRA times the physical length was found to be in agreement with the measured value, although the peak field was lower than predicted and the effective length longer. A 3-d

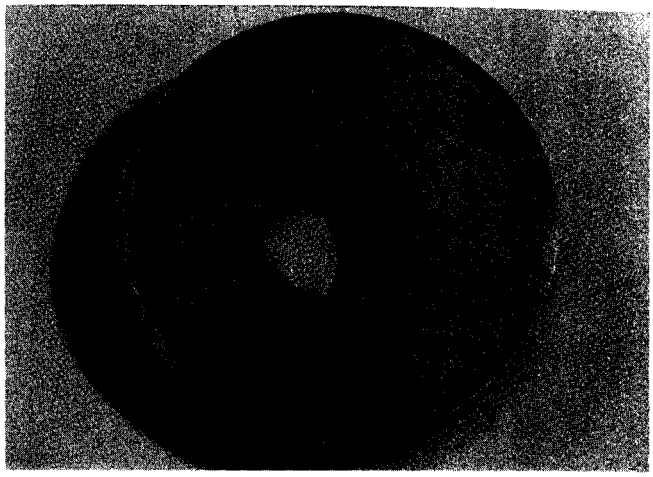

Fig. 1: The assembled dipole ring in its brass ring. The outer diameter of the magnetic material is 4", while the specified hole diameter is 1.56".

calculation of the field was done with PERMAG[2]. The ring was then mounted in the exit channel of the K800 and exposed to the full 6.6 kG in the exit channel and rotated while the field was on. The ring was then remapped. The results are shown in Figs. 2 and 3, as well as the PERMAG results normalized to the data (to account for uncertainties in the remanent field). As can be seen from Fig. 2, the field integral has been decreased by 10%. The radial profile is shown in Fig. 3. The pre-exposure calculations for the uniformity by the code PANDIRA predict a uniformity of 0.5% at a radius of 0.62", compared with the measured 7% at 0.5" radius. After exposure the eccentricity is more apparent- the profile is more asymmetric, reflecting the sensitivity of the different parts to the geometry dependent demagnetization fields. It is believed that the large eccentricity and the gaps between the segments are responsible for the production of large multipole components in the field, causing the difference between calculated and experimental results.

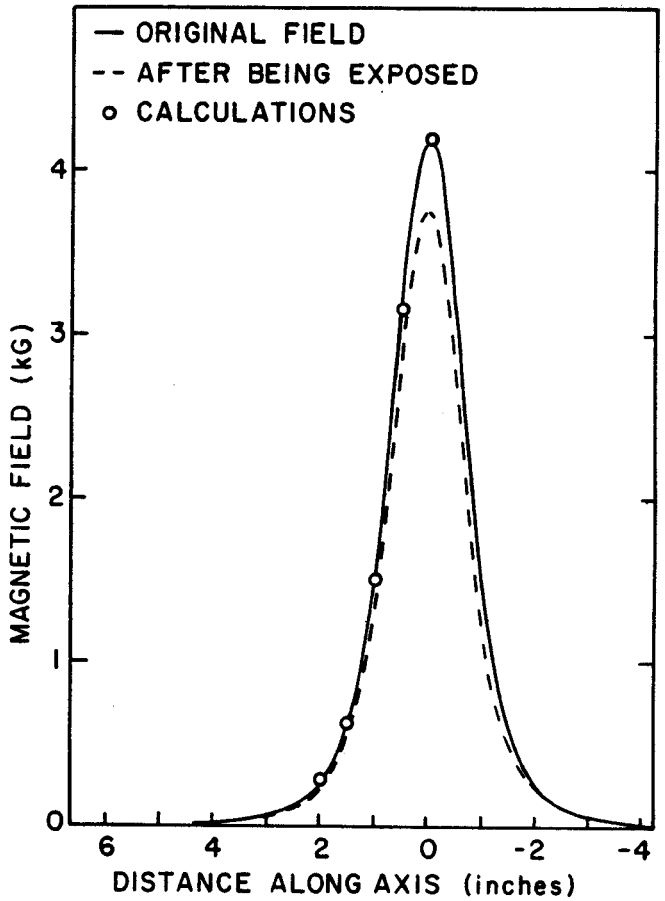

Fig. 2: Measurements of the magnet fields along the central beam axis. The calculations are made with PERMAG.

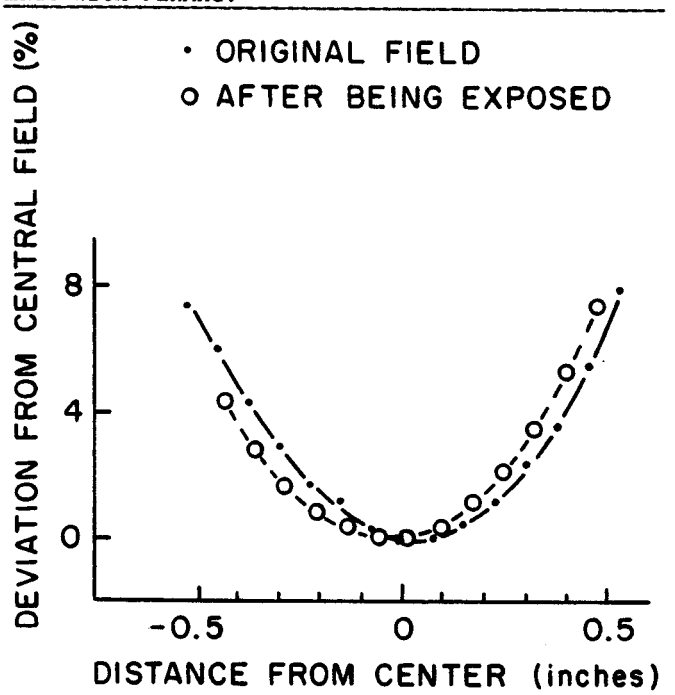

Fig. 3: Measurements of the field profiles in the middle of the magnet along the radius.

Because of the high cost for the permanent magnet system and the likelihood of poor magnets, we have changed our design to incorporate a resistive coil dipole and moved a superconducting quadrupole closer to the K800 to compensate for the elimination of the permanent magnets.

References

1. A. Zeller et al, 1986 Annual Report, p. 157.
2. Z.Q. Xie and T. Antaya, 1986 Annual Report, p. 196; and Z.Q. Xie and T.A. Antaya, NSCL Report MSUCL 622 (1987).

H. Laumer, J. Eicher, R. Fontus II, A. Gavalya[a], J.A. Nolen, D.E. Pendell,
R. Selden, and R. Zarobinski

Extensive modifications to the cryogenic distribution system have been completed in this reporting period. The temporary transfer lines for testing the K800 magnet coil have been replaced.[1] A comprehensive network linking the main(800 watt) refrigerator/liquifier and points of use is partially completed and presently in use. Liquid nitrogen from two 3500 gallon storage tanks, liquid helium from a 2500 l dewar and cold helium gas of variable temperature from the refrigerator are distributed via control boxes and transfer line channels. The return gases are being controlled and flow through the same box and channel system. The construction incorporates multilayer insulation and liquid nitrogen cooled shields and valve intercepts to minimize heat loads at 4 K. Figure 1 shows the relative position of various components. Box 7 is built but not installed. Box 4 is designed and the line to Box 5 will shortly be put in place. All other sections are operational. Box 2 has a small helium leak and the section between Box 1 and Box 3 has a nitrogen leak. They are being pumped on continuously and operate satisfactorily in this mode. The flow through the cryopanels is in series. There are Cajon fittings for quick disassembly on liquid nitrogen and liquid helium lines at the bottom of the DEE stems.

On 1/15/88 the K800 cryopanes where cooled down for the first time. One cryopanel circuit immediately developed a leak from the liquid nitrogen supply line into the beam chamber. It was bypassed and the two remaining panels operate as designed since 1/16/88. The liquid nitrogen cooled cryopanel shields can be cooled

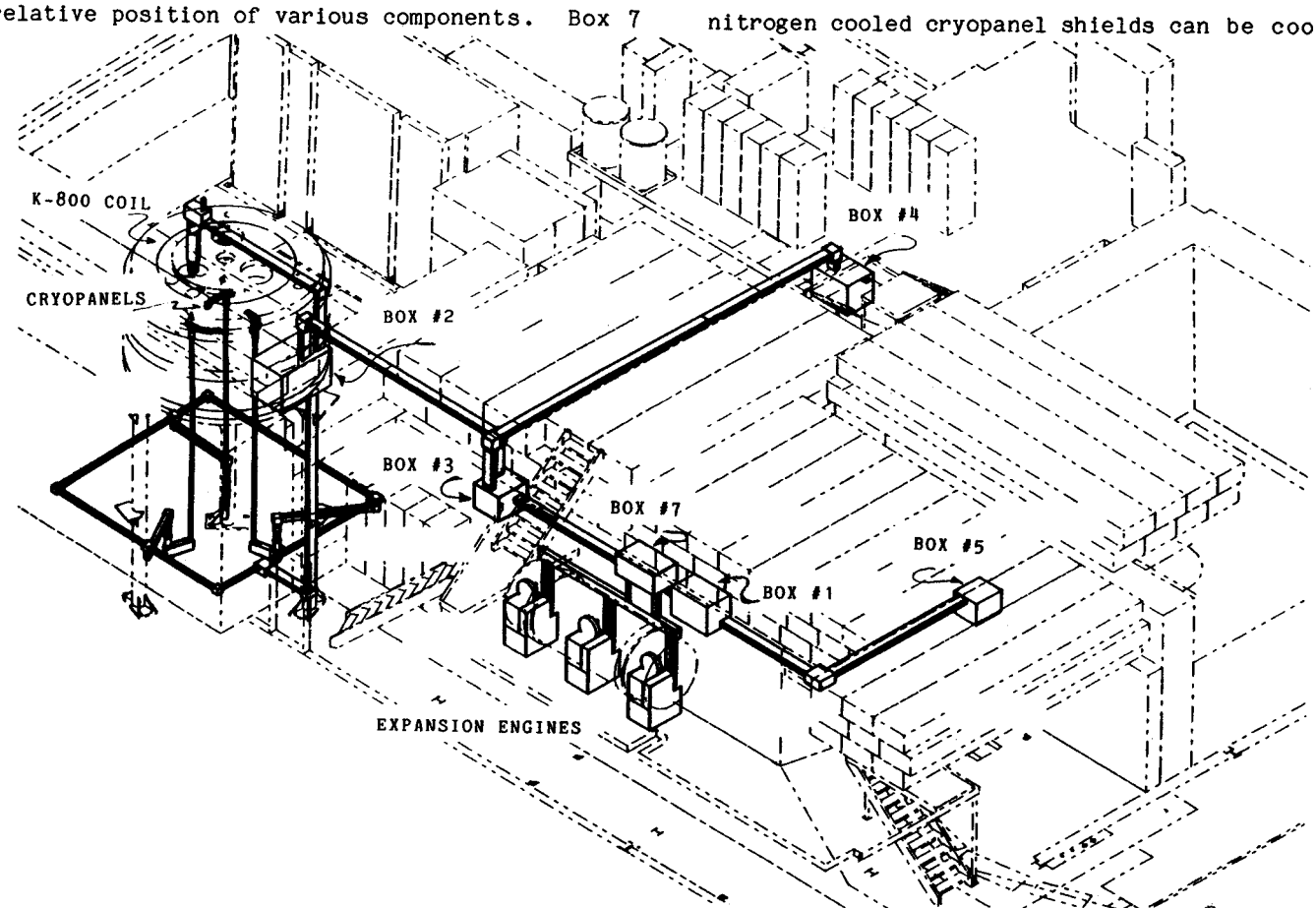

Fig. 1: Distribution system isometric drawing. The relative locations of control boxes and channels connecting them are shown.

as low as 80 K and helium cooled panels can then operate as low as 6 K. When nitrogen cooled shields are at about 200 K, the liquid helium cooled panels still operate below 20 K. The best vacuum achieved in the beam chamber with two out of a possible three cryopanels operating was $1*10^{-6}$ torr. The panels yield a factor of ten improvement over operation with only turbo molecular vacuum pumps. The actual improvement at the beam path is most likely even higher. Figure 2 represents a pump-down curve using a residual gas mass spectrum analyzer. Partial pressures and helium cooled panel temperature are plotted vs. time. As expected, water vapor is pumped first followed by sharp drops in partial pressures of O_2 then N_2 and finally H_2. The cooling of the second panel is less dramatic but is easily seen in the traces corresponding to oxygen and nitrogen. The thermal inertia of the panels is much larger than for those of the K500 cyclotron. Figure 3 shows a warm up curve (B and C shield temperatures are maintained at 125 K and 95 K respectively). It takes about 10 minutes, after liquid helium shutoff, for vacuum to deteriorate and it takes 40 minutes for the coldest panel to warm above 30 K at which point O_2 and N_2 are released copiously. Based on these preliminary observations the cryopanel performance appears very satisfactory and there is promise that a more open design for the nitrogen shield is possible and may yield higher pumping speed and improve the vacuum in the magnet gap if needed.

We have acquired a 6000 l liquid helium test dewar for testing superconducting coils. It has a liquid nitrogen cooled shield and was designed for operating at 1 atmosphere. It is being modified so that besides operating as a submersion test dewar it can also be used as a liquid nitrogen shielded cryostat for selfcontained coil testing apparatus.

The continuous operation of the 800 watt refrigerator/liquifier has become essential for simultaneous operation of K800 and K500

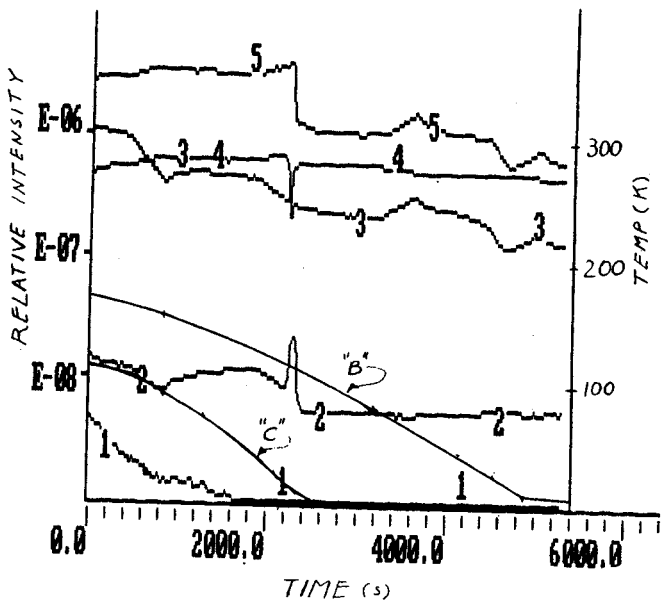

Fig. 2: Cryopanel cooldown. Residual gas mass spectrometer intensities (left ordinate) vs. time for 5 residual gas species. Cryopanel temperatures (right ordinate) vs. time for cryopanels in "C" and "B" dee. The traces represent 1 for C^{12}, 2 for H_2, 3 for O_2, 4 for H_2O, and 5 for N_2.

cyclotrons. Down time of components must be minimized. As reported in previous annual reports a number of startup problems have been overcome.[2] This past year equipment failures have caused little cyclotron down time. Expansion engine failures where limited to 2 per engine per year. Usually repairs are carried out while cyclotrons continue in operation. Compressor shut down was experienced once due to a malfunctioning switch of a cooling tower water pump. Two power failures were the only other occasions when compressors failed to operate. Contaminants in helium gas had little adverse effect on refrigerator operation. The problems in the past where principally due to oil aerosol from compressors and Ne impurity (30 ppmv) in the supply gas. The gas from our present supplier is low in neon (2 ppmv) though higher in nitrogen. Nitrogen is usually trapped out efficiently in the charcoal absorbers and has apparently not caused any plugging of transfer

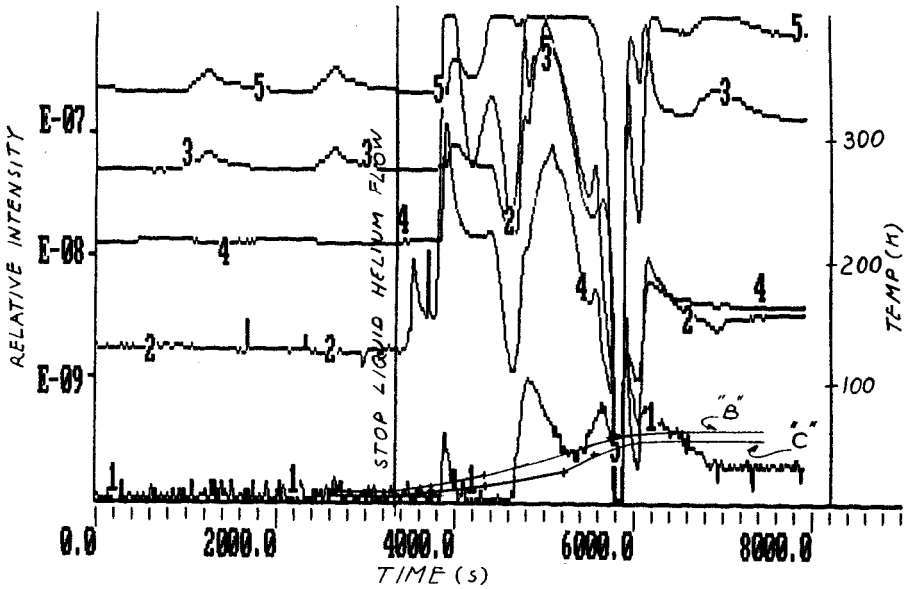

Fig. 3: Cryopanel warmup. Residual gas mass spectrometer intensities (left ordinate) vs. time for 5 residual gas species. Cryopanel temperatures (right ordinate) vs. time for cryopanels in "C" and "B" dees. The traces represent 1 for C^{12}, 2 for H_2, 3 for O_2, 4 for H_2O, and 5 for N_2. As pressure increases the sensitivity of the mass spectrometer to all components deteriorates . Towards end of scan the turbo pumps have restored vacuum to the $3*10^{-5}$ torr level.

lines or valves in the past. We had found that including a filter[3] in the liquid transfer lines alleviated plug formation by neon.

The oil aerosol burden for most of 1987 was 30 ppb, which leads to heat exchanger plugging at the rate of once in six months. A maintenance period of 2 to 5 days is then required before operations can be resumed. The buildup is gradual and scheduling of maintenance to minimize the negative impact is usually possible. By adding a coalescer filter in one high pressure compressor stage the oil aerosol level was reduced by a factor of two recently. We have a third stage coalescer filter ready for installation and thus expect to reduce oil carryover further in the future. There is good reason to expect that this cause for refrigerator maintenance can be eliminated.

The 800 watt refrigerator is presently supplying both coils and both sets of cryopanels with liquid helium. Operating with a compressor flow of 50 g/s at 240 psig. the refrigerator sustains this heatload and liquifies at the rate of 30 l/hr. The available compressor capacity is near 80 g/s. When operated at maximum capacity the pressure drop in the return side of heat exchangers is too high for routine coil operation. We have acquired a reciprocating cold gas compressor to correct this. A similar compressor was tested at Fermi Lab.[4] The unit is ready to be installed and tested in our application. As noted above box 7 which enables us to operate a third gas engine is also ready for installation. A modified transfer line linking reliquifier, cold compressor and the 2500 l liquid helium dewar has also been build. When all of these components are finally installed, the refrigerator will again be tested with a heater in the 2500 l dewar simulating refrigeration load. If this test is successful then the permanent installation of the cold compressor will be completed.

a. CEBAF, Newport News, Virginia.

References

1. Long Removable Cryogenic Transfer Lines. M.C. Mallory, H.W. Laumer, and A. Gavalya; 1985 Particle Accelerator Conference, May 1985.
2. Helium Liquifiers, Their Operation and Associated Equipment Modifications. H. Laumer, A. Gavalya, J.A. Nolen, M.L. Mallory, J. Yunker, R. Zarobinski; NSCL Annual Report, 130(1985).
3. Micron Size Filters in Liquid Helium Transfer Lines. M.L. Mallory, H. Laumer, A. Gavalya, J. Yunker, R. Zarobinski and J.A. Nolen; 11th International Conference on Cyclotrons and Their Applications; Tokyo Oct. 1986.
4. Tests of Cold Helium Compressors at Fermilab. T.J. Peterson and J.D. Fuerst; Adv. in Cry. Eng. 33,655(1987).

MAGNET SUPPLY INSTALLATION AND CONTROL FOR THE K800 INJECTION BEAM LINE SYSTEM

W. Nurnberger, T. Antaya, L. Foth, and J. Vincent

The power supply installation and control system for the K800 injection beam line is essentially an expansion and duplication of the system described in the 1986 annual report for the K500 injection beam line and room temperature ECR ion source (RT-ECR) system[1]. In addition to the K800 injection beam line, the new portion of the control system will also be used to control the superconducting ECR ion source (SC-ECR) when it goes into operation later this year.

It was decided early on, even before the installation of the K500 system, that it would be desirable to have the control systems for the devices associated with the K500 cyclotron completely separate from the controls for the devices associated with the K800 cyclotron. This approach has allowed the installation and de-bugging of the K800 injection line control system without significantly interfering with the scheduling or operation of the K500 cyclotron system. It should also pay dividends in the future by allowing one system to be shut down for modifications or repairs without interfering with the operation of the other cyclotron. The only exception to this arrangement is the compact ECR ion source (CP-ECR). The CP-ECR was designed to be used with either the K500 or the K800 cyclotron by simply moving it form one beamline system to the other, although it is always controlled by the K500 control system. Presently, it is being used as the ion source for obtaining initial beams in the K800 cyclotron.

EQUIPMENT LAYOUT

The power supplies and the control system for the K800 injection beam line and the SC-ECR ion source are located in equipment racks in the ECR complex. Although it has been necessary to increase the number of equipment racks by adding another single bay and a two bay unit to those described last year, they are still grouped in a relatively compact layout to minimize noise pick-up and grounding problems. See Fig. 1, ECR Area Main Floor Plan.

The racks in place last year are presently used as follows: The 5 bay unit's use has not changed - 2 bays are for equipment associated with the RT-ECR, 1 bay for K500 beam line equipment, 1 bay for CP-ECR equipment, and 1 bay for the Modicon 884 PLC system used for the ECR complex and the K500 ECR VME control system. In the 3 bay unit, one bay is reserved for the SC-ECR's power supplies, one bay is used for K800 beam line magnet supplies, and the last bay contains the VME crate for the K800 ECR equipment controls, the controllers for the K800 beam line steering magnets, and magnet supplies for the beamline magnets on the spur that ties the CP-ECR to the K800 injection line. The single bay unit still houses the power supplies for the first solenoid magnet in each injection beam line.

The new single bay rack contains the oven heater controls for the CP-ECR, turbo-pump controls and ion gauges for the CP-ECR, and the steering magnet power supplies for the K800 line. There is also room reserved for the future installation of oven heater controls for an oven planned for the RT-ECR. One bay of the new two bay unit houses the turbo-pump controls and ion gauges for all of the ECR equipment except the CP-ECR. The other bay is presently empty.

TECHNICAL ASPECTS

As noted above, the K800 system is an expansion and duplication of the K500 system whose technical design, construction, and operation aspects were described in the 1986 Annual Report.

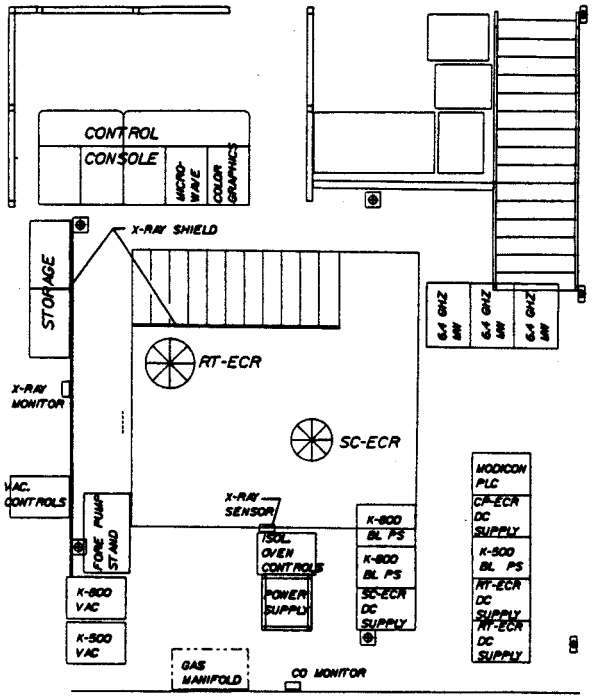

Fig. 1: ECR Area Main Floor Plan.

The only design change in the system components occurred in the beam current measuring devices (BCM's). These were referred to in last year's report as 'B-boards'. Experience with the K500 system showed that it would be advantageous to increase the sensitivity of the BCM's as they were located farther down the beam line from the ion source. Thus, the first 16 BCM's, located from the source to the divergence collimator (just before the first 90 degree magnet), are 'standard' units as described last year, with ranges of 0-10 and 0-1000 microamps for a 0-10 volt output. These are called BCM-A's. The next 27 BCM's (BCM-B's) are located from 4 jaw collimator No. 2 (just after the first 90 degree magnet) to Faraday cup No. 7 (just after the third 90 degree magnet). The BCM-B's have ranges of 0-10 and 0-100 microamps for a 0-10 volt output. The last 9 BCM's (BCM-C's) are located from 4 jaw collimator No. 7 to the cyclotron. The BCM-C's have ranges of 0-1 and 0-10 microamps for a 0-10 volt output.

OPERATING EXPERIENCE

The K800 ECR control system was installed in the December '87 - February '88 time frame in preparation for obtaining an accelerated beam in the K800 cyclotron. At the time of writing, the system has already been used for internal beam studies in the K800 cyclotron. It appears that there have been very few installation errors.

Experience with the K500 system over the past year has also been quite trouble-free. The main problem so far seems to be the heat generated by the magnet power supplies. Although the manufacturer claims they can be installed tightly spaced in the equipment racks, we found that, even with the doors removed from the back of the racks, the supplies (and, consequently, the other equipment in the racks) ran quite warm. In order to lower temperatures, re-arrangement of equipment in the racks with a view toward spreading the magnet supplies out, and installation of an area ventilation system is currently under consideration.

References

1. W. Nurnberger, et al., NSCL Annual Report, 120(1986).

MAGNETIC SHIELDING STUDIES FOR THE ECR-K800 BEAMLINE

A.F. Zeller and J.A. Nolen

Based on the ECR-K500 beamline, it was recognized that considerable magnetic shielding would be required to successfully transport the low energy heavy ions to the K800. The fringe field of the K800 at the position of the 90 degree dipole under the cyclotron is a factor of two larger than the 250 Gauss field under the K500. Therefore, a study of possible shielding configurations was done with the program POISSON. The basic geometry is a 20 x 20 in^2 cross section of a box along the beamline immersed in a uniform vertical field. A single layer of 1018 iron 1/2" thick in a 500 Gauss field admits 65 Gauss of internal field, consistent with levels measured with a Hall probe. Using a permeability curve for 1002 iron only reduced the internal level to 31 G. Since the most rigid ECR beams (capable of being injected into the cyclotron) are deflected by 5 degrees by passage thru 1 meter of even this reduced level, further shielding is needed.

Two obvious solutions consist of adding more shielding to the outside of the box or putting a smaller shield around the beamline. Adding a small shield around the beam tube is the most efficient solution; however, it is complicated by the necessity of having to go around leads, water manifolds, valves, etc. A thick iron beam tube also leaves gaps at the entrance and exit of each magnetic element. Placing added shielding around the outside raises the question of how to get the most shielding for a given amount of iron. Of interest is the choice of leaving a gap between iron layers, and how much of a gap is required.

Figure 1 shows the basic geometry of 1/4 of the 1/2" thick box with an additional 1/2" thick layer separated by a 1/2" air gap, immersed in a 500 G field. The internal field for this case is 7 G. But at higher fields the use of an air

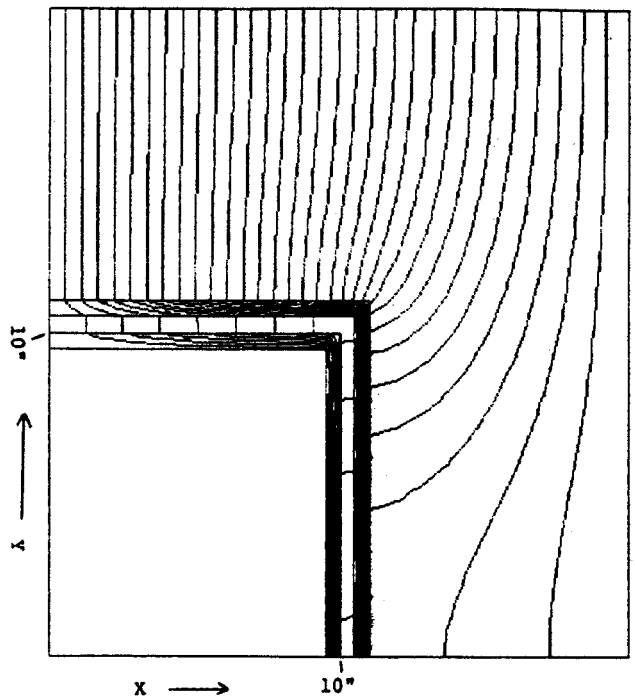

Fig. 1: One quarter of the ECR beamline shielding box in 500 G external field. The walls are 1/2" thick 1018 iron with a 1/2" gap between them.

gap is not so strongly indicated. Figure 2 shows the plates in contact at an external field of 1 kG, while Fig. 3 shows them separated by 3/4". The penetration of the flux is seen by the field lines in the interior of the boxes. From the position of the field line it is apparent that the air gap is less effective for higher magnetic fields than for lower fields. Figure 4 shows the internal field levels for three external fields as a function of air gap. Note that the 1 kG line is reduced by a factor of 8. The effect of the gap is more pronounced at the lower levels, while the high field does not show much reduction in internal field. At the 1 kG level going from no gap to a 1.5" gap reduces the internal field from 90 to 77 G. Note that for the 1 kG level the internal field starts to rise with very large gaps, the result

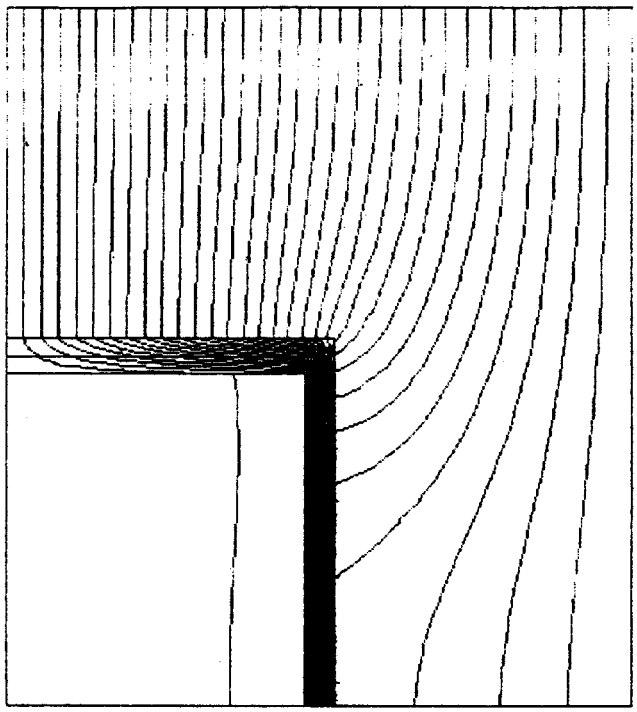

Fig. 2: No gap between the walls in a 1 kG field.

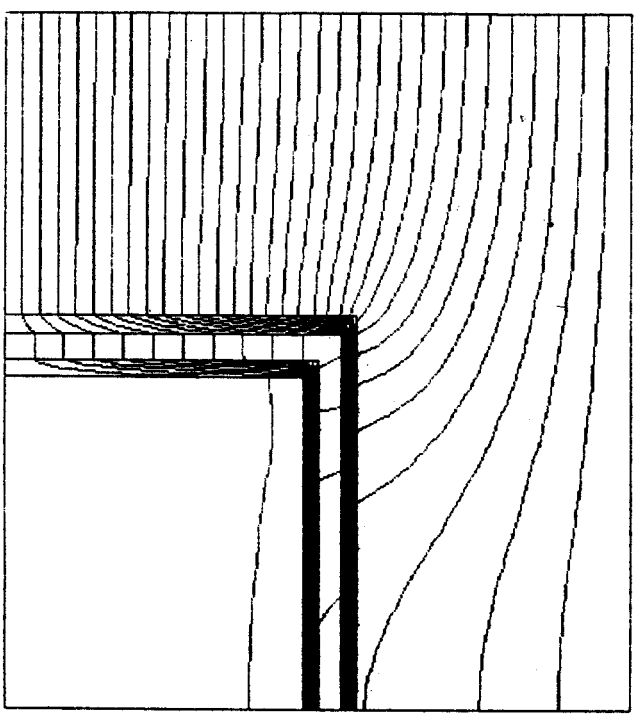

Fig. 3: A 3/4" gap between the walls in a 1 kG field.

of greatly increasing the area to be shielded. Figure 5 summarizes the effect of a 1/2" gap as a function of external field. Thus a gap is effective, vis-a-vis no gap, for external fields up to 600 - 700 G, for this geometry. For more compact geometries this level will increase.

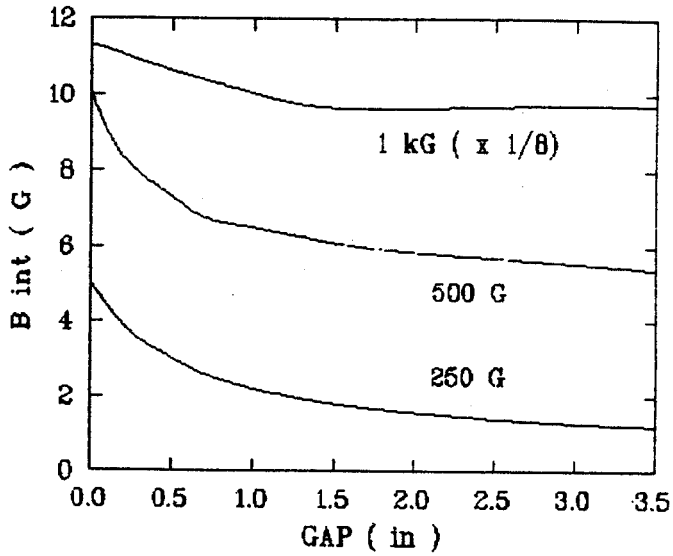

Fig. 4: The internal field as a function of gap for three levels. Note that the 1 kG data have been divided by 8 to get the same scale as the other levels.

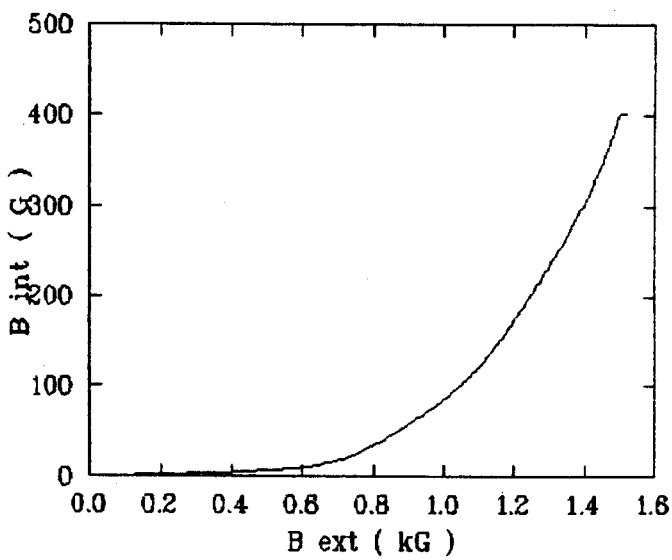

Fig. 5: The internal field as a function of external field for a 1/2" gap.

MEASUREMENT OF THE OBJECT AND IMAGE DISTANCE OF THE ECR 90 DEGREE MAGNET WITH A FLOATING WIRE METHOD

S. Tanaka, N.C. Bhattacharya, J.A. Nolen Jr, and E. Kashy

The 90 degree bending magnet[1,2] now used in the ECR beam line bears two special shims located at the entrance and at the exit to cancel the effect of the extended coil: this part of the coil distorts the magnetic field in the fringing field region and makes the edge rotation angle less than that of the iron yoke. Although the shim improves the magnetic field substantially, some irregularity still remains around the extended coil. Namely, equi-magnetic field lines are slightly curved. By field mapping we have attempted to set the edge rotation angles to the values predicted by RAYTRACE calculations. However, we felt it was important to independently verify the actual object and image distances of the magnet via the floating wire method.

The idea of the floating wire method[3-6] is that a path of a charged particle of a certain momentum is identical to a taught light and flexible wire carrying a DC current. Here the following relation holds,

$$T\ (\text{in gm}) = I\ (\text{in amp}) \times p\ (\text{in MeV/c}) / 2.94.$$

Where T, I and p denote the tension of the wire, the current carried by the wire, and the momentum of the charged particle, respectively.

Suppose the current I is 1 amp, the maximum rigidity of 30.5 MeV/c of the magnet needs a tension of 10.4 gm. The object and image distance is given by two intersection points between two trajectories.

For accurate measurements several precautions are necessary. First of all it is quite crucial to maintain a constant tension, current and magnetic field. Due to the momentum dispersion of 1.90 cm/% momentum at the image point, 0.01% change in momentum causes 0.19 mm transverse shift in the image position, namely 19 mm longitudinal shift of the intersection point between the central trajectory and a trajectory with a 10 mrad divergence. In order to get constant tension, we used a friction-free balance method as shown in Fig. 1, instead of a pulley. If the angle is chosen to be 45 degrees, the tension is equal to the weight. The change in tension is detectable from the position of the weight, which was observed via a telescope. Moreover, the current of the wire and the magnet excitation current were measured to an accuracy of 10^{-4}. Another important factor is the second order term of the beam transfer matrix. It has a term $\langle x|\theta^2\rangle$ of -1.98 $\times 10^{-4}$ cm/mrad^2 at the image point. Therefore a trajectory of 10 mrad gives a transverse shift of -0.198 mm from the central trajectory, and an image distance 19.8 mm shorter or longer than that obtained from a $\theta \approx 0$ mrad trajectory.

Keeping the above cautions in mind, we obtained a radial image distance of 92.5 cm for an object distance of 92.5 cm. A TRANSPORT calculation (the empirically determined fringing field parameters were used in the TRANSPORT code) with these values gives us an entrance and exit effective rotation angle of 29.3 degrees.

MSU-88-046

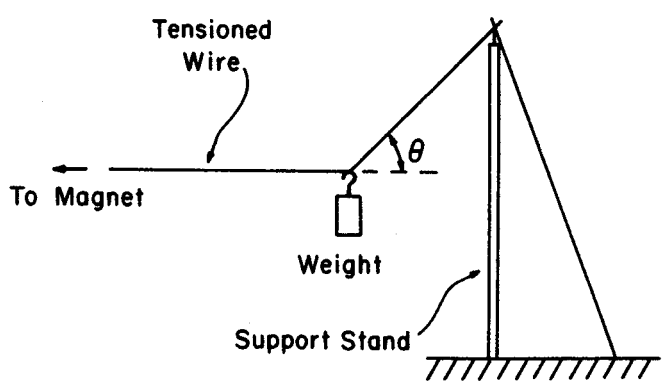

Fig. 1: The friction-free balance method to maintain constant tension on the wire. The angle θ should be kept at a constant value.

This value is slightly smaller than the desired value 29.8 degrees. The difference probably stems from a slight error in the shim placement. However, this disagreement is probably within the uncertainties of the two methods. Final adjustments of the shim positions should probably be done empirically with actual beams.

References

1. A.F. Zeller, J.A. Nolen, and R.T. Swanson, MSU Ann. Rep. 1983-84, 279.
2. A.F. Zeller, J.A. Nolen, and R.T. Swanson, MSU Ann. Rep. 1985, 167.
3. D.R. Bach, W.J. Childs, R.W. Hockney, P.V.C. Hough, and W.C. Parkinson, Rev. Sci. Instrum. 27 (1956) 516.
4. O. Chamberlain, Ann. Rev. Nucl. Sci. 10 (1960) 179.
5. P. Bounin and B. Milman, Rev. Sci. Instrum. 34 (1963) 1448.
6. A.P. Banford, "The Transport of Charged Particle Beams", E. & F.N. Spon Ltd. (London 1966), p.185.

DESIGN, FABRICATION AND TESTING OF A NESTED PAIR OF COSθ-DIPOLE X-Y STEERING MAGNETS

N.C. Bhattacharya, J.A. Nolen and S. Tanaka

The aim of the project was to design and construct a new type of air-core steering magnet for the ECR axial injection line of the K800 cyclotron. This magnet is mounted above the last bending magnet and directly below the K800 cyclotron and serves as a fine tuning device after the 90 degree magnet bends the beam upward into the K800 axial line.

Steel-core steering magnets[1] are in use in the ECR-K500 beamline and have been constructed for the ECR-K800 beamline. The purpose of this project was to design and construct air-core magnets having uniformity similar to the steel-core ones. The cosθ type design was chosen because two concentric coils could be wound to make an xy steering magnet with small components of higher-order multipoles.[2]

A "cosθ dipole" is a magnet in which the current or winding distribution varies as cosθ of the azimuthal angle. If the current distribution on a circular yoke goes precisely as cosθ, then the magnetic field at the median plane is a pure dipole over the full aperture of the magnet.

In a simple approximation to the "cosθ-dipole" with two separate blocks (separated by an angle) one can eliminate N = 3,5,7 (2N = number of multipolarity).[3] Figure 1 shows schematically the design of a 2-block dipole having outer radius, r_2, inner radius, r_1, constant current density, J, and the angles subtended by the blocks, ϕ_1, ϕ_2 and ϕ_3.

The ampere-turn requirements of the magnet

The magnet is required to produce a dipole field ~60G. The beam pipe has an O.D. of 8", hence r_1 and r_2 were chosen to be 4.0" and 4.25", respectively. Magnetic field computations were done using the POISSON code to find out the optimum design parameters.

MSU-88-035

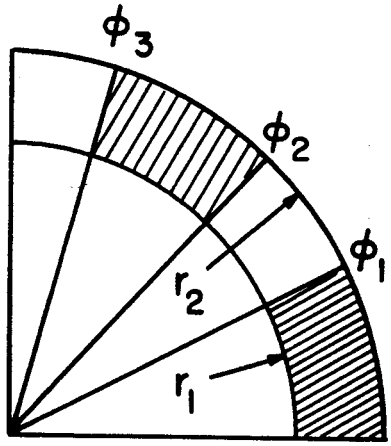

Fig. 1: Schematic diagram of a 2-block 'cosθ' dipole (4-fold symmetry, not to scale).

Because of space limitation and in order to have both x and y steering at the same place it was decided that both x and y magnets would be mounted co-axially, one around the other rotated by 90 degrees. For the outer coil r_1 and r_2 were chosen to be 4.25" and 4.50", respectively.

Various NI (NI = Ampere turn, N = No. of turns, I = Current) values were tried. With NI = 1000 for the inner coil and NI = 1200 for the outer coil, the magnetic fields at the median plane were found to be ~58 Gauss.

Tables I and II show the magnetic field distribution in the median plane up to 2" from the center of the dipole and the higher harmonic contribution for inner and outer coils, respectively. These are the results of POISSON calculations for infinitely-long coils. Also indicated are the calculated fields due to the dipole and first three allowed multipole components.

Fabrication of Coil

Physical dimensions of the dipoles are given in Table III. The coil winding fixtures were machined from co-axial cylindrical shells

Table I

X(in inches)	BTOTAL(Gauss)
0.0	57.124
0.256	57.123
0.512	57.122
0.768	57.120
1.025	57.117
1.281	57.112
1.537	57.104
1.793	57.092
2.050	57.072

N	Field at 2" radius
1	57.124
3	2.276×10^{-2}
5	1.408×10^{-2}
7	6.327×10^{-3}

Table II

X(in inches)	BTOTAL(Gauss)
0.0	58.479
0.255	58.479
0.510	58.479
0.765	58.480
1.020	58.481
1.275	58.481
1.530	58.482
1.785	58.482
2.040	58.480

N	Field at 2" radius
1	58.479
3	7.1644×10^{-3}
5	3.4202×10^{-3}
7	1.654×10^{-3}

of carbon steel. The coils were wound from 14AWG enamelled copper wire. The number of turns in the 43° and 15° blocks were decided in the ratio 43:15 so that the numbers of turns wound were 148 and 52 respectively. After winding, the coils were brushed with an epoxy mixture of 40% versamid 140 and 60% EPON 815, by weight. The epoxy was cured for four hours in a furnace at 200°C.

Magnetic field data

The magnetic fields in the steering magnets were measured with the NSCL X-Y mapper using a Hall probe with stability better than 1%.

The absolute magnetic field at the center of the magnet, near the effective edge, and the $\int B \cdot d\ell$ along the central trajectory and two trajectories 2" away from the central trajectory were measured.

The results are shown in figures 2 and 3 and tabulated in Table IV. So far as field uniformity at the magnet center was concerned it was found that in the case of the inner coil, the field uniformity was better than 1% up to a distance of 1.5" both ways from the center and better than 1.5% up to a distance of 2". In the case of the outer coil, the field uniformity was better than 1% up to a distance of 1" and better than 2% up to a distance of 1.5" from the center. With respect to field uniformity, the outer coil performance was slightly inferior compared to the inner coil, probably because of the higher ratio of diameter to length for the outer coil. However, the overall performance of

Table III

	Length	ϕ_1	ϕ_2	ϕ_3	r_1	r_2	NI	N	I	R
Inner coil	9"	43.2°	52.1°	67.3°	4.0"	4.25"	1000	200	5A	3.5Ω
Outer coil	6.5"	43.2°	52.1°	67.3°	4.25"	4.50"	1200	200	6A	3.8Ω

the outer coil, as measured by the variation of $\int B.dl$ over the 2" aperture at the center, was slightly better than the inner coil. The field integral is the most important parameter, hence the outer magnet is slightly better than the inner one. In this case the "end effect" better cancels the "3-D effect" on the internal field.

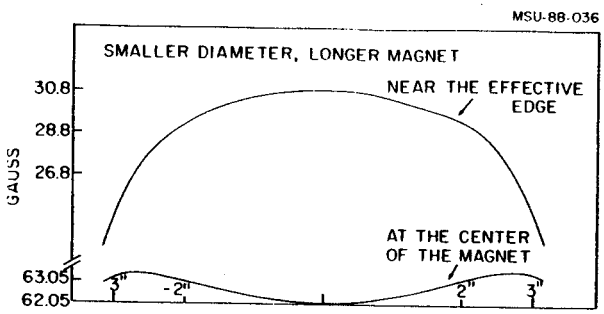

Fig. 2: Magnetic field distribution in the median plane.

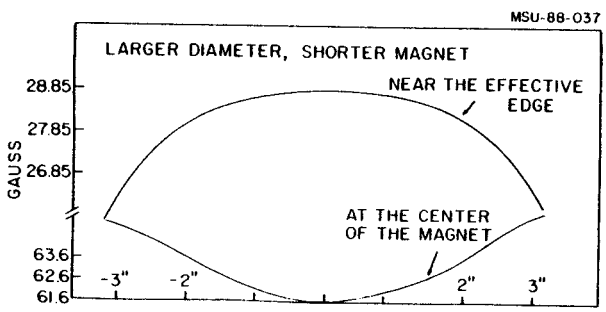

Fig. 3: Magnetic field distribution in the median plane.

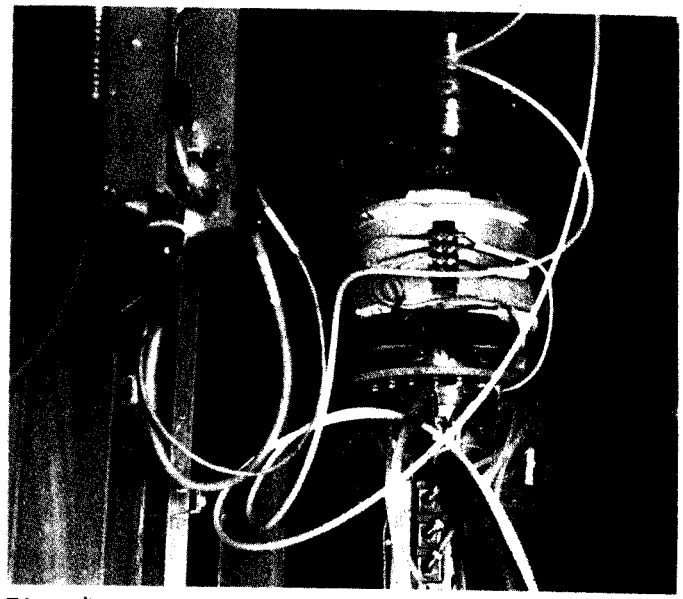

Fig. 4: The X-Y steering magnets installed in the K800 ECR beamline.

References

1. M.F. Williams, A.F. Zeller and J.A. Nolen Annual Report Cyclotron Lab (1985) p. 172.
2. AECL-9262 Progress Report of the Atomic Energy Canada limited, (1986) January-June 30, Section 3-20.
3. R. Perin Proceedings of the Workshop on CEBAF spectrometer magnet design April (1986) CEBAF Virginia Appendix.

Table IV

		axis	2" off axis		% variation	Central B(Gauss) @ 5 amps
Inner Coil	ΣBiLi (Gauss Inch)	2038.8	1998.7		1.97	61.6
	L effective (Inch)	9.96	9.61			
			right side	left side		@ 6 amps
Outer Coil	ΣBiLi (Gauss Inch)	1648.95	1644.9	1632.95	0.61	62.05
	L effective (Inch)	8.11	7.84	7.83		

CONSTRUCTION OF AN INTERIM VAULT FOR EXPERIMENTS WITH THE K800

B. Sherrill, N. Anantaraman, H. Blosser, R. Blue, S. Bricker, J.C. Dekamp, J. Easley, J.D. Johnson, H. Laumer, D. Lawton, F. Marti, L. Morris, J.A. Nolen, R.M. Ronningen, D.P. Sanderson, J.S. Winfield, and A.F. Zeller

In order to do nuclear science research with beams from the K800 cyclotron as soon as possible, while the Phase II experimental layout is being set up, an Interim Vault just outside the K800 cyclotron has been planned and is being constructed. Figure 1 shows a schematic layout for the vault. There will be two beamlines, one beamline for experiments, and one bending left from the switching magnet for beam emittance measurements. The experimental beamline will have two devices. The first is a large scattering chamber with a 92 inch diameter, labeled 92"SC in the figure. This chamber and its internal motions are described in a separate report by D. Sanderson. Directly in line with this chamber will be an additional vault to hold the 4π device, again described in a separate report by G. Westfall. Since the major experimental devices are described elsewhere, this report will present details of the vault layout, beam transport and data acquisition plans. The last section will be a short progress report.

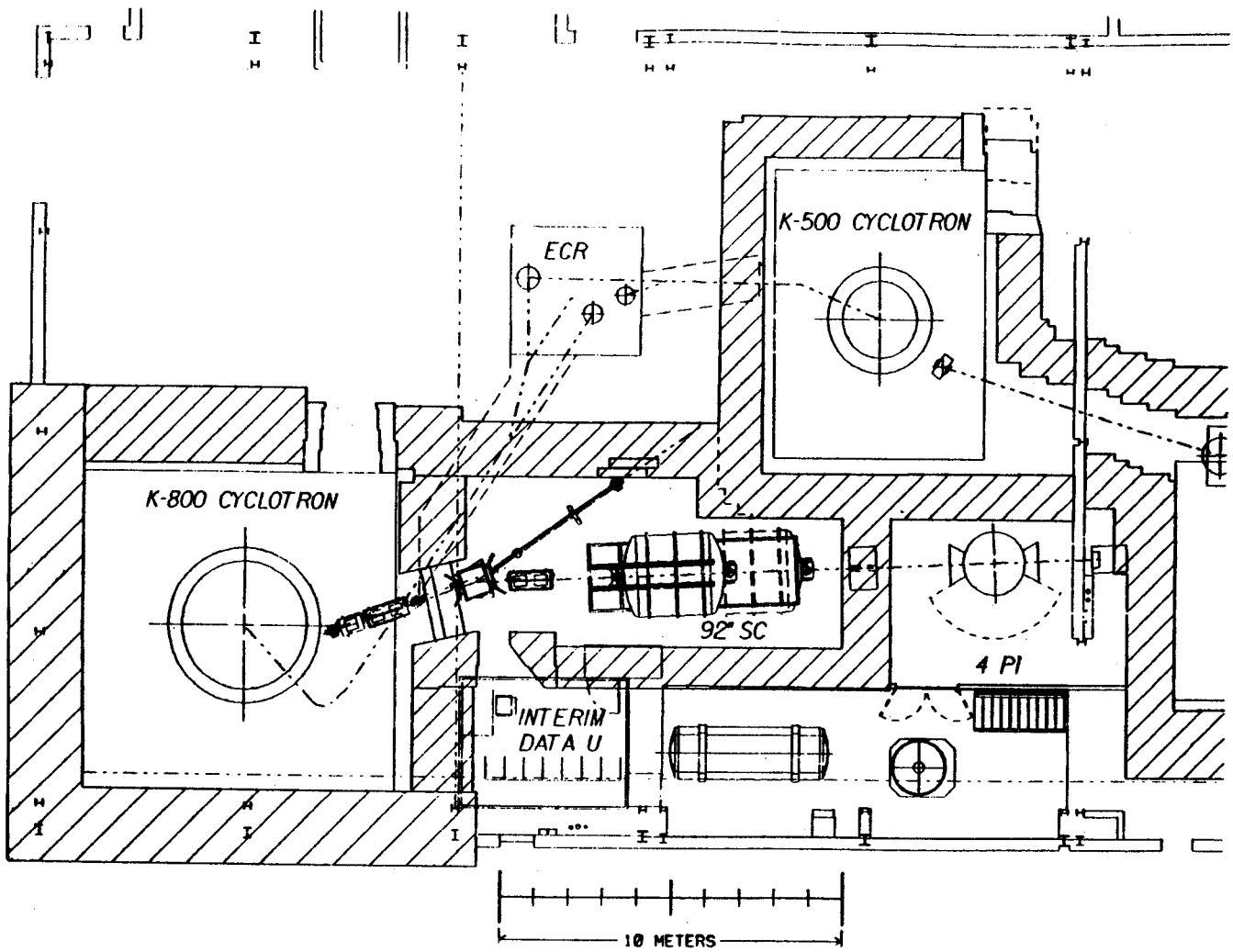

Fig. 1: Schematic layout of the Interim Phase Vaults.

Interim Vault Layout:

Beams from the K800 cyclotron are transported and focussed by a quadrupole triplet beginning 40 cm from the cyclotron return yoke. A beam diagnostics "box", a right circular cylinder holding pneumatically actuated slits, Faraday cups, beam monitors etc., follows the triplet and will be the object point for the following beam transport. An additional box is located between the cyclotron and the quadrupole triplet. In order to separate the K800 vault and the interim vault there will be a 12 inch steel wall with a 12 inch wall plug. The wall plug can be moved in and out of place to let the beam pass or to completely separate the two vaults. The steel wall is backed with a stacked concrete block wall of 24 inches thickness. Following this partition, the beam is switched by a standard NSCL ±16 degree superconducting dipole into either the beam line for emittance measurement, or the experimental beamline. Behind the bending magnet is a quadrupole doublet for focussing. The beam can be focussed anywhere from the front of the 92 inch chamber to the center of the 4π.

Space is provided next to the large chamber for two 7 foot high electronics racks. A third rack is located at the corner of the Interim and K500 Vaults and holds vacuum and chamber motion electronics. Access to the chamber is limited due to the small space available in this region of the building. However, if necessary, large objects can be brought into the vault by temporarily removing roof shielding. Potential difficulties may rise from stray magnetic fields from the K800 and K500 cyclotrons. At full field, the K800 produces approximately 5 gauss at the center of the 92" scattering chamber. At full field, the K500 produces a similar field of 5 Gauss. The gradients of the field are 1-2 Gauss per meter in the direction pointing toward the centers of the cyclotrons. Detectors which are sensitive to this level of field will have to be magnetically shielded either with iron or Helmholtz Coils. At the position of the 4π the K800 produces a field of less than 1 Gauss, but the K500 produces fields of approximately 10 Gauss. Therefore, it may not be possible to run the K500 while experiments using the 4π are being performed.

Behind the chamber is movable block shielding to protect detectors from back scattered neutrons from the beam dump, and an iron shielded beam dump. The shielding for the beam dump is in the form of a right circular cylinder. At 90 degrees to the position for stopping the beam is a 6 inch diameter hole in the beam dump, which can be rotated into position to allow the beam to pass into the 4π detector vault. After the chamber, the beam pipe will be enlarged to 6" i.d. and then to 8" i.d. near the Faraday cup. This is necessary to ensure that the beam does not strike the pipe, since there are no focussing elements in this section of beamline. An air conditioning unit will be placed in the vault in order to keep the temperature constant.

The 4π vault will have limited shielding, since the required beam current for typical experiments is very low (on the order of 10^8 pps). There are no ion optical elements in this section of beamline, and hence the beam shape is defined by collimation earlier in the beamline. As shown later, calculations show this should be straightforward, especially considering the low beam intensities required.

Beam Transport:

One concern for experiments using this area will be beam quality, since there is little space for beam analysis, unlike the situation for the Phase II facility (see the report on the A1200 beam analysis facility). Our hope is that the beam quality from the cyclotron will be good enough that it will not be necessary to have slits in the beamline. With proper tuning of the extraction system, this should be possible, as is true for the K500 cyclotron.

If, however, it is necessary to define the beam, there is a beam box just outside the cyclotron which can be used to define the beam divergence. A second box at the image of the quadrupole triplet can be used to define the object size for the experiment. A combination of small apertures in both locations will be used to attenuate and define a very parallel beam for 4π experiments. The slit thicknesses can be chosen to stop the beam or to degrade it sufficiently so that the 16 degree dipole will remove the energy degraded, scattered particles.

Sample beam envelopes are shown in Fig. 2 for the cases where the beam is focussed at the center of the 92 inch chamber and where it is focussed at the 4π target. The object of the system is assumed to be located at the position of the last extraction element of the cyclotron, and the emittance is taken to be 10π mm-mr. This is a conservative estimate; we expect a value closer to 10 mm-mr with proper extraction system tuning. In the first case, an image is required at the center of the second box. If this requirement is removed, then a beam tuning solution is possible which makes a unit transformation of the beam spot at the position of the last extraction element in the cyclotron to the scattering chamber target .

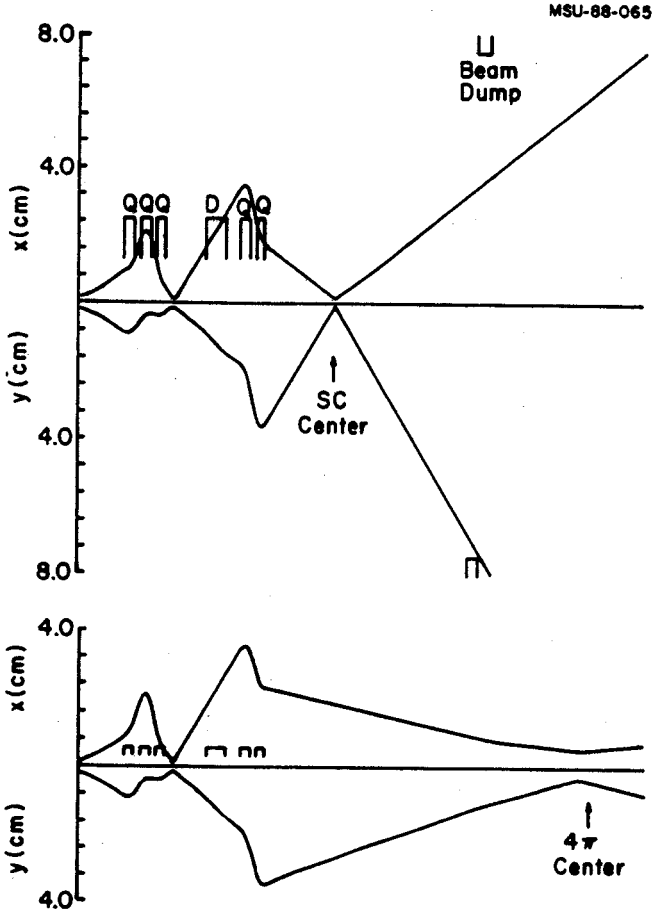

Figure 2: Beam envelopes for the case where the beam if focussed at the center of the 92 inch chamber (upper part), and where it is focussed at the center of the 4π detector. For beams sent to the 4π detector, collimators will be used to limit the beam spot size at the target.

Data Acquisition:

For experiments in the Interim Vault with K-800 cyclotron beams during Phase 1.5, a local Data Room, close to the Vault and at a height of about 15 feet above floor level, is being constructed. For most experiments with the 92-inch scattering chamber, the NIM/CAMAC electronics will be placed in this Data Room. For computer setup and online data monitoring a color display GPX Workstation will be provided. Thus the Data Room will be self-contained for setting up and debugging the electronics at the start of an experiment and also, if the experimenters choose to do so, for running the full experiment, except for the magnetic tape drive. A small amount of analog information, for monitoring purposes, can be sent to one of the existing data acquisition areas (Data-U's). The data-acquisition system will be based on CAMAC modules serviced by two 68020 microprocessors in a VME crate. Buffers of digitized physics data, scalers and run control information will be sent from the local Data Room via Ethernet cable to one of the Vax computers in the Computer Room, and from there to one of the existing tape units.

The size of the local Data Room will be about 16' x 12'. It will have 15-20 NIM bins distributed over 7 electronic racks. Two CAMAC crates, each capable of providing ±6 V, 85 Amp shared power, will be available. The GPX Workstation will have 8 color planes, a 19"

monitor, 9 Megabytes of physical memory and 0.5 Gigabyte of disc capacity. The existing AEDTASK program has been translated to run on the Workstation, so there should be no changes in the user software. There will be 250 signal cables and 25 high-voltage cables from the Interim Vault to the local Data Room. It remains to be seen whether the fringe magnetic field from the K-800 cyclotron will cause any problems for oscilloscopes, LED pulsers and the Workstation; if necessary, they can be covered by soft-iron shields.

Special attention has been paid to reducing noise pickup in the signal cables and to providing clean power to the local Data Room. Noise pickup is expected to be minimized for two reasons: (i) the length of cable from the Interim Vault to the local Data Room will be only about 50' (to be compared with the 250' length to one of the existing Data-U's); (ii) the signal cables will be of the "superscreened" type used at Daresbury Laboratory, U.K., with a noise pickup of about an order of magnitude less than for RG-58 at 10 kHZ and at least two orders of magnitude less for all frequencies above 100 kHZ. They are double-shielded by braid, with a mu metal foil sandwiched between the braids. The cables have a diameter of 6mm, compared with 5mm for a standard RG-58 cable. These cables were bought from Permanoid Ltd. of Manchester, U.K. (model MM 11/50). In a test under the actual operating conditions at the NSCL, a 250'-long cable of this type proved to be superior to both RG-58 and the double-screened RG-223. The (analog) signal cables will be run in an isolated tray different from the trays used for power cables and digital signals. Cable bulkheads will be made from a conducting material (brass) but mounted on insulating stand-offs; noise induced on one cable will thus be shared by all and therefore reduced. About 18 kW of clean power, obtained with a step-down isolation transformer, will be provided to the Data Room. The "clean ground" will be isolated from the computer ground and, of course, the ground for pumps, motors, etc.

Present Status:

At the present time (March 1988) construction of the Interim Vault is well underway. The schedule is such that it should be possible to perform the first experiments shortly after the beam is extracted. However, before final placement of magnets it is desirable to check the effect of the cyclotron fringe fields on the direction of the extracted beam. Thus, some extraction studies will be needed before the full interim facility can be ready. Therefore we expect that approximately one month after beam is extracted we will be ready to do experiments.

A brief description of the status of the various components follows. The west and north shielding walls are almost completed. The platform and room for the data area are also almost finished. The superconducting beamline magnets are finished and ready to be placed and their cryogenic lines connected. Various beamline vacuum parts have been ordered and most are already here. Development is in progress for beam diagnostic devices, but at first standard Al_2O_3 scintillators will be used. However, these will be viewed with CCD cameras, which will have better dynamic range and less sensitivity to the K800 fringe field, than our standard cameras. The beam pots have been ordered from Huntington, and will arrive shortly. Turbomolecular pumps have been ordered for the vacuum. All vacuum flanges will be standard CONFLAT type. All parts and steel for the beam dumps, wall plug, and steel shielding have been purchased and are in the process of assembly, placement, or machining. The radiation safety system, described in the report the R.M. Ronningen, has been designed and tested. The components are currently being fabricated and assembled. Finally, all electronics, cables, etc. for data acquisition are on order, or have already arrived.

SUPERCONDUCTING BEAMLINE QUADRUPOLES PROGRESS

J.C. DeKamp, C.T. Magsig, J.A. Mooney, J.A. Nolen, A.F. Zeller

Progress on beamline quads has centered on the completion of 2 quadrupole doublet assemblies and modifications to the original prototype quad singlet, all of which are needed for the first experimental vault (interim vault) setup for operation with the K800 cyclotron. The quad singlet is needed because of changes in the extraction channel design.[1]

Quadrupole Doublet Construction

Both doublets needed for the interim vault setup are completed. The two iron-coil assemblies in each doublet are held in alignment by 4 stainless steel tie bars fastened to the yoke on each flat as shown in Fig. 1 and 2. Each magnet has voltage taps for trouble shooting, and a carbon resistor to monitor cooldown temperatures. The He is fed to the container at the bottom in the back and leaves at the top in the front to provide for even and efficient cooldown. The total cold mass is 450 kg. Net operating LHe capacity is 50 l. A doublet iron-coil assembly is shown in Fig. 3. The LN_2 shielding also uses carbon resistors to verify shield temperatures. The stainless steel shield bore tube is copper plated to improve thermal performance. The plating is removed in narrow strips so eddy currents are not induced whose associated forces could cause the tube to collapse. Aluminum tape is used on the LN_2 and LHe surfaces which face each other to reduce radiation heat loads, which has proved successful on the prototypes.[2,3] MLI is used to insulate between ambient and LN_2 surfaces. Unlike the prototypes, no glass cloth spacer material is used between layers. This improves initial pumpdown times and is easier to cut and apply but the effects on heat transfer are yet to be determined. Although others use this technique with crinkled MLI, conclusive results

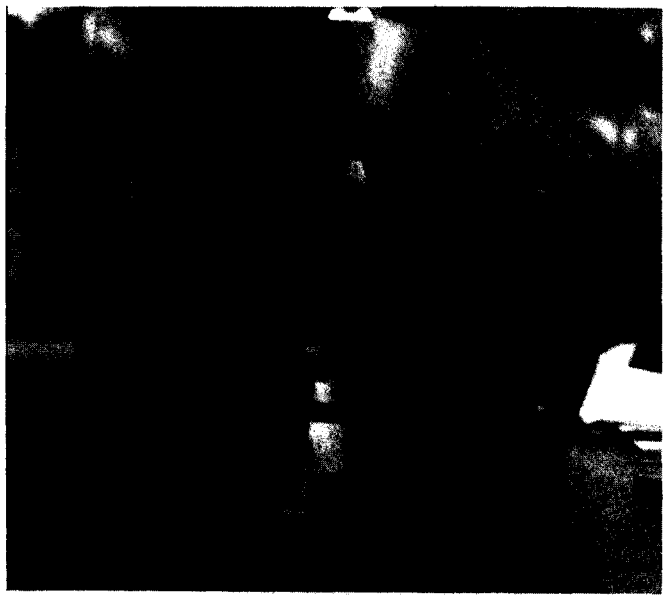

Fig. 1: Doublet yoke/pole tip assembly showing pole tip alignment.

of effects of the glass cloth spacer material have not been found. The net LN_2 operating capacity is 58 l. Conflat flanges are used on the cryostat to connect beamline sections to the warm bore. System controls include electro-mechanical valve actuation, LHe level sensing, and He system pressure monitoring. The completed quad doublet is shown in Fig. 4.

Prototype Quad Singlet Modifications

The prototype quad was found to have thermal accoustic oscillations present in He feedlines, contributing to a higher heat load. Further design of the K800 vault including this magnet made relocation of valves and feedlines necessary. The cryostat has been disassembled to make these modifications. As this magnet is in close proximity to the K800 cyclotron, a steel cryostat vacuum box will replace the original stainless steel box to shield the quad from the K800 fringe field. Completion of these modifications is expected before its required date of installation in the vault.

Fig. 2: Doublet yoke/pole tip assembly showing stainless steel tie bars holding magnets in alignment.

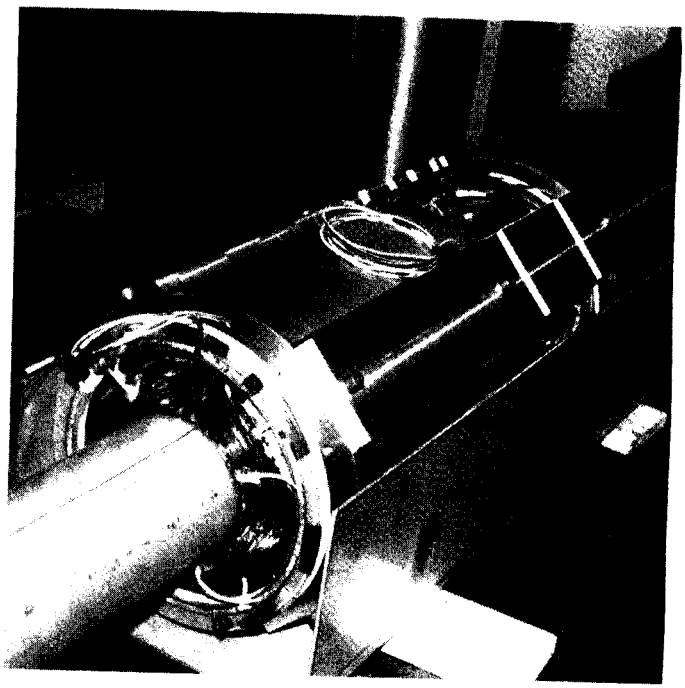

Fig. 3: Doublet iron-coil assembly sitting in its LHe container bottom with bore tube partially installed.

Phase 2 Doublet Construction Progress

The remaining coil wire was recieved and accepted. Coil winding has continued at intervals throughout the year as permitted by competing projects. A total of 40 superconducting quad coils were wound, with 16 already installed in the 2 completed doublets. Over 100 end forms for coils were cast from epoxy to support coil winding. All necessary conductor pieces needed for the magnet buss rings have been fabricated. Orders have been placed for 21 more doublet steel cryostat vacuum boxes to be received in Feb. 1988. GMAW (MIG) welding equipment was purchased for efficient cryostat box welding. Orders for the remaining parts for the 21 doublets will be placed soon, with all parts expected in-house by July 1988.

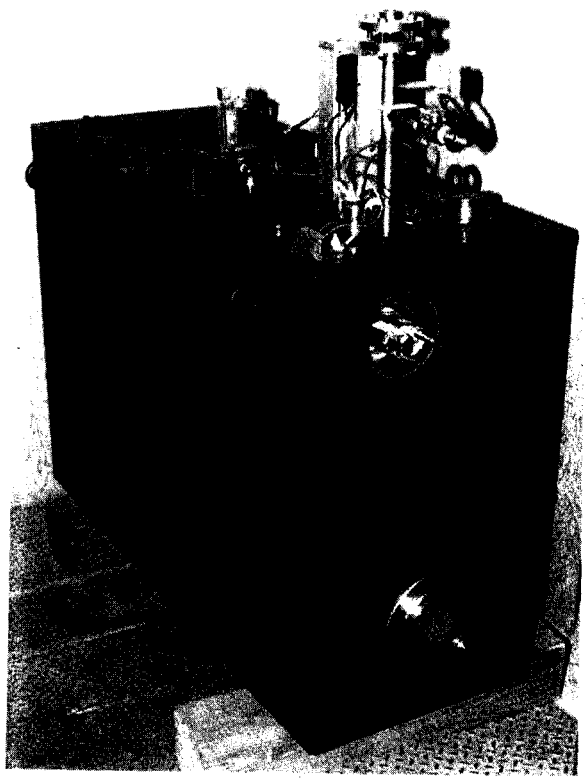

Fig. 4: Completed Doublet assembly.

References

1. A.F. Zeller et al, MSU Annual Report, 1987, pg. 165.
2. A.F. Zeller et al, Proc. Ninth Int. Conf. Magnet Technology, 160 (1985).
3. A.F. Zeller et al., MSU Annual Report, 1985, 176.

SUPERCONDUCTING BEAMLINE DIPOLES PROGRESS

J.C. DeKamp, C.M. Magsig, J.A. Nolen, A.F. Zeller

The beamline dipole project has expanded from the prototype to final design of the ±16° dipole and 22.5° 'X' magnet needed for Phase 2 operation.

Prototype ±16° S.C. Dipole Modifications

Results of initial testing[1,2] showed heat loads higher than expected and He system operation problems which needed correcting. The upper cryostat was separated from the rest of the magnet and disassembled. The LN_2 shielding was improved by better heat sinking to the LN_2 container. Shielding was improved in other areas where inspection showed it was necessary. New current leads were fabricated, installed, and vented to the LHe container through an added line. This was done to equalize the He pressure in the system so that boiloff gas produced in the LHe container could be used to help cool the leads. An added benefit will be a reduction in cooldown time as this line enables a higher mass flow through the bobbin. A reduction of 12 hrs. is expected. The LN_2 heat load will most likely be unchanged since it is thought the extra contributions are from poorly insulated areas in the bobbin cryostat which was not modified because of the expense involved. The upper cryostat is now fully reassembled and partially reconnected to the rest of the magnet. Completion is expected in January, 1988. It will then be installed in the K800 interim experimental vault.[3]

±16° and 22.5° 'X' Magnet Final Design

The prototype magnet design was changed to provide more room in the bobbin cryostat area for heat shielding and insulation. This resulted in a small increase in outer yoke dimensions and a slight change in pole tip design. The 'X' magnet design is similar to the ±16° magnet, having the same cross section as the large end of the ±16° magnet throughout it's length. At 115 cm long, it is about 34 cm longer than the ±16° magnet. The 'X' magnet also runs at a slightly lower current density. The bobbin support system has been redesigned from 3 links at each corner (1 horizontal and 2 vertical) to 2 links at 45 degrees. This reduces the number of parts, saves assembly time, eliminates fragile components in the vertical links, improves shielding through fewer penetrations, and lowers space requirements for the magnet assembly. A cryostat corner section is shown in Fig. 1. Both magnets share the same basic designs, adjusted only when necessary for different geometries. We have received bids from vendors on the magnet steel and an order has been placed. Orders for the remaining parts are expected to be placed by June, 1988.

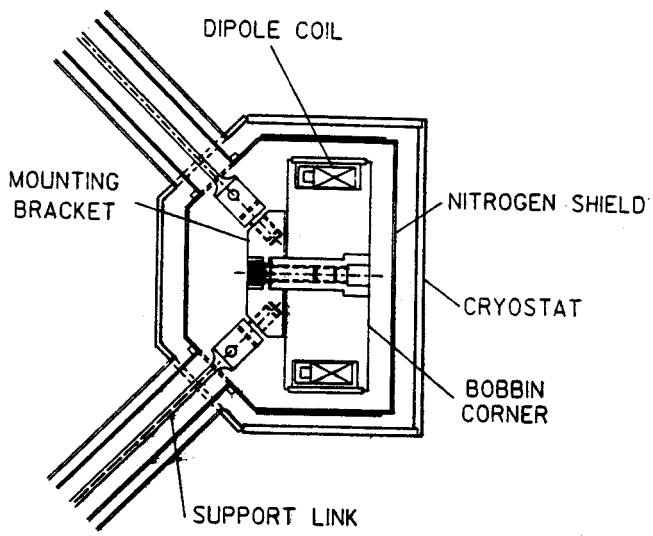

Fig. 1: Bobbin cryostat corner section showing support link geometry.

References

1. J.C. DeKamp et al., MSU Annual Report, 1986, 186.
2. J.C. DeKamp et al., IEEE Trans. on Mag. Mag-23, No. 2, 524 (1987).
3. B. Sherrill et al., MSU Annual Report, 1987, pg. 183.

A BEAM ANALYSIS DEVICE FOR PHASE II BEAMS AND THE PHASE II BEAMLINES

B. Sherrill, E. Kashy, D. Lawton, and J.A. Nolen

Plans have been made for the layout of the Phase II experimental facility. Included in these plans is a beam analysis device called the A1200. The primary function of the device will be to analyze the beams from the K800 cyclotron, i.e. define the beam energy, beam energy spread, and emittance as required by the various experiments. It can also be used to dispersion match the cyclotron beam to the beam lines for the rest of the experimental areas. In addition, with an absorbing wedge at one of the intermediate images, it can be used as a secondary fragment separator to provide beams of radioactive particles for calibrations and experiments. This technique has been successfully used at GANIL[1,2] to separate and study radioactive nuclei, and will be used in the GSI SIS-18 fragment separator[3,4]

A schematic layout of the planned Phase II facility is shown in Fig. 1. The initial plan is to have four experimental areas. Area N1 will hold the S320 and a general purpose line. In area N2 will be the 4π device. Vault N3 will be dedicated to the large 92" scattering chamber, and S1 will hold the RPMS and a general purpose line. These areas can be fed by either the K500 or the K800 cyclotrons. This is accomplished by the use of two kinds of dipoles in the transfer hall, the normal ±16 degree bending magnets[5], and a newly designed X-magnet which will allow crossing beams, or can be used to bend 22.5 degrees.

Focussing of the beams is done in a special way which uses ion-optical cells consisting of two doublets. Each cell has waist-to-waist and point-to-point imaging with a unit matrix

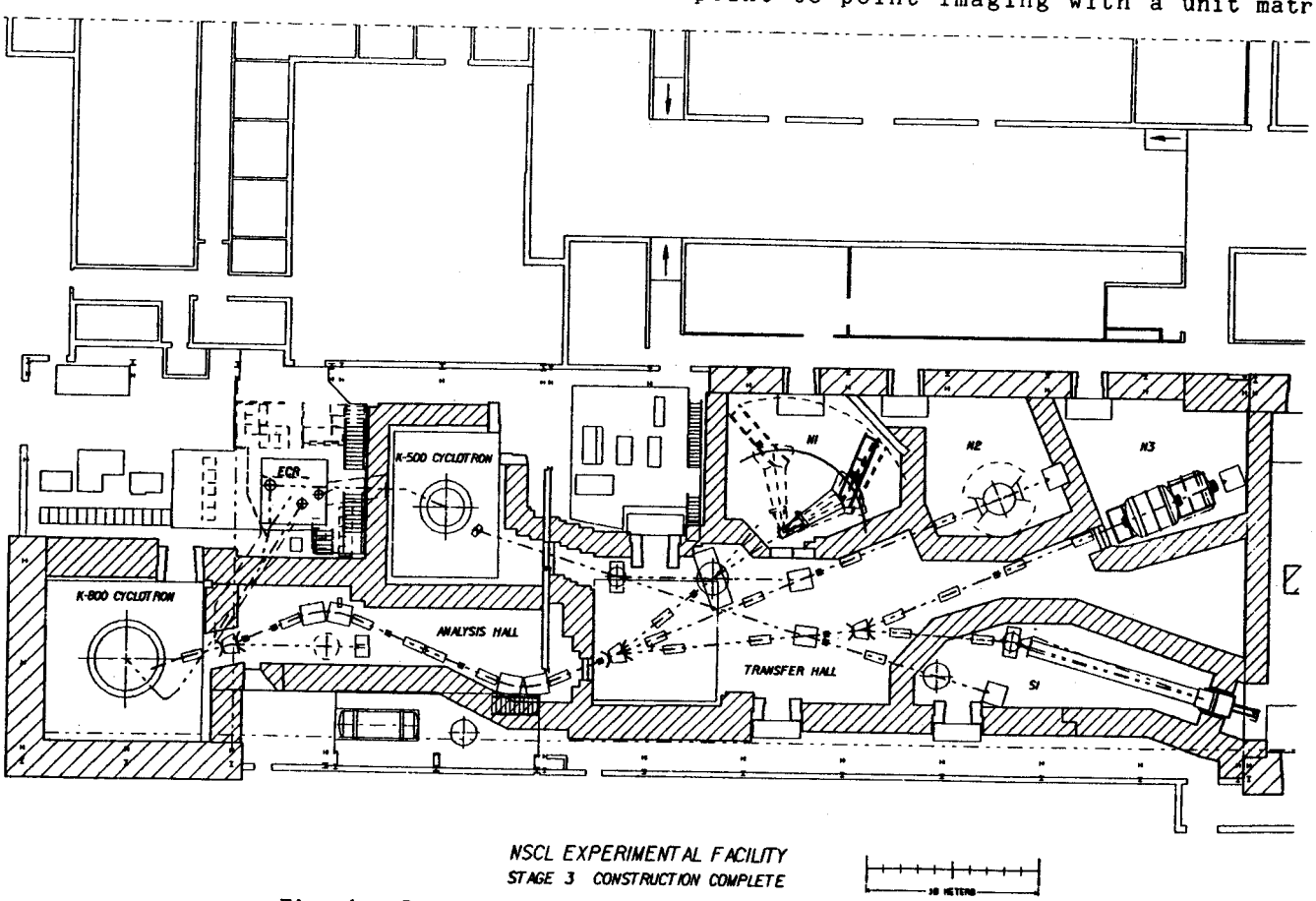

Fig. 1: Proposed layout for the NSCL Phase II facility.

transformation. By placing the images of the cells just beyond the exits of the bending magnets, the edge focussing effects of the non-normal magnet edges are small and the dipoles do not perturb the unit cell transformation. The image of the A1200 is just before the ±16 degree magnet in the center of the transfer hall. Using unit cell optics, this point can be imaged at the various target positions of the experimental areas. This type of optics also has the advantages of large phase space acceptance, and low quadrupole fields.

The beam properties will be defined in the section of beam line between the K800 and the transfer hall by the A1200. This device is shown in the analysis hall in Fig. 1. The parameters for the A1200 are listed in Table 1, and the beam envelopes are shown in Fig. 2. The beam envelopes shown in Fig. 2 are for one of the two possible optical modes of the device, and assume a 2% momentum spread with ±10mr horizontal and ±20 mr vertical divergences from the target. In this case the system is achromatic, as shown by the dashed line which represents the dispersion for a particle with +1.5% momentum from the central ray. For the dispersion line, the axis of the figure represents plus and minus x direction.

It is also possible to run the A1200 in a chromatic mode with one horizontal cross over in the center of the device. This mode can be used to energy analyze K800 beams or fragmentation products, produced at the object of the device, for detector calibrations. In general the achromatic mode will have the largest acceptance, and hence would be used for collection of secondary fragments. Experiments at GANIL on the production of secondary beams using LISE (which has acceptances similar to the A1200) have shown that secondary intensities of 1×10^{-6} of the initial beam intensity can be expected for ions near stability[6]. Hence, for example, with a ^{22}Ne beam of 100 MeV/A and

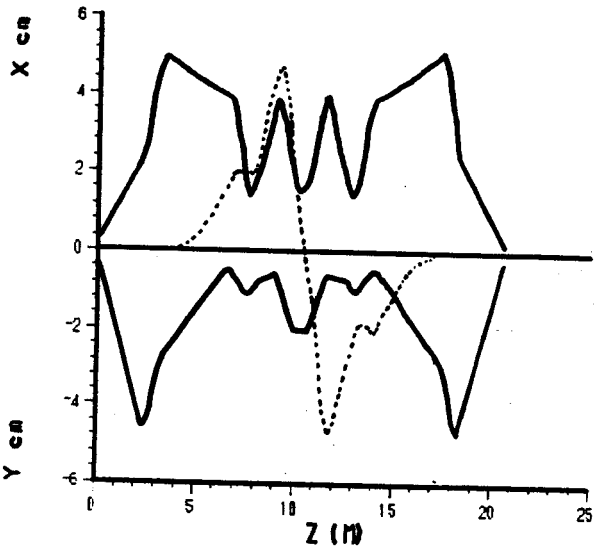

Fig. 2: Beam envelopes for the achromatic mode of the A1200. The envelopes are shown for a momentum acceptance of ±1% and horizontal and vertical emittances of 40π mm-mr. The dashed line represents the dispersion for a particle with +1.5% momentum from the central ray.

several hundred nanoamps, we would expect ^{16}C intensities of greater than 10^6 pps.

The resolution of the device has been checked with a third order version of TRANSPORT and with the program TURTLE[7]. The chromatic aberration ($x/\theta\delta$) is large at the intermediate images and at the end of the device. However, the symmetry of the device reduces the geometric abberations. The first order image is enlarged about a factor of two due to the chromatic effects. Interestingly, the term ($x/\theta\delta$) can be made zero without significantly affecting the resolution by the addition of one sextupole following the second dipole, and a second sextupole in the symmetric position before the third dipole. In all calculations the second half of the system is constrained to be the mirror image of the first half. With this constraint and fitting to make ($x/\theta\delta$) zero at the itermediate image, the chromatic aberration at the end of the device is also corrected, with the sign of the second sextupole opposite to that of the first. This can be understood in

Table 1: Parameters for the A1200 beam analysis device.

Acceptance:		Ω = 0.8 msr
		$\Delta\theta$ = ±10 mr
		$\Delta\phi$ = ±20 mr
Momentum Acceptance:		$\Delta p/p$ = ±1 %
Magnification:	intermediate	0.5
	system end	0.97
Momentum Dispersion:		
(X/δ), cm/%		
Achromatic -	intermediate	1.71
	system end	0.00
Chromatic -	system end	3.42
Momentum		
Resolution:	achromatic	3000/mm
	chromatic	6000/mm
Maximum Rigidity:		5.3 T-m

terms of the multipole coupling coefficients of Brown[8]. The first order term (x/θ) is identical at both locations due to the system symmetry, but the dispersion term has changed sign, hence the change in sign of the sextupole. With the use of the sextupoles, more than 95% of the initial first order resolution can be achieved.

For experiments with secondary beams, a movable Faraday cup will be installed between the first two dipoles. To cover extreme cases where the beam rigidity is very different from the fragments of interest, stationary Faraday cups will be installed inside the first dipole. They will be electrically isolated in order to read beam current and will stop all beams. Hence except for beams with rigidities within 7% of the fragments, the primary beam can be separated from the secondary products.

In general the beam analysis and transport system will be very flexible, and allow for a wide range of applications. Particularly interesting is the possibility for performing experiments with radioactive beams, or high resolution experiments with analyzed K800 beams.

References

1. R. Anne et al., NIM A257 (1987) 215.
2. J.P. Dufour et al., NIM A248 (1986) 267.
3. H. Geissel et al., Projectle-Fragment Separator, A Proposal for the SIS-ESR Experimental Program, private communication.
4. H. Geissel et al, 8th Heavy Ion Study Conference, Nov. 1987, Berkeley, CA.
5. J.C. Dekamp et al., IEEE Trans. on Magnetic Technology, MAG-23 (1987) 524.
6. R. Bimbot et al., Z. Phys. A322 (1985) 443.
7. D. Carey, TURTLE, Fermilab Report 64-02041.000, 1971.
8. K.L. Brown et al., SLAC-75, Stanford 1982.

RADIATION MONITORING SYSTEM FOR PHASE II

R.M. Ronningen, J. Bailey, R.A. Blue, B.L. Jiang, T.R. Jones, E. Kashy, Y. Lan, M. Maier and J. Yurkon

We are developing a radiation monitoring system for Phase II operations. It consists of components designed and built in-house including two kinds of neutron detectors, preamplifiers and power supplies, radiation level logic boards, and a programmable logic controller (PLC) with personal computer (PC) interface. Logic signals from the logic boards indicate count rate levels for each detector and are input to the programmable logic controller, as are vault interlocks related to personnel access, and beam injection and transport. Three detectors and the K800 vault interlocks are currently in operation for evaluation and K800 start-up, using two logic boards, the PLC+PC and software.

Two kinds detectors are employed, a BF_3 counter for lower energy neutrons and a plastic scintillator for higher energy neutrons. The BF_3 tubes, with 45 cm fill pressure, 1" diameter and 4" active length, are placed in 5 gallon plastic pails of paraffin which are wrapped with cadmium. The scintillators are 5" X 5" cylinders of NE110 plastic.[1] Five of both detector types have been assembled. Both types use the same charge sensitive preamplifier design but with different gains. Attached to each preamp box is a box containing a detector/preamp power circuit. A single coaxial cable connects each detector to its logic circuit, carrying 24V DC from a power supply in the control rack to power the preamplifier and the DC-to-DC converter for the detector high voltage. The 3-4 volt unipolar preamp output pulses are sent along the same cable back to the logic board where they are picked off. Figure 1 shows a photograph of a BF_3 tube, preamp and power supply.

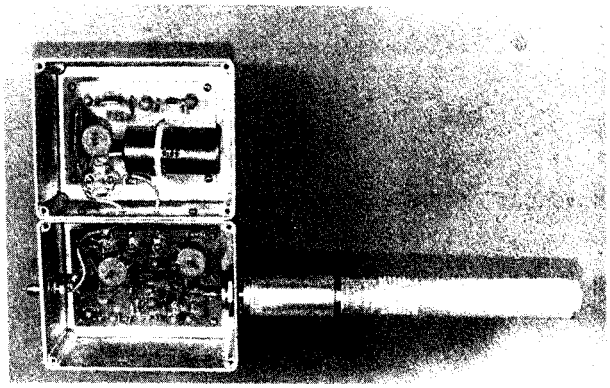

Fig. 1: A BF_3 neutron detector with preamp and local power supply. The 50 Ω signal cable carries 24V DC to supply the preamp and to be converted to the approximately 1800V DC detector bias. The same preamp power supply is used with plastic scintillator detectors, with slight modification.

Each logic board, one is shown in Fig. 2, has two logic circuits. The board is VME compatible in size; an inexpensive VME "test crate" holds 20 cards. The back plane is a panel holding 16 pin "half C" connectors. The 24V DC and 5V DC, for logic board power, are bussed along the back plane and wire pairs bring information to the PLC or to the control room. The circuit counts the pulses and compares the number to dip-switch adjustable rate limits. Two limits are used, giving three "states" indicated visually by green, yellow and red LEDs. The status of both limits is communicated to the PLC by the opened/closed states of board mounted mini-relays. A current sensing circuit detects when the preamp is not using power (e.g. when the detector cable is removed) and uses a separate LED and mini-relay. There is also a count rate monitor output. We plan to construct 15 boards for use over the next several years.

The K800 vault has a security system of arming buttons, chain + microswitch barriers, and a door-open/closed microswitch. This system is like the one used for the K500 and will also be used in the experimental vaults. Wall plug

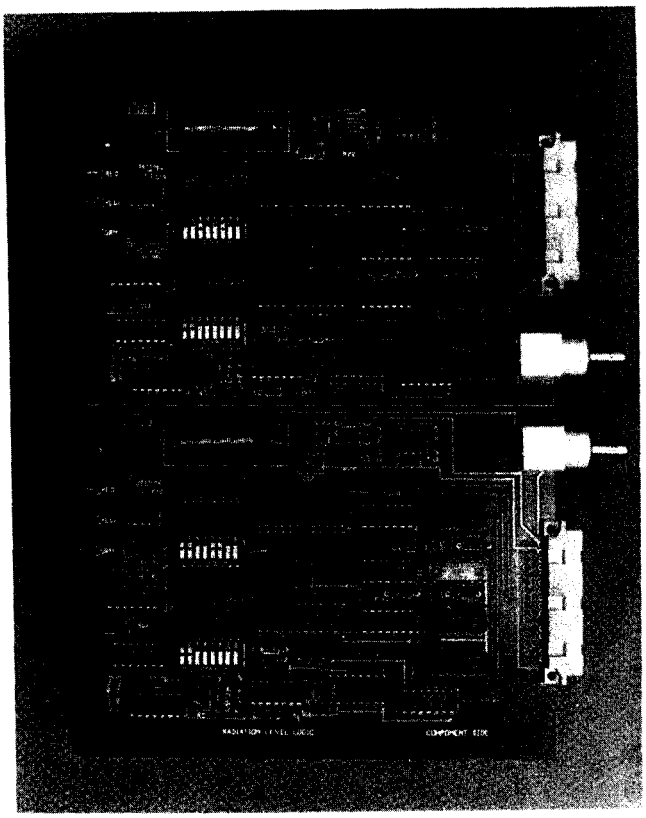

Fig. 2: A radiation monitor logic board. There are two independent circuits. The size is VME crate compatible.

("neutron shutter") positions, when the plugs are installed, will be sensed by microswitches.

The programmable logic controller is made by the Square-D Company. It has a 2K RAM CPU and is is dedicated solely to the radiation safety task. It is interfaced to the user by an IBM PC-XT personal computer, running SY/MAX (Square-D) and "ScreenWare" (Computer Technology Corp.) software. Ladder logic rungs, register assignments and labels are the bases of the radiation interlock logic. The logic rungs collate the status of the vault security hardware, the radiation level logic states, and other input information such as ECR Faraday cup position and RF bypass status. Satisfied logic rungs can close internal output relays, e.g. a "RF enable" logic signal to the RF PLC.

Using the PC software one may program ladder logic on- or off-line. Animation screens, associated logic and alarm messages can be developed. Figure 3 shows a "live" animation screen for K800 vault security. Logic status changes can be depicted by changing colors, symbols and messages.

In regards to PLC I/O we are presently using five input and three output registers, each having 8 bits, at one station. This number is sufficient for 5 detectors and the K800 vault logic. We are adding a remote station for vault logic from the experimental vaults and the K500 vault. In addition, we are investigating the use of 32 bit registers in the local station so that thirty neutron detectors can be accommodated there.

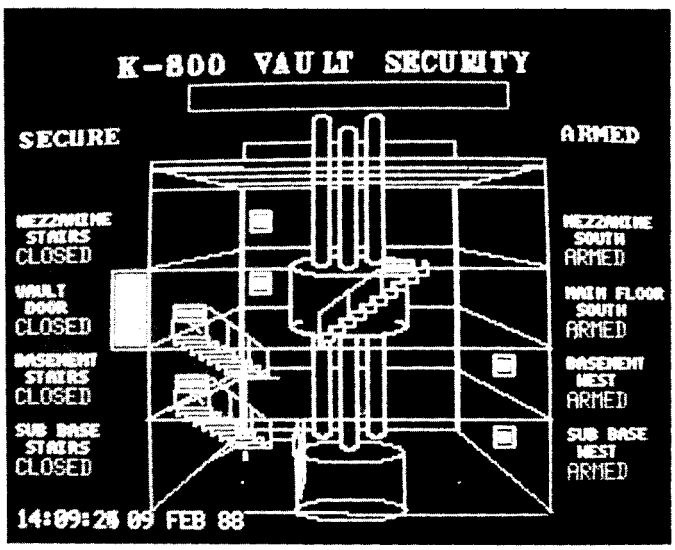

Fig. 3: An animation screen for the radiation monitoring system. This gives the "live" status of the K800 vault security.

References

1. E. Kashy, B. Remington, and J. Yurkon, NSCL Annual Report 1982-83, p. 101.

THICK TARGET NEUTRON YIELDS FROM 250 MEV PROTONS

C.E. Scripter and R.M. Ronningen

There appears to be a renewed interest in intermediate energy proton accelerators, stimulated in part by superconducting magnet technology. Shielding to reduce the high energy neutron flux from such accelerators to acceptable levels will be an important consideration in designing new facilities. We have calculated the thick target neutron yield for 250 MeV protons incident on a water target and also calculated expected dose rates outside of some given shielding.

Monte Carlo calculations of intranuclear cascade and evaporation neutron spectra have been analytically fit by Alsmiller, Leimdorfer and Barish[1] for proton-nucleus collisions at selected energies from 25 to 400 MeV. By interpolation techniques we used these fits to generate a surface in neutron energy and proton energy space for protons incident on oxygen. Using ranges[2] of protons in water we then performed an integration over proton energies from 25 to 250 MeV to calculate a thick target yield. This is shown in Fig. 1.

Shielding calculations were done using a Moyer model approach.[3] Figure 2 shows the neutron flux per unit energy as a function of neutron energy for the above reaction at a distance of 18 ft with shielding consisting of 6 ft of concrete and 1 ft of steel. A beam intensity of one nanoampere was assumed. The integrated dose rate was then calculated by folding the energy dependent flux-to-dose rate conversion with this result, as done in Ref. 3, and integrating the resulting curve.

References

1. R.G. Alsmiller, Jr., M. Leimdorfer, and J. Barish, Oak Ridge National Laboratory Report ORNL-4046 (April, 1967).
2. Joseph F. Janni, At. and Nucl. Data Tables 27, 147(1982).
3. J. Naryanaswami, J. Duffy, Z. Koenig, R. Ronningen and E. Kashy, NSCL Annual Report 1980-1981, p. 117.

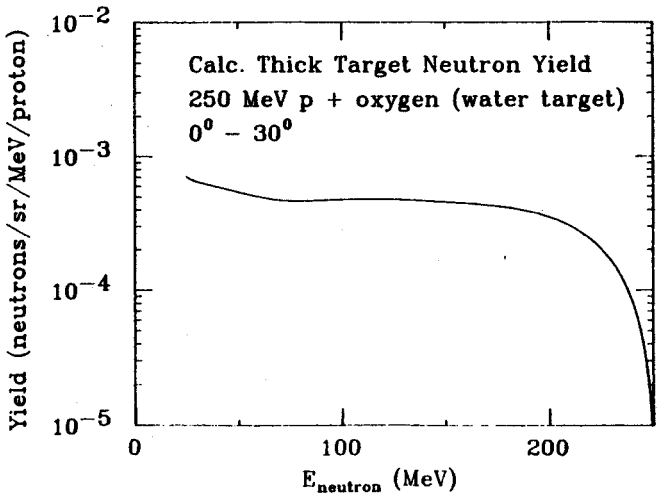

Fig. 1: Neutron yield from 250 MeV protons stopping in water. The cross sections for protons on oxygen were assumed. The angular range is 0-30 degrees.

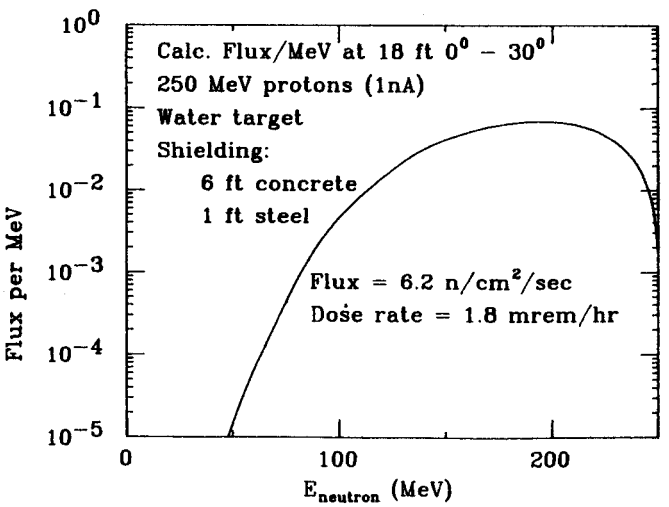

Fig. 2: Neutron flux per unit energy at 18 ft, after transverse shielding with 1 ft of steel and 6 ft of concrete, for the p + oxygen reaction at 250 MeV. The stopping medium was water and a 1 nA beam intensity was assumed. The integrated dose rate from the neutron flux is given.

COIL STRESS ANALYSIS

J.C. DeKamp and A.F. Zeller

A 2D finite element fortran code has been developed for general in-plane stress/strain analysis. The program follows the same format as most modern programs of this type[1], utilizing 8 node isoparametric parabolic elements and Gauss quadrature 3-point integration. The program handles plane stress, plane strain, and axisymmetric problems. Anisotropic as well as isotropic materials can be modeled, with concentrated, uniformly distributed, gravity or load/unit volume, and temperature element loadings available. Some programs are also available for generating element-node locations and node coordinates for input files for combinations of simple geometries. The program has been initially used to handle potted coil analysis. Some problems, results, and outputs from the superconducting ECR coil analysis[2] will be discussed to demonstrate the program's usefulness.

Two different current densities and several different boundary conditions were investigated for the ECR coil design. The basic structure section analyzed is shown in Fig. 1. Coil forces were calculated with the POISSON codes. The low current density design was settled upon after analysis showed that high shear stresses relative to epoxy-wire bond strength were present in the high current density design. A comparison of different boundary conditions was then investigated for the low current density design. Maximum principal stress contour maps for two boundary cases investigated: 1) fully potted in place and 2) potted to the adjacent coil and the coil form only, are shown in Figs. 2 and 3, respectively. This shows the advantage of the latter restraint condition, reducing tensile stresses in the coil over its entire volume to the point where tensile stress exists only in one corner of the coil. The maximum

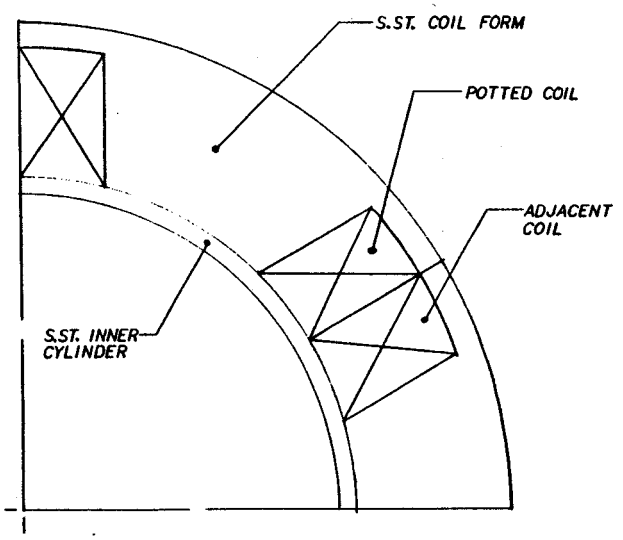

Fig. 1: 1/4 of cross section of ECR Hexapole assembly used for analysis.

tensile stress is reduced from over 700 psi to just over 200 psi, a much safer value to use relative to wire-epoxy bonds. An interesting case analyzed included a coil, fully potted in place and banded under tension around the outside. This is the system used on the K500 and K800 to apply an initial compression to the coil which offsets the tension when the coil is energized, but is used here on a potted instead of an open-latticed coil. The initial analysis was for the coil form in contact with the inner cylinder. Results showed little compressive preload was added to the coil because of the larger stiffness of the coil form, which carried 95% of the added radial compression. Another analysis was then done leaving a gap between the coil form and the inner cylinder. This created a large stress concentration in the corner of the coil where the coil form approaches the inner cylinder. A high, localized compressive stress was present in the radial direction with an associated high tensile stress present in the circumferential direction. This showed that for banding to be effective, a buffer material would

be needed between the coil form and the inner cylinder.

References

1. Klaus-Jurgen Bathe, Finite Element Procedures in Engr. Analysis, Prentice-Hall, Inc., Englewood Cliffs, N.J., 1982.
2. T.A. Antaya et al, MSU Annual Report 1986, 176.

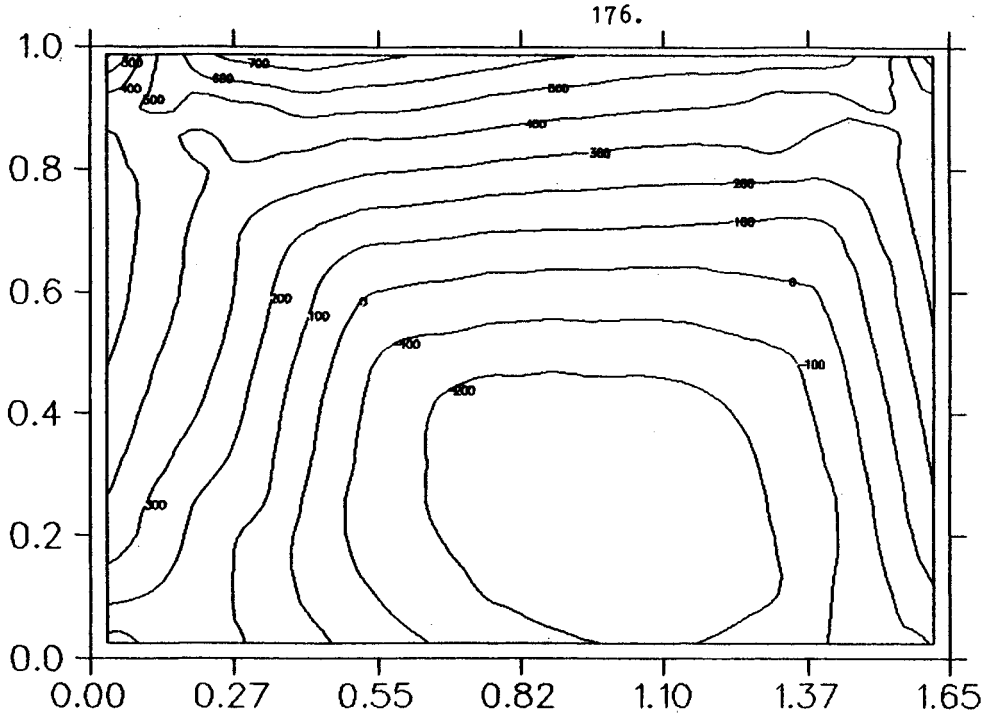

Fig. 2: Maximum principal stress map of coil cross section for fully potted in place coil. Contour units are lb/in^2 and coil dimensions in inches.

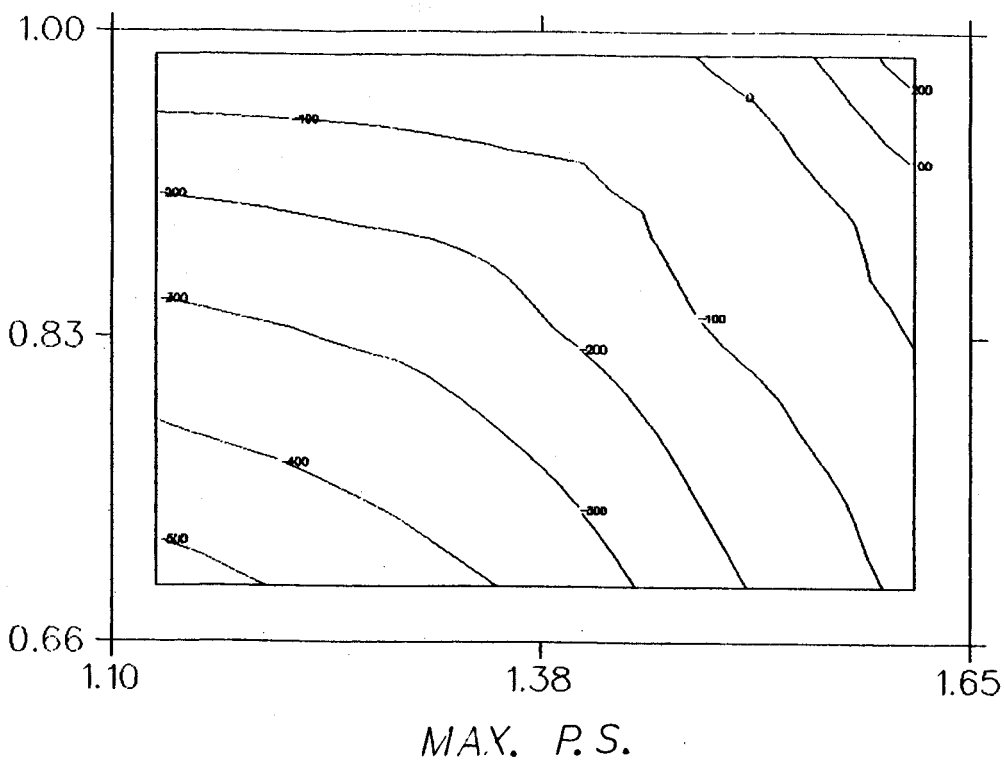

Fig. 3: Maximum principal stress map of the coil cross section for a coil potted to the coil form and restained in the incumferential direction by the adjacent coil. Note that this is an enlarged section of the coil shown in Fig. 2. Contour units are lb/in^2.

EFFECTS OF INSULATION ON POTTED SUPERCONDUCTING COILS

A.F. Zeller, J.C. DeKamp, C.T. Magsig, J.A. Nolen, and A.D. McInturff[a]

While considerable attention has been paid to epoxy formulations used for superconducting coils, little study has been devoted to the effects of the wire insulation on training behavior. If the insulation does not bind well with the epoxy, the wires will not be held securely in place, and training will be required to make the coil operate at its design limit. In fact, the coil may never reach its design current, showing considerable degredation. Conversely, if the epoxy - insulation reaction is to soften or weaken the insulation, then shorts and/or training may result. We have undertaken a study of the effects of the insulation on potted coils wet wound with Stycast epoxy (which is used for our dipole, quadrupole and test coils). The wire was insulated with one of two insulating varnishes: Formvar (a polyvinyl formal resin) or Polyesterimid (a phenolic resin). Formvar is the standard insulation in the United States while Polyesterimid the European standard. All the early test coils, the prototype quads and dipoles were insulated with Formvar, while all the beamline quads that will be used in Phase II will have Polyesterimid insulation. The initial tests of the quad coils with Polyesterimid insulation showed considerable training. However, the wire has a much higher critical current and quenches only occurred at that current at which the Formvar insulated coils quench. The Formvar insulated quad coils were fabricated from different batches of wire obtained over a long time period. Some of these trained while others immediately ran at short sample limit. Therefore a more systematic study using wire from the same run, but with with different insulation, was required.

Small racetrack coils were wound with 610 turns of 0.356 mm wire (Cu:SC = 2:1) using Stycast 2850 FT epoxy. These coils were wound on the same form as the test coils described earlier.[1] Three coils used Formvar insulated wire while two had Polyesterimid insulation. Air core calculations with POISSON and the measured short sample limits supplied by the manufacturer allowed calculation of the load line provided by the coil's self-field. The calculated short sample current for the coil cross section (using a 65% packing factor found in our test coils) is 135 Amps with a peak field of 3 Tesla at an average current density of slightly over 70 kA/cm^2.

The results of the tests conducted at Fermilab are shown in Fig. 1. Coils D and E have Polyesterimid insulation. Only two of the coils reached the calculated short sample limit, one of each type of insulation. The Polyesterimid insulated coils showed slightly fewer quenches to reach the maximum current than the Formvar insulated ones, but started training at a lower current. Coil D had a known short which reduced the maximum ramp rate to 1/4 A per sec, while the other coils could be ramped at 4 A per sec without degredation. Except for coil

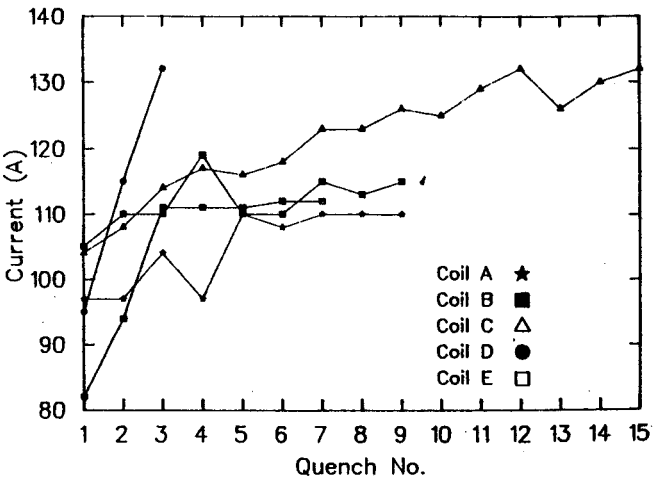

Fig. 1: Training history of the test coils. Coils A - C use Formvar insulated wire, while coils D an E use Polyesterimid insulation.

C the other coils reached a hard limit after 3 - 5 quenches, with most of them in range of 110 to 120 Amps. Sectioning some of the coils after the tests revealed that the windings were not uniform in the high field region. As even small displacements of the wire and a higher than calculated packing factor result in large changes in the peak field experienced by the conductor, these lower hard limits are probably the short sample currents at the enhanced fields. Thus with the exception of coil C, 3 - 5 quenches were sufficient to reach short sample limit, with little difference between the types of insulation. It should be noted that the lowest initial quench occurred at an overall current density of 45 kA/cm^2, while the peak current density exceeded 70 kA/cm^2.

We found that the only difference between the two types of insulation is the price: In the US Polyesterimid is nine times more expensive than Formvar, while in Europe Formvar is more expensive and not readily available.

---

a. FNAL, Batavia, Illinois.

References

1. A.F. Zeller, et al, MSU Annual Report 1982-83, p. 151; and J.C. DeKamp, et al, ibid., 1983-84, p. 266.

MULTIPOLE MODIFICATION OF INTENSITY DISTRIBUTIONS

B. Sherrill, J. Bailey, E. Kashy, and C. Leakeas[a]

In many applications of charged particle irradiations it is necessary to have a uniform spacial distribution. For example, in proton oncology it is essential to insure that all parts of the tumor receive the same dose, so that all cancer cells in a given volume are destroyed and the complications to surrounding normal cells can be kept to a minimum. Presently in charged particle oncology, uniformities of better than 10 percent are used[1].

There are several techniques used to make uniform irradiations. The standard technique is to scan a small beam spot either by raster scan, wobbling, or fast sweeping. Other techniques have been developed which use more passive methods. One of these techniques involves spreading the beam using multiple scattering in a thick absorber, and then by a series of occulting rings and additional scatterers, smoothing the resulting Gaussian distribution[2]. Another technique, which will be discussed in this contribution, uses multipole magnets to transform a Gaussian intensity distribution into a uniform distribution[3]. The principle of the technique is not limited to Gaussian shapes, but these are the most typical for the applications where the technique might be used.

THEORY

The use of multipole magnets for changing intensity distributions can be thought of as an integral transform. In this case, the kernal of the transformation is just the delta function. For the discussion we will use the coordinate system where the z dimension is along the beam direction and x and y are the transverse coordinates. The angle θ is in the x-z plane, and the angle ϕ is in the y-z plane. The integral transform can be written:

$$I(x) = \int I_0(x,\theta,y,\phi)\ \delta(x - f(x,\theta,y,\phi))$$

where I_o is the initial intensity distribution as a function of the initial coordinates and f is the function which describes the optics of the system of how the final x of the system depends on the initial coordinates. The integral simply adds up all the contributions at the final position x which come from all different intial coordinates combinations which give a particle at position x. For illustration, if we assume that the final position depends only on the initial angle θ, then the above equations simplifies to:

$$I(x) = \int I_0(\theta_0)\ \delta(x - f(\theta_0))$$

where θ_o is the initial angle.

This expression can be evaluated by using the identity that:

$$\delta(x - f(\theta)) = \sum 1/[f'\ \delta(\theta - \theta_i)]$$

where f' is the derivative of f with respect to θ, and the sum is over the i zeros of the function (x-f(θ)). Therefore, we see that if we want the final intensity distribution to be uniform, then we must adjust f(θ) such that:

$$\text{constant} = I(\theta_0) / f'(\theta_0).$$

If we consider a Gaussian distribution, and expand it in a Taylor's series, then we see the first term to cancel must be of order θ^2, and hence the term in f(θ) must involve θ^3. Such

third order terms, n=3, are optically controlled by octupole magnets. Hence the first order correction for a Gaussian distribution must involve an octupole magnet. Higher order corrections will obviously require higher order magnets of odd symmetries, i.e. n=5,7,9, etc. In general, it is more difficult to see how the corrections must be made, since all coordinates contribute to the integral and the optical transformation may be complicated.

EXPERIMENT

The calculations which were done in Ref. 3 to test the principle of the method, were performed with the program TURTLE[4]. In order to check these calculations and the program we made a test using the octupole magnet in the S320 spectrometer. By placing a 0.0016" diameter hole at box 1 of the K500 beamline, and detuning the bean, we were able to get count rates of 500 to 1000 per second at the S320 focal plane with the spectrometer at 0 degrees and looking directly at the beam. Targets were placed at the target position of the spectrometer to spread the beam into a Gaussian distribution. The resulting intensity distribution was measured at the focal plane using the standard S320 position sensitive detectors. The octupole was turned on, and its effects studied. In all cases the measured results were in agreement with TURTLE calculations[5].

To further test the level at which intensity distributions can be flattened, we have made TURTLE calculations for a sample beamline with optics similar to those discussed in Ref. 3. However, in this case multipoles up to 16-pole were used to flatten an initial Gaussian shaped beam. Figure 1 shows the results. The upper part shows the finial distributions with the multipoles turned off, and the lower part of the figure shows the effect with the multipole on. In this case almost 100% of the initial beam is flattened to

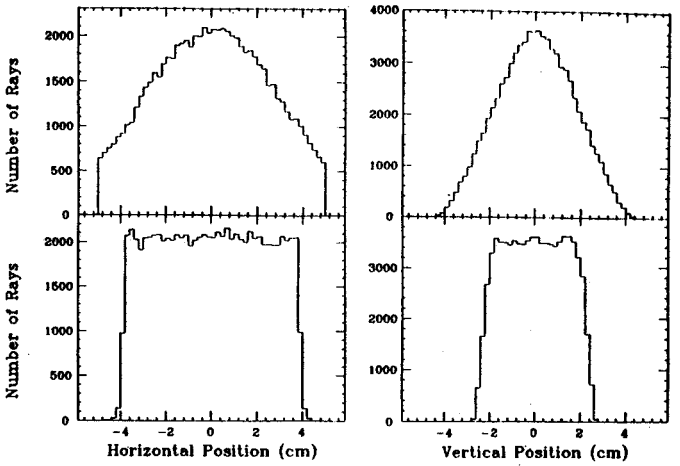

Fig. 1: Intensity distributions calculated with the program TURTLE showing the effect of multipole flattening. In the upper part the multipoles are turned off, and in the lower part the multipoles have been set to flatten the particle distributions.

the statistical uncertainty of the TURTLE Monte Carlo calculation.

FUTURE DEVELOPMENTS

We hope to build a superconducting multipole magnet, with variable multipole components, in order to further test the technique. A cross section of 1/4 of the magnet is shown in Fig. 2; included are the magnetic field lines calculated with the program POISSON. The 7 independent coils per quarter are, in this calculation, excited to give an octupole field. The currents in each coil are determined the expression

$$I_{coil\ m} = I_0 \cos[n*(m-1)*15]$$

where n is the multipole number and m is the coil number. Table 1 gives the possible maximum multipole fields for this magnet. With two of these magnets a test beamline could be set up using K800 or K500 beams. After the initial testing, this beamline could be used for actual experimental irradiations studies.

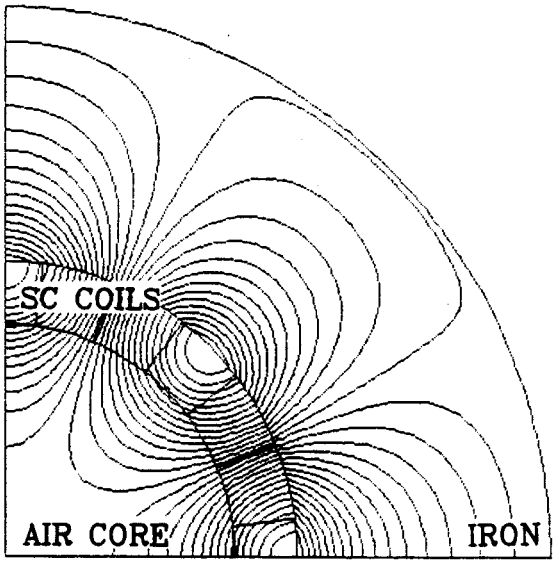

Fig. 2: POISSON calculation for one quarter of a variable strength multipole magnet. In the figure the currents are set to make an octupole field. The magnet has 7 independent superconducting coils.

TABLE 1: Field strengths for the multipoles of the magnet show in Fig. 2.

Multipole	N	Field(kG)
Quadrupole	2	6.2479
Octupole	4	2.1777
Dodecupole	6	0.7876
16 - Pole	8	0.2962
24 - Pole	12	0.0820

Figure 3 shows a schematic layout for such a beamline, and the corresponding beam envelopes. The energy degraders are used to change beam energy and the monokinetic wedge is used to correct the energy straggling generated by the degrading wedges. The final energy

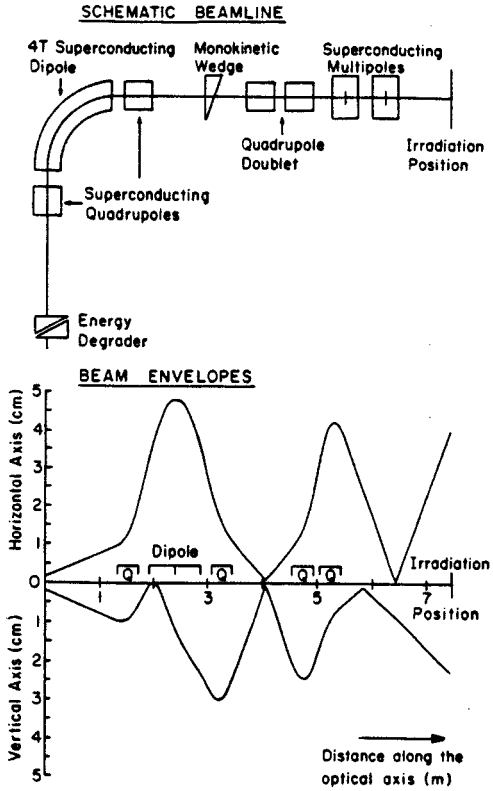

Fig. 3: Figure showing a proposed beamline for investigating the field flattening technique. The upper part shows a schematic of the beamline, and the lower part the beam envelopes.

spread is limited by energy straggling in the monokinetic wedge to about .2%. Waists are set at the centers of the multipoles in order to decouple the x and the y planes.

---

a. NSF Summer Program Science Student; present address, Purdue University.

REFERENCES

1. A.M. Koehler, R.J. Schneider, and J.M. Sisterson, Medical Physics, 4 (1977) 297.
2. B. Gottschalk, private comm., Harvard Cyclotron Laboraty.
3. E. Kashy and B. Sherrill, NIM B26 (1987) 610.
4. D. Carey, TURTLE, FermiLab report 64-02041.000.
5. C. Leakeas, 1987 NSF Summer Student Report, NSCL.

ENERGY DEPENDENCE OF THE $\nu_r + 2\nu_z = 3$ COUPLING RESONANCE LIMIT IN A SUPERCONDUCTING CYCLOTRON

M.L. Mallory and P. Miller

The $\nu_r + 2\nu_z = 3$ coupling resonance limits the lower operation boundary of the K500 cyclotron. In a series of light particle computer studies on the K500 cyclotron, it was observed that the resonance was encountered at magnetic field levels considerably lower than obtained for heavy ion particles. Figure 1 shows the relationship between the central magnetic field and the deflector radius for various charge to mass ratio ions at the resonance. A change of ~.8T in central magnetic field (B_o) between protons and heavy ions occurs for the resonance crossing at 26.3".

A simple analytic expression has been derived for this relationship and it is given in equation 1.

$$B_o = \frac{1}{\gamma}\left[\frac{2}{9} N^2 \frac{[1 + 2\tan^2\zeta]}{N^2 - 1}\left[B_H - B_V\right]^2\right]^{\frac{1}{2}} \quad (1),$$

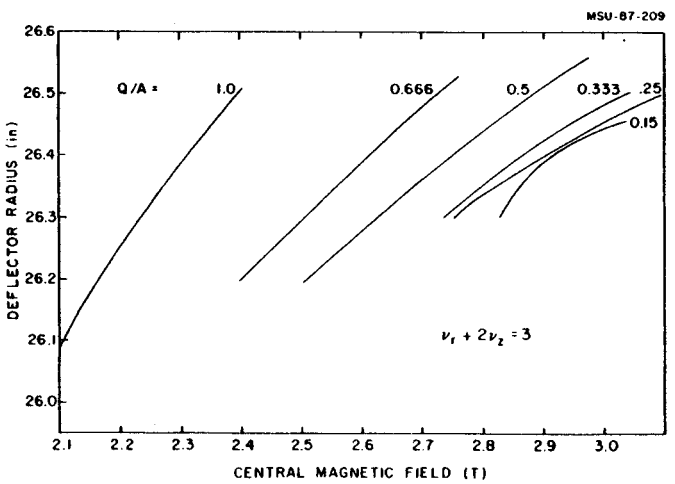

Fig. 1: The deflector radius at which the coupling resonance is crossed has been computed for the K500 cyclotron as a function of central magnetic field for different charge to mass ratio beams. Nominally the deflection of the beam occurs near 26.3 inches. For most heavy ions (Q/A < .33) the resonance is crossed near 3T. The value for protons is found to be 2.3T.

where γ is the relativistic parameter given by the ratio of total energy to rest energy, N is the magnet sector number, zeta (ζ) is the pole tip spiral angle, B_H and B_V are the magnetic fields of the hill and valley respectively. This equation was derived by substituting the betatron smooth approximation into the coupling resonance equation and making appropriate assumptions for flutter and the field index at the resonance crossing.

Figure 2 shows the agreement of the analytical expression with the computed results for various charge to mass ratio ions. The analytical curve fairly predicts the trend. The deviation of the points from the curve can be attributed to the small differences in the radius of the resonance crossing, assumed particle phase history, and to magnetic field extrapolation problems, especially for Q/A=1.0 ions.

Figure 3 is the new operating diagram for the K500, where light ion acceleration has been emphasized. This figure shows the possibility of lower energy acceleration of $^4He^{2+}$ than previously assumed. The acceleration of $^3He^{2+}$ in the K500 cyclotron now seems possible with the present upper limit of the radio frequency system (28.2 MH_z).

Figure 4 is a 40.2 MeV/u $^4He^{2+}$ beam versus cyclotron radius and this beam is within the new operating region of the K500. An extracted beam of 10 enA was obtained. The operating point for the K500 magnet is outside the field mapped. The magnet field for isochronism involves extrapolation that may produce a magnetic field that has large deviations from the actual field, thereby producing phase errors and lead to the observed beams loss versus radius.

In summary, the coupling resonance which determines the low energy cut off for external

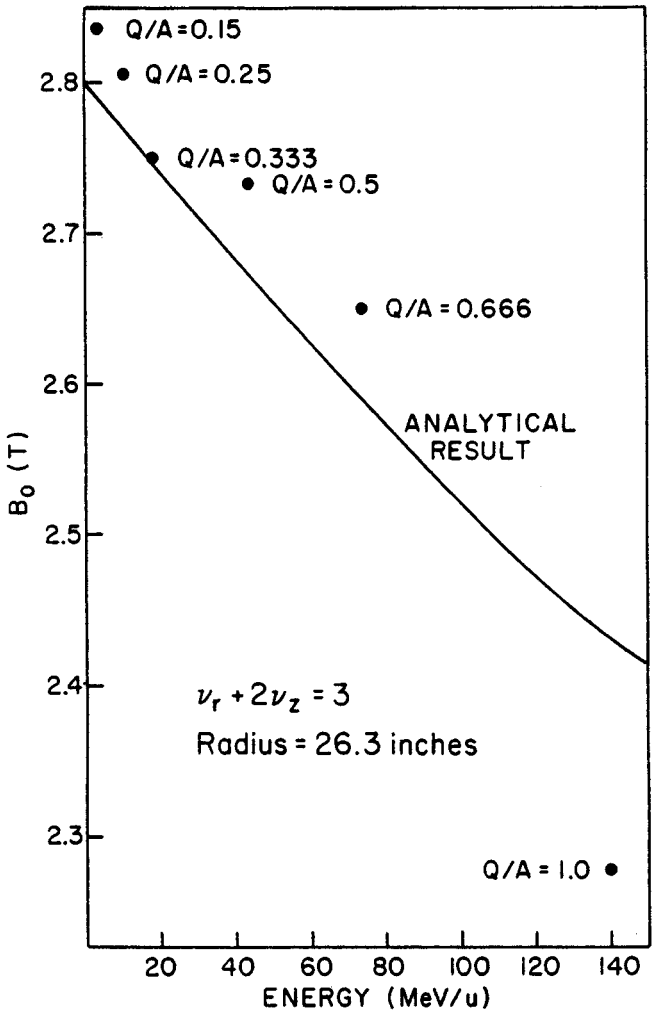

Fig. 2: The computed central magnetic field for different charge to mass ratio beams are plotted against the particle energy, where each beam encounters the $\nu_r + 2\nu_z = 3$ coupling resonances at a radius of 26.3 ± .1 inches. The theoretical curve is shown (solid line), where B_o equal to 2.8T at $\gamma = 1$ has been assumed. The scatter of the points from the theoretical curve is attributed to the variation of the radius at which the resonance is encountered and slightly different assumed phase curves in the cyclotron acceleration.

beams varies in a favorable way as Q/A increases. For future superconducting cyclotrons, this information could influence the range of magnetic field measurements, design of the radio frequency range and design of the extraction system.

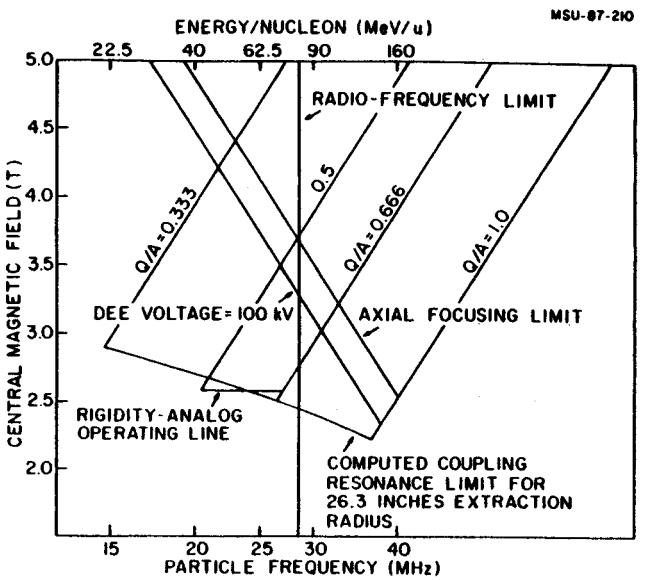

Fig. 3: The operating diagram for the K500 cyclotron with the computed limits on the coupling resonance occurring at 26.3 inches is shown. This operating diagram predicts the successful acceleration of $^3He^{2+}$ with the achieved radio frequency limit of the K500.

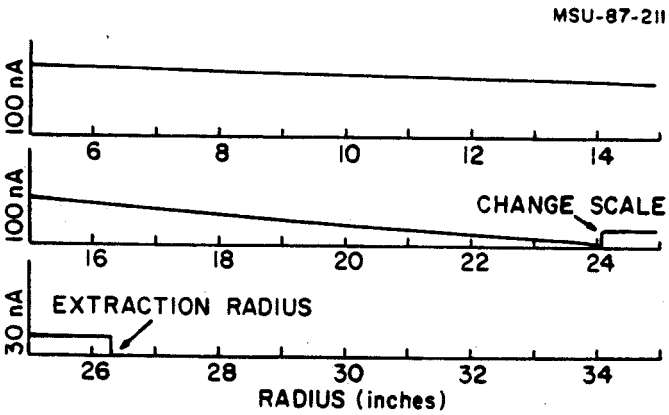

Fig. 4: The radial beam trace of 40.2 MeV/u $^4He^{2+}$ is shown and this is within the new operating boundary. The beam is gradually lost as a function of radius and this is attributed to problems with calculating the correct trim coil settings. 10 enA was successfully extracted. This beam is near the calculated coupling resonance limit.

^{7}Be STUDIES FOR WEAR RESEARCH

M.L. Mallory, R. Ronningen, H. Schock[a], B. Sherrill, and W.C. McHarris

Introduction

We have previously reported the production of short half-life radioactive ion beams (^{6}He), produced by the fragmentation of heavy ions in the K500 acceleration region.[1] At the Tokyo cyclotron conference, H. Schweikert from KFK, suggested that we should look at the fragmentation of heavy ions into ^{7}Be. At his laboratory in Karlsruhe, they have developed the surface layer activation (SLA) method for measuring wear rates of certain material surfaces. This technique uses the ion bombardment of surfaces like iron or chromium with beams of proton, deuteron, or alpha particles, producing radioactive isotopes. Because these radioisotopes are produced in a very thin surface layer, the wearing away of this layer can be monitored by their decay. A large class of materials, for example ceramics and light metals with atomic number Z<24 are not easily accessible to their technique, since a suitable isotope with a reasonable half-life and a detectable γ-ray cannot be made.

^{7}Be Characteristics and Production by Fragmentation

^{7}Be has a half-life of 53.2 days and a single 478 keV γ-ray (10.4% intense). In the early 1970's, physics studies with a proton beam from the MSU K50 cyclotron, demonstrated that ^{7}Be is produced with a large yield in carbon and nitrogen targets[2]. Figure 1 shows the measured cross-sections versus proton beam energy on a carbon target. With the development of the K500 cyclotron, it is now possible to do the kinematically reversed reaction, i.e., we can bombard light targets with energetic carbon and nitrogen beams. The consequence of this is that the nuclear fragments are made having the beam

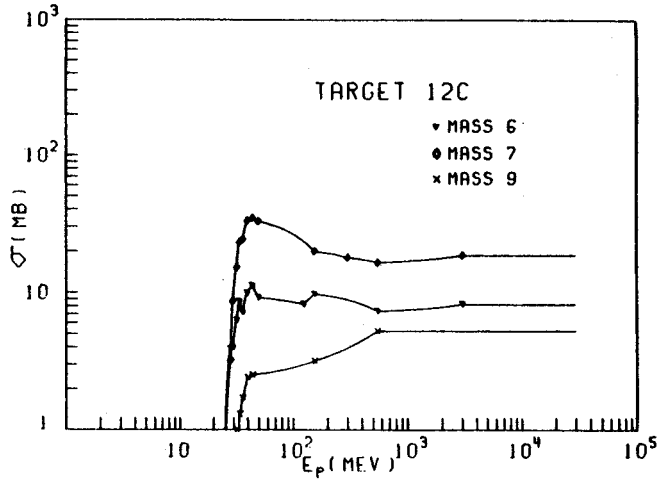

Fig. 1: Total cross-sections as a function of proton energy for spallation products of mass 6 to mass 9 from a carbon target.

velocity and then can escape from the target in the forward direction of the primary beam. A cross-section measurement for producing various fragments, including ^{7}Be, from a 35 MeV/u $^{14}N^{5+}$ beam on a ^{165}Ho target at 10° from the forward beam direction was done recently at MSU[3]. These ^{7}Be fragments are referred to as quasi-elastic fragments from heavy-ion collisions and the cross-sections obtained were large.

We have now done a stacked foil experiment and measured the yield rate for producing ^{7}Be. A total of 10^{12} particles of ^{7}Be were made in a two hour bombardment of 35-MeV/u $^{14}N^{5+}$ on a 0.070" thick carbon target, with an integrated beam current of 9 x 10^{14} particles. A partially stopping catcher foil stack of Al behind the carbon target detected the implantation of 10^{10} ^{7}Be per each 25 micron thick foil. Figure 2 shows the experimental data for the foil stack. Scaling the K500 cyclotron to its maximum $^{14}N^{5+}$ output yields a 1μCi γ-decay rate of ^{7}Be with a 24 hr bombardment. This maximum beam current would require cooling the electrostatic

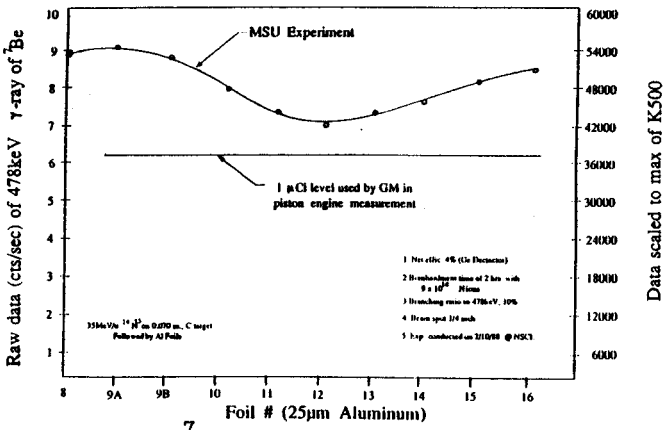

Fig. 2: The ^{7}Be count rate in Al foils stacked behind a carbon target (foils 1-7). The right side of the graph is the data scaled to the maximum output of the K500 for a 24 hour run and produce greater than a μCi dose for each 25 μm foil.

deflector and the target with water. The above yield rates would be equal or better than the 1μCi levels used by General Motors (GM) in their piston engine wear measurements[4].

The difference in stopping for ^{7}Be and $^{14}N^{5+}$ allows a clean separation of the primary beam from the fragment within the foil stack. Radioactivity from other short half-life fragments is found to be of no significance several days after bombardment. A slight background, of academic interest, was detected in the Al foils and is attributed to light fragment activation of impurities in the Al.

Summary

It now appears that implanting ^{7}Be produced by a fragmentating heavy-ion beam can be a new tool of potential value to a tribiology program by allowing new materials to be studied that were not possible in the past. Depending on the beam stopping cut off results, which it is expected to be sharp compared to the traditional SLA method, this tool may be immediately available for use at MSU.

We have established a cooperative working arrangement with the MSU Mechanical Engineering Department with primary emphasis on wear detection on internal and external combustion engines. Preliminary discussions have been held with researchers at NASA, Ford, General Motors, and with top management of Lansing based BOC Division of G.M. All have expressed an interest in using ^{7}Be samples for wear analysis when available.

---

a. Mechanical Engineering Department, MSU, East Lansing, MI.

References

1. M.L. Mallory, Proc. 11th Int. Conf. on Cyclotrons and their Applications, Ionics, Tokyo, (1987) 558.
2. H. Laumer, S.M. Austin, L.M. Panggabean and C.N. David, PRC 8, (1973) 483.
3. G. Caskey, L. Heilbronn, B. Remmington, A. Galonsky, F. Deak, A. Kiss, and Z. Seres, MSUCL-626 (1978).
4. E.W. Schneider, D.H. Blossfeld, and M.A. Balnaves, GMR-6033, (1987).

DESIGN STUDIES FOR A 250 MeV SUPERCONDUCTING SYNCHROCYCLOTRON

M.M. Gordon and X.Y. Wu

Work is continuing on the design of the extraction system for a 250 MeV superconducting synchrocyclotron to be used in cancer therapy. A paper describing preliminary results was presented at the Particle Accelerator Conference held in Washington, and this paper has now appeared in the Proceedings of that conference.[1] A report on subsequent progress is scheduled for presentation at the APS meeting in Baltimore in April, 1988.

As described in last year's annual report, beam extraction is based on the use of a regenerator to produce turn separation. Radial phase plots at a sequence of energies show that as the beam accelerates out to the regenerator, the stability region shrinks rapidly to zero thereby spilling the orbits onto the outflowing asymptote along which the radius gain per turn increases until they can clear the septum and enter the magnetic channel. The rapid decrease in the stability region between 252.0 and 253.5 MeV is shown in Fig. 1, and this region completely disappears at 253.7 MeV.

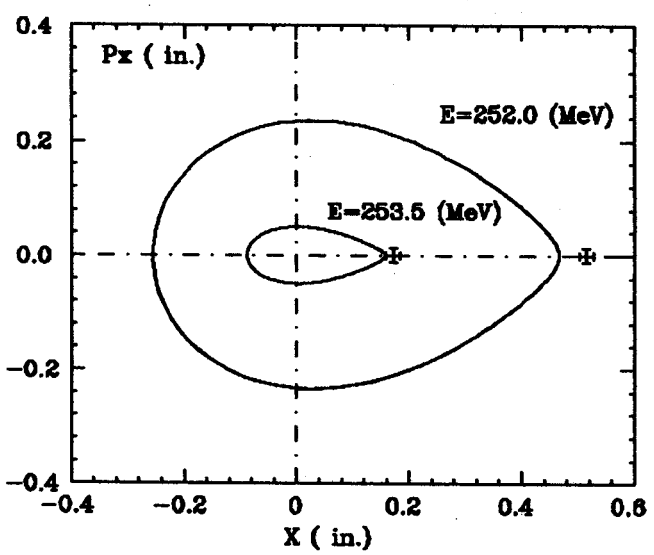

Fig. 1: Radial phase plots at 252.0 MeV and 253.5 MeV showing the rapid decrease in the stability region between these energies. The stability region shrinks to zero at 253.7 MeV.

Vertical stability requirements ultimately limit the maximum radius gain per turn to about 0.6 in. at the channel entrance. That is, as the orbits move progressively further off center, strong coupling effects eventually cause the vertical height of the beam to expand beyond the allowed limits. The magnetic channel entrance must therefore be positioned well before this point is reached.

Vertical stability also depends quite strongly on the radial displacement of the orbit centers prior to extraction, and because the stability region shrinks with increasing energy, protons with large orbit center displacements begin extraction at lower energies than those with small displacements. As a result of the coupling action, the lower energy extraction orbits with their larger displacements suffer a greater growth in vertical amplitude.

This effect is shown in Fig. 2 where the beam height Δz is plotted as a function of turn number for four different energies from 252.0 to 253.5 MeV. In each case, the initial height is 0.1 in., and the initial (r,p_r) point was chosen so that the protons reach the channel entrance in about 24 turns. These results demonstrate that at 252.0 MeV the height Δz increases by a factor of about 3.4, an uncomfortably large value, while at 253.5 MeV, the growth factor is only 1.3. Clearly, it would be quite advantageous to restrict the range of orbit center displacements (or radial emittance) in the central region as far as possible since this would not only improve the extraction efficiency, but would also narrow the energy spread in the extracted beam.

Other results from these orbit studies show that as the initial height is increased above 0.1 in., the nonlinear coupling of the vertical into the radial motion becomes progressively

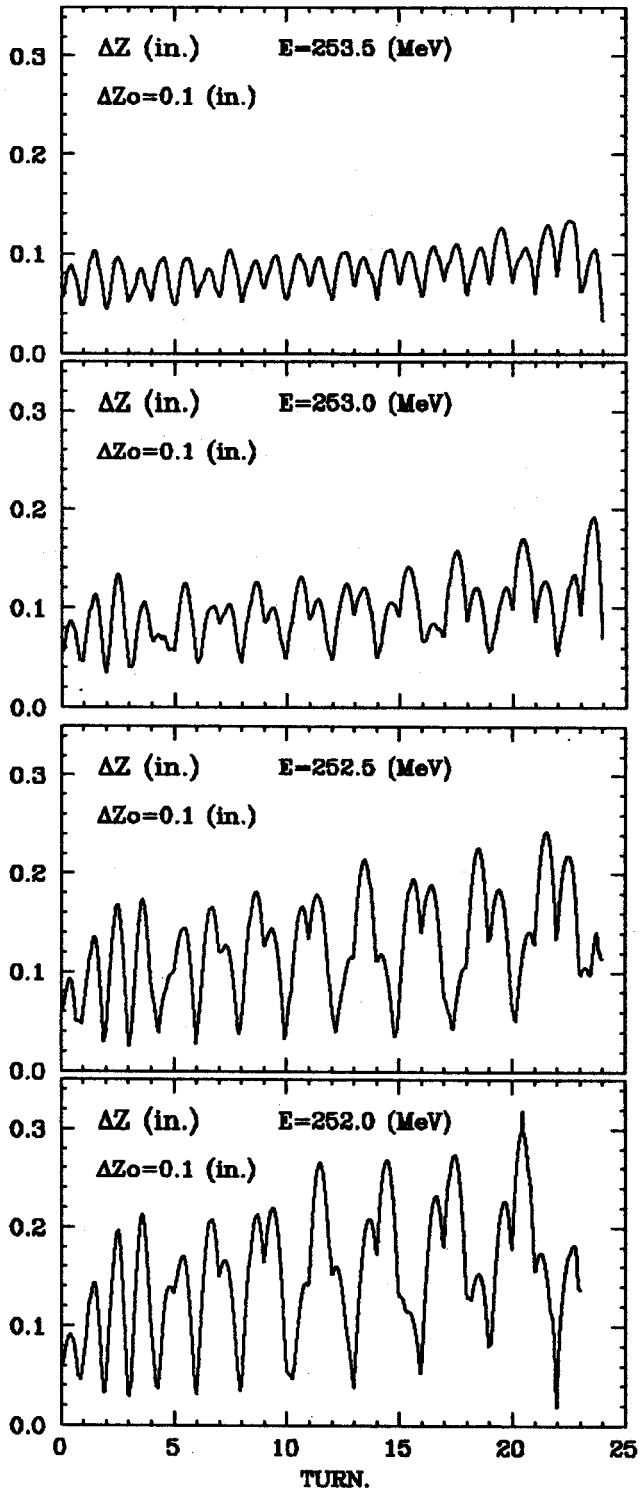

Fig. 2: Plots of height Δz vs. turn number for a group of orbits having an initial height Δz_o = 0.1 in. and energies from 252.0 MeV (bottom) to 253.5 MeV (top). All orbits run for about 24 turns to reach the channel entrance.

more obvious and corresponds, in effect, to an undesirable weakening of the regenerator action. That is, the orbit radius at the channel entrance sweeps across the septum repeatedly as the initial vertical amplitude increases. From the point of view of extraction efficiency, it would therefore also be advantageous to restrict the vertical height of the beam (or vertical emittance) prior to extraction. In this connection we should note that the adiabatic damping factor in this machine will cause the beam height to decrease by a factor of two between the central region and the start of extraction. Thus, for example, a height 0.2 in. just prior to extraction would correspond to an initial height of 0.4 in. in the central region, a quite reasonable value.

Our conclusions on the relation between extraction efficiency and the control of radial and vertical emittances are fairly well borne out by the experience at CERN. As a result of the upgrading of the CERN 600 MeV synchrocyclotron in the early 1970's, the extraction efficiency increased dramatically to values as high as 70%, and a significant part of this improvement can be attributed to a completely revised central region based on a closed ion source that provides good control on the emittance values for the injected beam.[2]

---

1. M.M. Gordon and X.Y. Wu, Proc. of the 1987 Particle Accelerator Conf., (IEEE, New York, 1987) p. 1255.
2. B.W. Allardyce, Proc. Tenth Intl. Cyclotron Conf. (IEEE, New York, 1984) p. 744.

RECENT DEVELOPMENTS IN BETA DECAY STUDIES OF LIGHT EXOTIC NUCLEI WITH THE RPMS

D. Mikolas, N. Bhattacharya, T. Glynn, A. McGilvra, M. Maier, M. Samuel, C.E. Scripter, H. Takayasu, K. Tyson, A. Vander Molen, R. Harkewicz, S. Gil[a], W. Rogers[a], A. Garcia[a] and J. H. Gundlach[a]

The Reaction Product Mass Separator (RPMS) at NSCL has now been used in a large number of experiments to study the production and decay of nuclei far and close to stability. A summary can be found in Ref. 1. We discuss here many developments, both hardware and software, and ongoing projects to increase the usefulness of the RPMS, and to increase the information available from the study of decay properties of isotopes separated. These are be divided into five main categories, those associated with the RPMS itself, with the aquisition of data, with its analysis, with the containment of separated activity within small volumes for better decay studies (monochromation) and those with an experiment by the group from Seattle.

I. Developments of the RPMS itself.

The yield of exotic isotopes from the projectile fragmentation reaction fills a cone with about a 3° half-angle for E/A = 35 MeV ^{22}Ne on Ta. Most of the primary beam leaves the target within a much smaller cone. N. Bhattacharya has designed and constructed a small permanent magnet dipole to be placed just before the target of the RPMS. The effect would be a vertical downward deflection of the beam. The acceptance of the RPMS is typically a factor of four smaller in the vertical direction than the horizontal, and extends from 0° upward, so that a 1° downward deflection is sufficient to keep the primary beam out of the Wien filter, while maintaining most of the aperture of the RPMS illuminated by the 3° cone of the reaction. Fig. 1 shows the completed magnet, and Fig. 2 shows a two-dimensional calculation of the resulting field. The materials used are described in the caption.

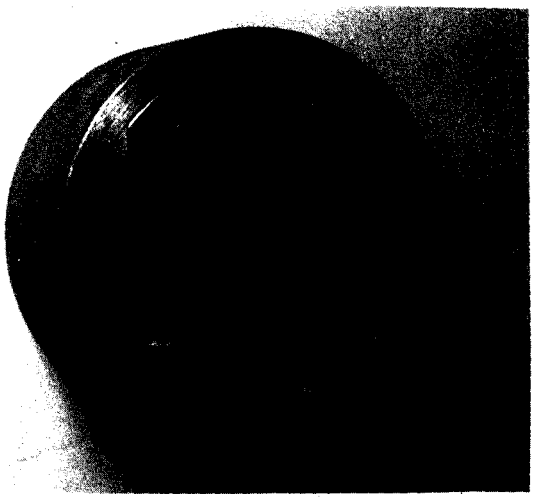

Fig. 1: The 1° magnet for the RPMS. The four large (2" × 2.1" × 0.5") Samarium Cobalt permanent magnets are all magnetized in the horizontal direction in the photograph. Of the four small (1" × 0.5" × 0.5") Samarium Cobalt magnets, the lower two are magnitized with their field pointing upward into the gap, and the upper two, out of the gap. The line integral B•dℓ is constant to within 10% across the 2 inch aperture.

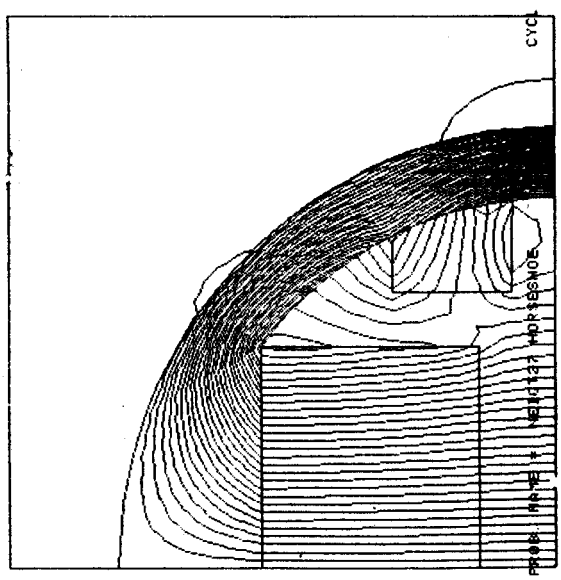

Fig. 2: Two-dimensional Poisson calculation for the magnet in Fig. 1.

Figure 3 shows a position spectrum of two isotopes with nearly identical m/q. This demonstrates the mass resolution of the RPMS. The resolution is optimized by varying the dispersion of the second dipole (Cornell magnet) while tracking the deflection by adjusting the tail-angle. The focus of the quadrupoles must be correct before such a study is useful. The two most useful diagnostic 2D spectra to observe while tuning up are energy vs. vertical and horizontal vs. vertical. The former clearly indicates how close the tune is to a momentum focus, and the latter to a spatial focus.

New power supplies have been purchased for the second quadrupole doublet, Q22 and Q23. Previously, these were driven by two channels of the Perkins Supply. With increases in beam energy and m/q, and corrections in the ratio of focusing between the first and second doublet, the Perkins reached a voltage limit below the operating point of the doublet. The distance from the last doublet to the focal plane has also been increased to ~2m from the original 1m.

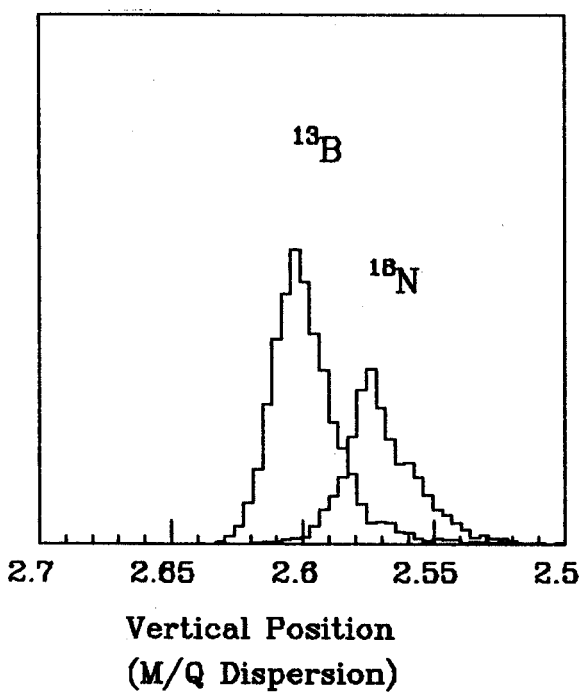

Fig. 3: Vertical position spectrum of ^{13}B and ^{18}N from the fragmentation of ^{22}Ne. These isotopes are only 1.1 % different in m/q. The FWHM m/q resolution is only 0.8 %.

The increase in the final quad-to-focus distance places the focus just past the existing tail support structure. This fact, plus the increasing complexity of detector arrangements prompted the design of a new detector mounting carriage. The choice was a standard 95 mm square optical bench rail manufactured by Klinger. This product has been adopted as the standard support structure for detector arrays in the 92" scattering chamber described elsewhere in this report. A steel support frame was designed to hold two 2.5m long Klinger X95 rails solidly and parallel, 26" apart, mounting to the existing non-parallel I-beams that comprise the tail structure of the RPMS. See Fig. 4.

To date, the RPMS has been used almost exclusively to separate reaction products to facilitate the study of their subsequent beta decay.[1-5] In order to extend the use of the RPMS to the study of the details of the reaction phenomena themselves, more needs to be learned about the transport of particles through

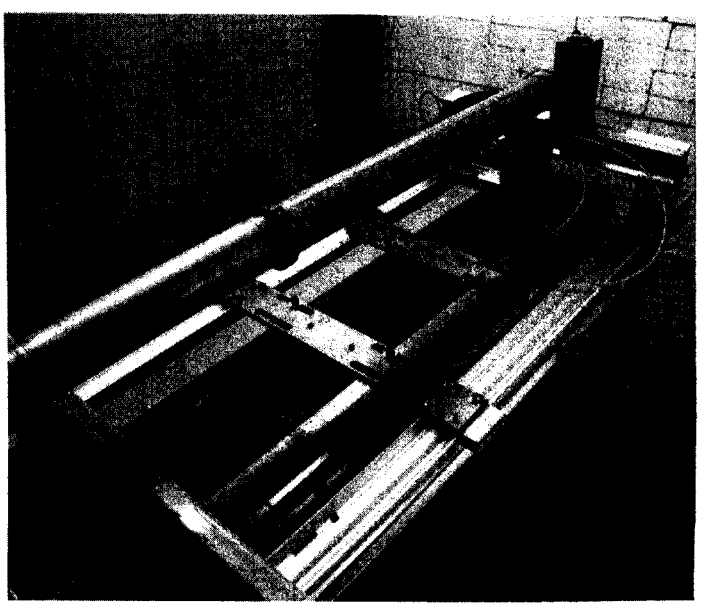

Fig. 4: Klinger X95 optical bench rail and associated support structure for the tail of the RPMS. These pieces are of modular construction and can be extended to accomodate increasingly complex detector set-ups. See text.

the RPMS. The transmission as a function of energy, direction and m/q must be accurately determined before actual cross-section measurements can take place. To facilitate diagnostic measurements of the trajectories of ions through the RPMS, a two-dimensional position sensitive detector has been designed and constructed. The detector may be run in vacuum, and thus may be placed at any accessible point in the RPMS. For example, it may be run in the drift between the velocity filter and the dipole for intermediate focus diagnostics, or a fraction of a meter before final focus, where correlations between the existing focal-plane detector and this detector will provide angle information. It is shown in Fig. 5. It presents a square active area 2" × 2", and fits into a slightly modified beam-box, with a hole enlarged to accommodate the detector. The aluminum mounting flange is electrically isolated from beam-line ground by means of a Lexan intermediate flange, and Lexan inserts in the bolt-holes. It is divided into two separate chambers, each with a resistive 0.3 mm dia. Nicrome wire crossing the center of the volume, one horizontally and one vertically. It is nearly transparent to light reaction products. There are three windows of 0.00025 inch thick aluminized mylar (the center window is aluminzed on both sides), and 0.75 inches of gas volume. At an operating pressure of 25 Torr of Isobutane, the detector presents a total thickness of 2 mg/cm^2, or a 0.3% loss in momentum of a ^{13}O ion at E/A = 25 MeV. The forward momentum straggling is then only 10% FWHM of the momentum loss. The windows are also thin enough to allow α particles from a standard ^{241}Am source to penetrate both chambers of the detector in order to give a signal for both the horizontal and vertical position. This feature will allow for extended periods of off-line diagnostics.

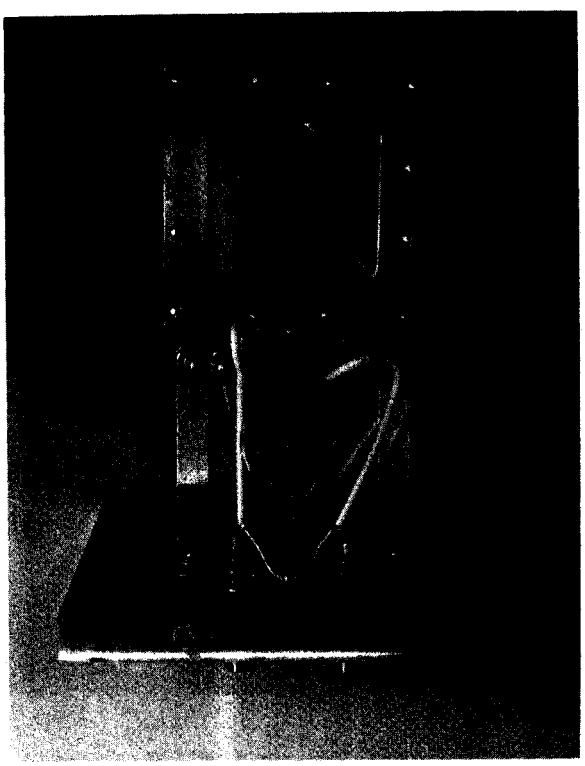

Fig. 5: Two-dimensional position-sensitive proportional chamber for beam diagnostics of RPMS. See text.

Developments in Data Aquisition

The arrival of ions within a silicon detector can deposit many hundreds of MeV, while the decay may involve only a few hundred keV. For instance, the measurement of the branching ratio of ^{9}C to the ground state of ^{9}B was accomplished by the detection of the breakup of the ^{9}B into 2α + p within the silicon, releasing only 0.29 MeV[2]. Standard instrumentation is not capable of maintaining a good signal to noise ratio over this dynamic range. Therefore, a preamplifier with a fast gain-switching FET associated with the input capacitor has been designed to switch the gain by a factor of 10 in a few μs, responding to the level of a TTL input. Five channels are incorporated into a small unit requiring only ± 12 V to operate. The preamps are divided into two groups that can be individually gain-switched. Typically the gain is switched 10 μs after the arrival of an isotope of interest in the silicon, and is then lowered after a preset period appropriate for the isotope of interest, but see below.

While the new preamp has greatly improved immunity to broadband noise associated with the electronics while maintaining a good dynamic range, other sources of noise were discovered. These non-statistical, sharp spikes seem to be quasi-synchronous to the 60 Hz line frequency. In order to improve the detection and possible rejection of these signals, a 'Phase Box' was constructed. This device generates a saw-tooth wave, continuously ramping from 0 to 1 volt and abruptly resetting to 0 V at each upward-going zero-crossing of the line voltage. Thus, when the signal (the output voltage is proportional to the instantaneous phase of the AC) is digitized along with the rest of the signals associated with decays, any correlations become obvious.

Much of the non-statistical noise was indeed correlated with AC phase, but would vary on the scale of minutes. In fact, the phase of the pulses could change continuously for up to 720° of phase in 5 minutes! This indicates that the pulses can not yet be simply related to the line voltage noise.

It was later discovered that the pulses were picked up passively by the long coax cables from the Data-U to the vault, coupled into the pre-amplifier, and then amplified and sent to the Data U. A solution was found to inhibit the transmission of these pulses along the shield of the coax. 'Noise Suppresser Modules' were constructed. Each contained eight high-Q high frequency Ferrite cores of approx 2.5" dia. Short lengths of coax were wound twenty times on the cores, and both ends were brought to electrically isolated BNC connecters on the front panel. When all signals, including power and gain-switch, were fed through these supressers, the spurious noise pulses could be suppressed by a factor of 10.

After this, some pulses still remained. It was the discovered that while the noise pulses from the fast output of the fast/slow amplifier (now in the experimental vault) were well above the threshold of the CFDs, they resulted in very little or no signal in the slow channel. They carried voltage and little charge, or more simply, had a faster time-constant that the 'real' pulses associated with ionization in the silicon. Now, the fast signals are split, and while one continues to the CFD, the other is digitized by a peak-sensing ADC (Lecroy 2259), in addition to the slow pulse (digitized by an EGG AD811). In a two-dimensional plot of fast vs. slow, a clear separation emerges between the 'real' pulses and 'noise' pulses, and thus they can be removed from the data during off-line analysis.

Another source of contamination to the recorded spectra of beta-delayed charged particles is the energy loss of the beta particle itself as it leaves the silicon. See References 1 and 2 for a discussion of this. A device has been constructed that would allow for the detection of the beta particles, giving signals when they would leave with an angle less than about 60° with respect to the normal of the silicon detector surface. The device consists of an array of four plastic scintilator donuts, each coupled its individual photo-multiplier tube. These are interspersed with mounts for four silicon detectors (see Fig. 6). The device

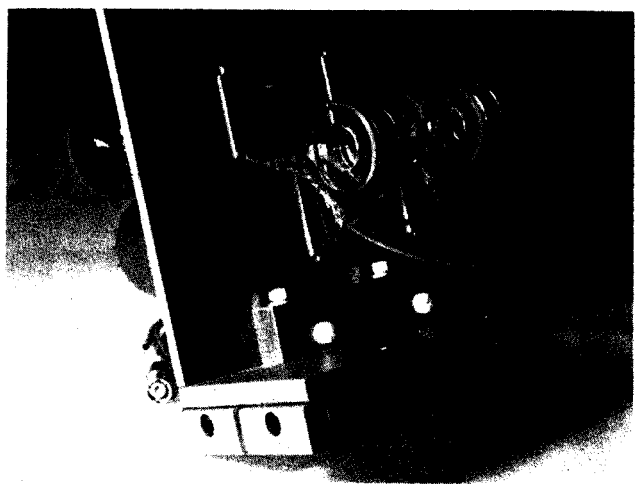

Fig. 6: Plastic scintilator donuts, with light-guides and photo-multiplier tubes, for triggering on the beta particle leaving the silicon detector. See text.

operates in air, and it can be mounted directly to the X95 rail at the focal plane of the RPMS.

As isotopes studied with the RPMS move further from stability, and further up the chart of the nuclides, two factors rapidly increase the difficulty of the determination of accurate half-lives. The first is the rapid decrease in yield of the isotope of interest, and the second is the increase in both the number of daughter beta decays following the decay of interest, and in the ratio of the half-lives of the daughter to that of the parent. The former calls for more efficient use of the activity - and the latter calls for physical separation of the primary activity from daughter activity. Implementation of both has been made by the construction of a computer-controlled rotating wheel and associated soft-ware, and by new data-analysis software.

A new device, HIRO (High-speed Implantation and ROtation) has been built as a method to accumulate and manipulate individual atoms after production and BEFORE their decay. It consists of a 12" diameter wheel of Kapton, 0.001" to 0.010" thick, bound to a 9" disk of 0.0625" Al. The disk is coupled to a high torque DC motor, of the type used in the K800 RF transmitter tuning circuits (see Fig. 7). A shaft encoder keeps track of the instantaneous rotational position of the disk at all times. While a standard 1024 pulse-per-turn shaft-encoder is used, a special circuit in the control unit discussed below interpolates the pulses to achieve a position resolution of one part in 4096; one fourth of a mm at the edge of the disk! The motor is driven by a commercial driver board, which receives signals from the motors tachometer and from a special control unit designed for this purpose. The control unit accepts NIM signals from the Data -U, and delivers the proper voltage to the card amplifier to move the wheel to the desired position as quickly as possible. The motor can accelerate the wheel from a complete stop, rotate 180° and settle to within 1 mm of the desired location in 50 ms. At all times, the instantaneous position can be recorded in the data-U by counting encoder pulses from the encoder unit. The wheel may be kept at rest or rotating at any constant speed, then either stopped at a desired absolute location immediately after a NIM pulse from the Data-U, or stopped once it has rotated a certain angle past the point when the pulse arrives. Thus, when a radioactive atom stops in the wheel, it can be rotated so that the part of the wheel containing the atom can be accurately positioned within the sensitive volume of a detector. All of the signals to and from the control unit are optically isolated from the data-U electronics to avoid inducing noise into the aquisition electronics.

Fig. 7: The HIRO device, described in text.

A collection of soft-ware has been written in order to control the wheel, gain-switching preamp, and cyclotron beam-interrupt. The input allows the user to set up to 16 isotope gates on the data as it enters the VME crate in data-U 2. Each isotope gate is the combination of up to 16 logical tests of one-dimensional windows on the various parameters recorded for each incoming ion event. Pseudo-parameters are also calculated. Thus, within a few ms, the software PID is completed, and the decision can be made

as to how to move the wheel, and for how long to turn off the cyclotron beam and raise the gain of the preamp. For short-lived isotopes with daughter activity of much longer half-life, the atom can be quickly moved into the sensitive volume of a detector, the decay observed, and the beam may be re-activated since a 'fresh' part of the wheel is ready to catch the next atom. This prevents build-up of long-lived activity that would occur in a static silicon detector telescope.

A prototype beta-detector has been designed for the activity in the wheel, and is presently under construction. It consists of two layers of 0.25" plastic scintilator 1" × 2", in shapes designed to present nearly 4π sR to the emitted beta from a 0.5" dia. circular area on the wheel. The two layers will be operated in coincidence. This will reduce the background count-rate due to noise in the phototubes and electronics to practically zero. The scintilators are surrounded by a cosmic-ray detection box made from 0.5" plastic scintilator, and run in anti-coincidence mode. The box is viewed by a single 5" dia. phototube.

For heavy, low-energy recoils, such as those from fusion reactions with the ^{3}He target discussed below, the silicon detectors must remain in vacuum. They are then inaccessible to γ-ray detectors. Therefore, three re-entrant windows have been built to allow close access to the silicon detectors containing $\beta+\gamma$ activity, for standard 3" × 3" NaI detectors (see Fig. 8). They present a 0.150" Aluminum window, which has a negligible effect on photons above 100 keV.

In order to extract accurate half-lives from data representing the decay of only hundreds of events, a set of fitting codes and systematic procedures has been developed by M. Samuel. The fitting is based on the concept of Maximum Likelyhood[6], and allows for various types of time background to be accounted for. The technique of Least Squares breaks down when the number of counts in a given channel is small and can not be used to extract the full statistical potential of the data when only a few hundred atoms decay, accompanied by background events. A Monte-Carlo simulation is used to directly calculate the true uncertainties in each of the calculated parameters, (e.g. half-life), without the ambiguities from coupling between uncertainties in two or more parameters.[3]

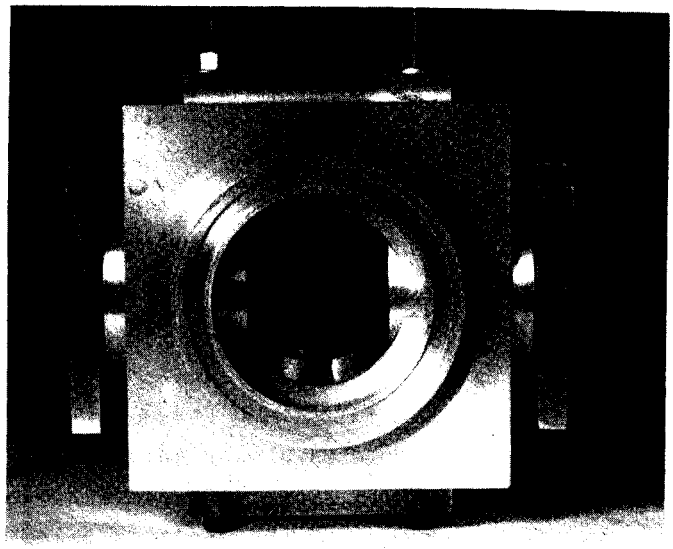

Fig. 8: Re-entrant windows for gamma-ray detectors. A third window at the front of the box has been removed for the photograph. The 0.5" spacers between the flanges and the beam-box can be removed to bring the inner surfaces of the windows 1.5" apart.

Monochromation

In experiments where the beta-delayed charged particles are to be detected and their energies accurately determined, the contribution of the beta-particles energy must be minimized. The detection of the direction of the beta can reduce this effect (see above), but is limited by solid angle conditions and multiple scattering within the silicon. The effect of the beta upon the resolution is to first order directly proportional to the thickness of the detector (see Refs. 1 and 2). The yield of particles of a given isotope separated by the

RPMS is distributed within a fixed set of final stopping ranges, typically hundreds of microns. Whereas this calls for a thick detector, resolution considerations call for a thin detector. In order to circumvent this problem, a technique was developed to minimize the width of the distribution in final stopping depths of the ions. The RPMS is first tuned to produce a momentum focus. This gives a spot size of approximately 4 mm. Then the momentum dispersion of the dipole is slowly adjusted to degrade the momentum focus. The beam spot enlarges vertically, with the position being correlated with the velocity of the particle. Once the spot has expanded to 20 mm (the diameter of a standard 300 mm^2 silicon detector), the position of the ion is directly proportional to the velocity of the particle with a resolution of 4/20, or 20%. A graded absorber is then introduced, with a thickness which increases with vertical position. The gradient of the thickness is chosen to compress the range of energies of the ions leaving the absorber and entering the silicon detector, until it is a factor of five narrower. This then puts the ions that would have originally spread out into 250 μm of range, into a single 50 μm thick detector.

Since the compression is accomplished by a deliberate degradation of the m/q resolution, this technique is limited to very light isotopes, such as those of Helium through Boron, where the distance in m/q space is large from one isotope to the next. We are presently developing a second system that will maintain the m/q selectivity while allowing for even better compression. It involves the addition of one quadrapole and one dipole magnet. The horizontal (non-dispersive) focus is extended to a point 1 m past its present location. There is still a focus in the vertical direction at its present location, where slits select ions of a fixed m/q ratio. The ions are then momentum dispersed by the dipole, and refocused by the new quadrapole. If the magnification is 0.5 in the direction of the dispersion of the new quadrapole, range compression of 10 to 1 can be accomplished. To this end, the prototype magnet for the K50 cyclotron has been disassembled, and sand-blasted clean. After painting, it will be re-assembled and new pole-tips fitted. Pancake coils will be manufactured with the facility presently used to wind ECR coils. An additional support structure will be necessary to bear the weight of this magnet at the tail of the RPMS.

The Seattle Cryogenic ^{3}He target

Recently, the group from Seattle performed an experiment which required a thick target of ^{3}He. The depth of field of the RPMS constrained the length of the target to 10 cm. In order to produce a target dense enough, a gas cell was designed and built in Seattle, that can maintain up to two atmospheres of ^{3}He gas at a temperature slightly above that of boiling liquid Nitrogen. It is shown in Fig. 9.

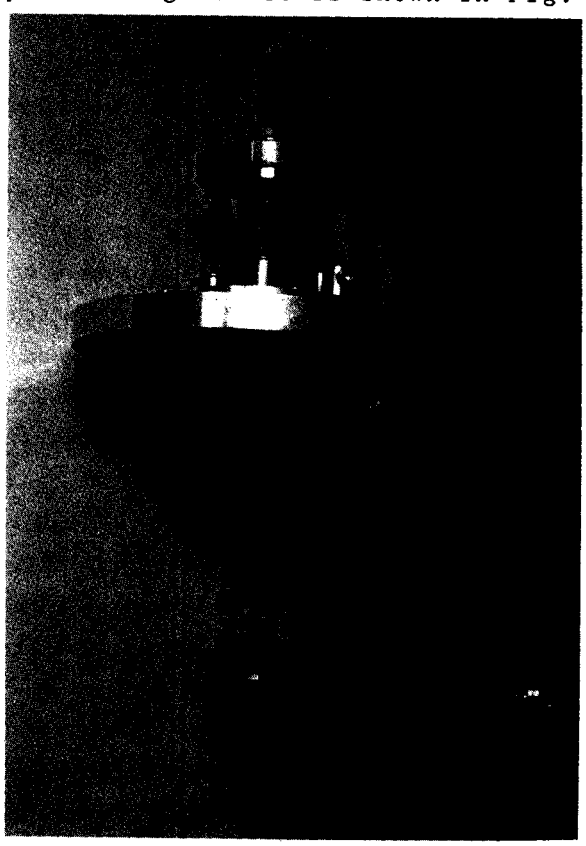

Fig. 9: The Seattle ^{3}He gas cell. See text.

Collimators on both entrance and exit to the gas cell lie outside of the Nickel windows, and are electrically insulated from the cell in order to monitor the alignment of the cell with respect to the beam. A 1" diameter copper 'finger' served as the mechanical support for the cell. It extended into air where it can be inserted into a LN_2 dewar. The ^3He is fed into the gas cell through a stainless steel line, and could be pumped in and out by cycling the temperature of both the gas cell and an external holding vessel.

---

a. Nuclear Physics Laboratory, GL-10 University of Washington, Seattle, Washington 98195.

References

1. D. Mikolas, B.A. Brown, W. Benenson, Y. Chen, M.S. Curtin, L.H. Harwood, E. Kashy, J.A. Nolen Jr., M. Samuel, B. Sherrill, J. Stevenson, A. Vander Molen, J.S. Winfield, Z.Q. Xie, R. Sherr, M. Gai, Z. Zhao, Proceedings of the 5th Internat. Conference on Nuclei Far From Stability, Rosseau Lake, I. Towner, Ed., AIP, NY, (1988).

2. D. Mikolas, B.A. Brown, W. Benenson, L.H. Harwood, E. Kashy, J.A. Nolen Jr., B. Sherrill, J. Stevenson, J.S. Winfield and Z.Q. Xie, Phys. Rev. C37, (1988), 766.

3. M. Samuel, B. A. Brown, D. Mikolas, J. Nolen, B. Sherrill, J. Stevenson, J. S. Winfield and Z. Q. Xie, Phys. Rev. C37, (1988), 1314.

4. J. Stevenson, B. A. Brown, Y. Chen, J. Clayton, E. Kashy, D. Mikolas, J. Nolen, M. Samuel, B. Sherrill, J. S. Winfield and Z. Q. Xie, Phys. Rev. C37, (1988), 2220.

5. Z. Zhao, M. Gai, B.J. Lund, S. M. Rugari, D. Mikolas, B.A. Brown, J.A. Nolen Jr., M. Samuel, "Beta decay of ^{18}N to alpha emitting states in ^{18}O, and parity violation in ^{18}O," NSCL Annual Report, 1987 (this volume).

6. T. Awaya, Nucl. Instr. Meth. 165, (1979), 317, ibid. 174, (1980), 237.

ECR ION SOURCE STATUS

T. Antaya, Z. Xie, D. Sanderson and K. Harrison

During 1987 work proceeded in several main areas. The RT-ECR continued to be used as the main ion source for the K500 cyclotron. The CP-ECR was completed in late March 1987 and the first lithium ions beams were extracted from the K500 cyclotron in April. Several lithium experiments were completed using the CP-ECR during the spring and summer. During these runs new development work was completed on the RT-ECR. This included the production of ions from solid materials by solid feed and vapor pressure oven techniques, and the operation of the source with a single transmitter via a power divider. During the fall the operating program shifted back to high charge state ion production using the RT-ECR, and this period was used for further alkali metal ion development using the CP-ECR. Work also continued on the design of the SC-ECR ion source, with the main focus of this effort being the development of prototype superconducting coils for the hexapole magnet. We decided that Z. Xie would study the charge dependence of the emittance of beams extracted from ECR ion sources, and towards this effort work, was started on a 3D extraction code ERAY, in order to study theoretically the dominant beam formation processes.

In November an International Conference on ECR Ion Sources and their Applications, sponsored by NSCL, was held at Michigan State University. There were 90 participants and over forty papers presented at this meeting, with approximately 1/2 of the papers from outside the U.S. and 1/4 of the papers on applications of ECR ion source technology. The next ECR Meeting, organized by R. Geller, will be held in Grenoble, France in September 1988.

RT-ECR Ion Source Status

The RT-ECR has operated 9000 hours since the first operation in July 1985, primarily in the mode with two Minimum B stages at 6.4 GHz. During the period from November 1, 1986 to November 6, 1987, the RT-ECR was under vacuum without component failures logging approximately 4000 hours of ion production. With the operation of the CP-ECR in 1987, several periods were available for continued development of the

Table 1. RT-ECR DC Performance for gaseous feed materials, Mar. 1988.

	^{12}C	^{14}N	^{16}O	^{20}Ne	^{40}Ar	^{86}Kr	^{127}I›
4	28.Ø	>1ØØ	87.	67.	19.		
5	6.1	68.	61.	5Ø.5	*		
6	*	25.5	52.	41.1	42.		
7		*	12.2	16.5	55.		
8			*	5.Ø	94.		
9				1.Ø	44.		
1Ø				*	*	23.	
11					7.6	*	
12					2.Ø	23.3	
13					Ø.33›	29.Ø	1.7
14					Ø.15›	29.Ø	2.3
15						23.2	3.Ø
16						*	*
17						6.8	2.7
18						3.2	*
19						1.4›	2.5
2Ø						Ø.4›	2.3
21							2.1
22							1.8
23							1.Ø
24							*
25							.Ø35››

Conditions: 1Ø kV ext. voltage; 8 mm ext. aperture.
› Vertical emittance decreased by 2.Ø to increase resolution.
›› Vertical emittance decreased by 6.Ø to increase resolution.
* Mixed M/Q

Table 2. RT-ECR DC performance for solid feed materials, Mar. 1988.

	^{7}Li	^{19}F	^{24}Mg	^{28}Si›	^{51}V	^{56}Fe	^{181}Ta
1	14.5	5.Ø	4.5	2.5			
2	14.5	5.Ø	8.4	1.Ø	6.1	8.Ø	
3	1.5	8.Ø	11.3	Ø.6	7.8	11.5	
4		14.Ø	13.5	1.7	8.7	15.7	
5		12.Ø	16	2.1	11.7	15.9	
6		7.Ø	*	3.Ø	12.6	11.4	
7		2.Ø	Ø.7	*	15.2	7.3	
8		Ø.1		Ø.6	13.5	1Ø.Ø	
9				Ø.2	6.5	5.5	Ø.4
1Ø					4.Ø	4.2	*
11					1.7	2.7	Ø.5
12						1.5	1.Ø
13						.42	*
14							1.6
15							*
16							3.1
17							3.6
18							3.6
19							3.1
2Ø							2.7
21							2.Ø
24							Ø.6
27							Ø.11
29							Ø.Ø8

Conditions: 1Ø kV ext. voltage; 8 mm ext. aperature.
› Vertical emittance decreased by 2.Ø to increase resolution.
* Mixed M/Q

RT-ECR. New beams of ions from solid materials were developed. The present performance of the RT-ECR is summarized in Tables 1 and 2.

CP-ECR Ion Source

Design work began in November, 1986 on a single stage ECR, the CP-ECR, ion source for low charge ions and lithium. This ion source, shown in Fig. 1, began operation in March, 1987, with the first lithium beam injection into the K500 cyclotron in April, 1987. During 1987, the CP-ECR was used primarily for lithium ion production, where vapor produced by the high temperature oven diffuses into the main stage where it is ionized. In order to minimize condensation in the main stage, a heated stainless steel liner is maintained at about 400°C. A typical lithium spectrum is shown in Fig. 2.

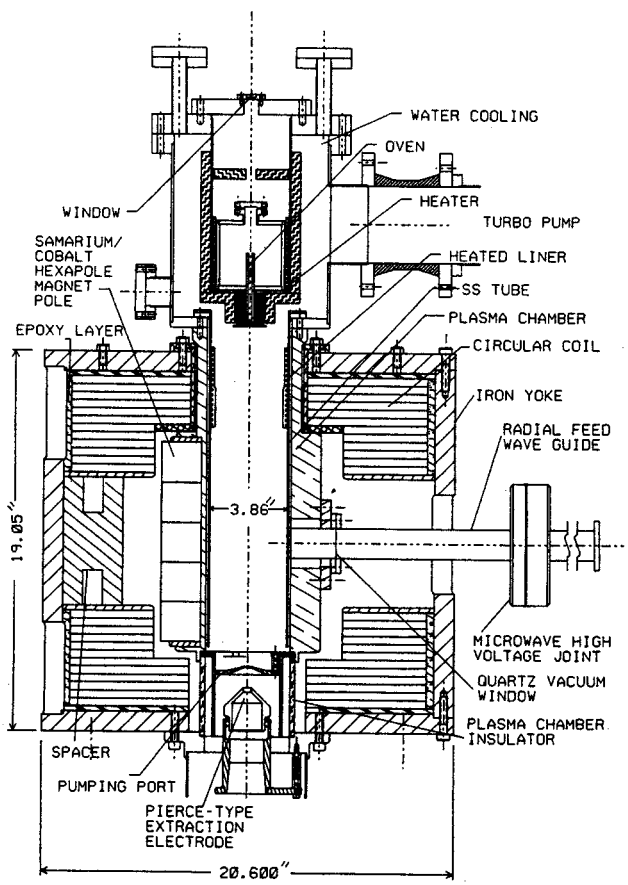

Fig. 1: The new CP-ECR, first operated in March 1987, is shown.

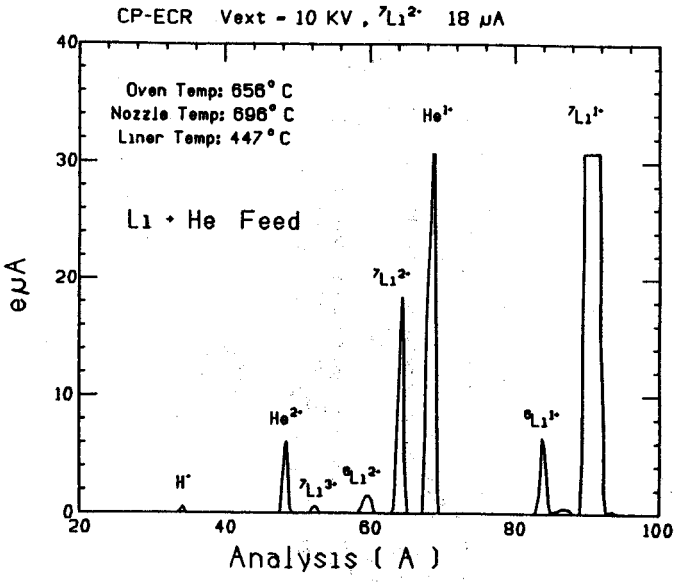

Fig. 2: Lithium ion production in the CP-ECR.

SC-ECR Ion Source

Work is proceeding on the design of the variable frequency SC-ECR ion source, shown in Fig. 3. The resonance frequency range is set at 5-35 GHz. In order to produce the required magnetic fields at the high frequency end, the SC-ECR has a full superconducting coil set. In other respects the SC-ECR design features are the same as the 6.4 GHz RT-ECR. The main motivations for this source are to provide a flexible design for wide ranging studies of magnetic confinement and resonance heating at fixed frequency, and to study cw ionization rate scaling with frequency.

The present effort is directed towards hexapole coil development with testing of prototype epoxy-impregnated coils to begin in early 1988. Initial operation of the ion source magnet should occur in mid 1988 if the coil development effort is successful. Ion source components will be built in parallel with the magnet development, so ion source operation, initially at 6.4 GHz, should follow shortly after the successful operation of the magnet sub-system.

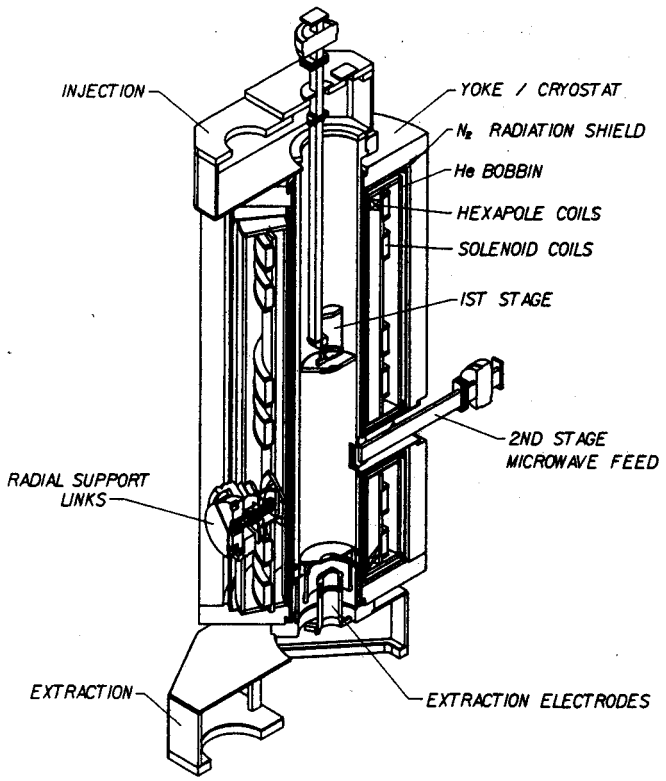

Fig. 3: The SC-ECR ion source, now in the design phase, is shown in schematic form for operation at low frequency.

STATUS OF STREAMER CHAMBER/CCD CAMERA EXPERIMENTS

C.A. Ogilvie, S. Angius, G. Crawley, C. Djalali, S. Howden, D. Krofcheck, R. Tickle[a], A. Vander Molen, G. Westfall, and K. Wilson

Two years ago an experiment that measured central collisions between Nb+Nb at 100 MeV/nucleon was performed at the streamer chamber facility at LBL. The events were viewed with three CCD cameras as described in a previous Annual Report.[1] Since then, approximately one hundred events have been analysed.[2] Manual corrections were made to tracks that were partially recognized by software. The tracks from different views were then matched (again by software with manual assistance) and the event was constructed into three dimensions. An approximate intensity for each track was found and used with the extracted rigidity in an attempt to identify the mass and charge of the particles.

It was found that the overall brightness of picture changes from event to event. This is thought to be due to different voltages applied to the streamer chamber by the Marx generator. As a result only sub-sections of the particles (in the forward cone and near beam rigidity) can be assigned a mass and charge with certainty. This required the use of a normalization factor for each event's brightness.

A second streamer chamber experiment was performed in November 1987. One of its aims was to reduce the variations in event brightness. Central collisions of Nb+Nb at 60 and 120 MeV/nucleon and La+La at 50, 70 and 130 MeV/nucleon were measured. The trigger was the absence of energy deposited in a forward scintillator that was co-linear with the beam.

Several improvements to the experimental technique were implemented. The engineers at LBL improved the stability of the voltage applied to the chamber. A voltage signal was picked off from the cathode and recorded along with the event. This may be used to normalize any remaining variation in the brightness. The signals from the trigger scintillators were recorded as well and will be used to determine the hardness of the trigger.

In order to take full advantage of the fact that the data are stored in digital form, this second experiment will be analysed fully by software. In this way sufficient statistics can be achieved in order to compare the results to theoretical models.

The track recognition program has been improved and its development is nearing completion. The major advance has been to use the information already obtained about a track fragment to find the rest of the track. The next task is to automate the track matching between the three views. It is planned to use, the intensity and the intensity-pattern along each track, in addition to geometrical information. Once reconstructed the intensity analysis will be improved by 1) taking into account overlapping tracks, 2) correcting for the changing solid angle as the particle moves towards or away from the camera, 3) including the transmission of light through the central electrode, and 4) the measured response of the CCD pixels[3] will be folded into the intensity values.

The intensity of each track will be used with the rigidity in an attempt to identify the mass and charge of the particles. It will be then possible to extract information from the distribution of particles and momenta in each event, e.g. the transverse momentum flow[4].

A possible enhancement to this project is the use of image intensifiers with the CCD cameras. This would enable the chamber to operate with lower voltages, thereby reducing the competition in the development of

streamers[5]. This will make the light output more directly related to the initial ionisation and hence improve the possibility of identifying a wide range of particles.

---

a. Physics Department, University of Michigan.

References

1. S.P. Angius et al., NSCL Annual Report p23, (1986).
2. S.P. Angius, PhD Thesis Michigan State University (1987).
3. D. Krofcheck et al., NSCL Annual Report (1987) and Y. Hiraoka et at., Science Vol. 238, 36 (1987).
4. P. Danielewicz and G. Odyniec, Phys. Lett. 157B, 283 (1985).
5. P. Rice-Evans, 'Spark, Streamer, Proportional and Drift Chambers', The Richelieu Press, London (1974).

INITIAL CCD CAMERA SYSTEM PERFORMANCE MEASUREMENTS

D. Krofcheck, G.M. Crawley, C. Djalali[a], S.D Howden, C. Ogilvie,
R.S. Tickle[b], A.S. Van der Molen, G.D. Westfall, D.K. Wilson

The MSU Charge-Coupled Device camera system has been used in two experiments[1,2] at the Lawrence Berkeley Laboratory. During the November 1987 run, an initial attempt was made to characterize the overall CCD system performance. The measurements included multiple exposures of the CCD chips to uniform light levels while the cameras were mounted in their holders on the LBL streamer chamber. This data also provided for each camera a pixel by pixel renormalization file which can be used in future picture enhancement and analysis efforts.

Uniform illumination of the CCD chips was accomplished with a red, diffused head light-emitting-diode (LED). A red diode was chosen as a close match to the color of the light produced by a charged particle's passage through the 90% Ne + 10% He gas mixture inside the streamer chamber. Such a choice was necessary due to the pixels frequency dependent quantum efficiency for detecting photons. The diode was supported on a stand placed inside the chamber's magnet yoke. A CCD chip to diode distance of 30 cm was used. An extra diffusive element, consisting of a sand blasted piece of 0.5 cm thick plexi-glass, was taped to each camera's aperture prior to exposure to the LED light.

A variety of light levels was simulated by increasing the exposure time for a fixed LED light level and distance. Multiple pictures were taken for the individual exposure times. The numerous pictures were averaged in order to minimize the uncertainties due to statistical fluctuations in photoelectron production inside the pixels. An overall average pixel value for the 221184 pixels, on a full scale of 4096, was then calculated and plotted versus the exposure time as shown in Fig. 1. The point labeled dark field in this figure represents the contribution to the pixels of thermally generated noise. Electrons shaken loose from the CCD chip silicon lattice by thermal vibrations are indistinguishable from electrons produced by incident photons. The small pixel value from the dark current contributed about 0.3% of a full scale saturation. This fraction can be reduced by running the cameras at even lower temperatures than the -35 to -40 degrees Centigrade used in the Nov. 1987 experiment.

A pixel by pixel renormalization file, also known as the 'flat field response' (ffr), was obtained from an average over many pictures using a single exposure time. This ffr file can be used as in Eq.1

$$F_p = (F_{exp} - F_{dark})/(\bar{F}_{ffr}/F_{ffr}) \qquad (1)$$

in which F_{exp} is a raw, exposed field. The quantity F_{dark} is the dark current produced in each pixel, F_{ffr} is the individual pixel

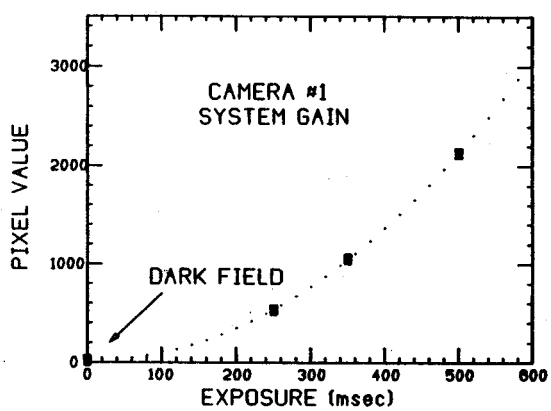

Fig. 1: System gain defined as the change in the average pixel value for a change in the exposure time when the CCD chip is uniformly illuminated. The dotted curve is drawn to guide the eye.

response to a uniform field and $\bar{F}_{ffr}$ is the overall average value of all of the individual pixel responses to that same uniform field. Here, F_p represents the final raw data field. Typically, averaging 10 to 15 pictures to obtain F_{ffr} is sufficient to produce a negligible deterioration in the quality of the $(F_{exp}-F_{dark})$ field. The effect of dividing by the ffr function is to make all of the pixels appear to have the same sensitivity to a given light level. Image enhancement and subsequent track recognition can then be performed using the F_p field. Figure 2 illustrates a typical response curve. In this figure, the average y pixel values in the two dimensional ffr field (576x384) have been calculated and placed in the corresponding x channel. Maximum pixel variations of <7% from $\bar{F}_{ffr}$ were observed. The shape of this curve was checked by moving the diode to different locations in front the CCD chip and retaking the pictures. A large spike near channel 576 may be due to an electronics or readout problem.

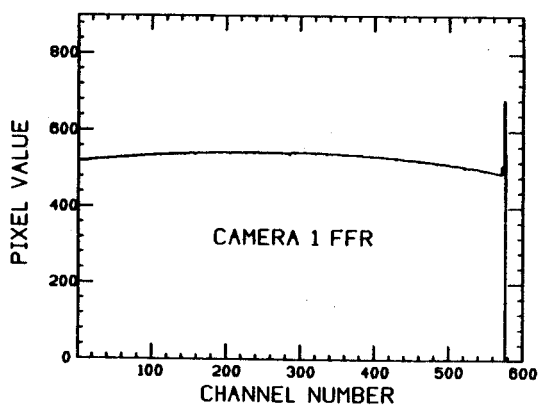

Fig. 2: A typical ffr response curve illustrating a maximum in the photon detection efficiency near the center of the CCD chip.

Presently, work is proceeding to remeasure the ffr function in a more secure optical environment than that provided by the streamer chamber. The system gain measurements are also planned to be extended to the full 4K saturation value of the CCD chips.

---

a. Insitute de Physique Nucleaire, Orsay FR.
b. University of Michigan, Ann Arbor MI.

References

1. NSCL 1986 Annual Report, p.23.
2. Ogilvie et al., 1987 MSU Cyclotron Laboratory Annual Report, pg. 220.

A CERENKOV RANGE TELESCOPE FOR HIGH ENERGY GAMMA RAY DETECTION

J. Stevenson, R.J. Radtke, W. Benenson, J. Clayton, K. Hanold, J.E. Hendrickson, E. Kashy, M. Mohar, D.J. Morrissey, T.K. Murakami, and C.L. Tam

Since the discovery of high-energy(E_γ>20 MeV) gamma ray production[1,2] in intermediate energy heavy-ion collisions in late 1984 there has been a rapid expansion of experimental and theoretical work on the subject. Detection of high-energy gamma rays produced in heavy-ion collisions is particularly difficult because of the large background of fast neutrons, penetrating charged particles, thermal neutrons and low energy gamma rays produced in the collisions. All of the background particles have production cross sections which are 10^4-10^5 times larger than the high-energy gamma ray production cross sections. This difficulty has stimulated the development and use of several novel detectors, including the Cerenkov range telescope[3,4] described in this report.

The basic idea behind the detector is to convert the gamma ray to an electron-positron pair in a thin BaF_2 detector and then stop the electron and positron in a stack of plastic Cerenkov detectors. The Cerenkov light output would then be used to determine if one or two electrons were present in the detector and thus determine the range of both the electron and positron in the pair.

The detector is shown schematically in Fig. 1. It consists of a .63 cm thick BaF_2 scintillator with a 10 cm X 10 cm active area followed by a stack of eight cerenkov detectors with active area of 23 cm X 23 cm The first and second Cerenkov detector elements were respectively, 1.27 and 2.54 cm thick The remaining 6 detector elements were each 5.08 cm thick. The Cerenkov detectors have a 23 cm X 23 cm active area which is connected by tapered light guides to 5 cm diameter phototubes (Hammamatsu R329) on the top and bottom of the detector element. The solid angle of the detector is defined by the solid angle of the converter and was 40 msr. The efficiency of the detector is determined by the pair conversion probability of the gamma ray in the BaF_2 converter and ranged from 10% at E_γ=20 MeV to 20% at E_γ=100 MeV. The minimum gamma ray energy was determined by the requirement that an electron or positron reach the second Cerenkov element. This corresponds to a threshold of about 10 MeV.

MSU-87-256

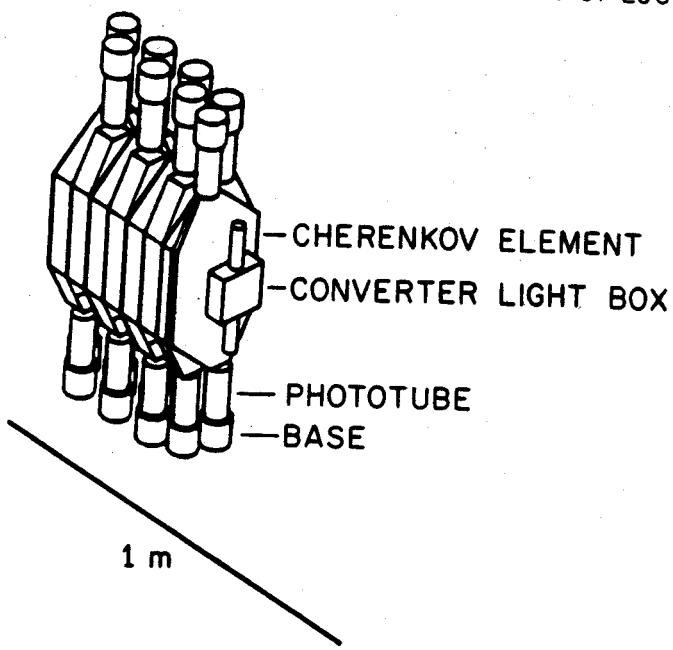

Fig. 1: A schematic figure of the detector, consisting of a .63 cm thick BaF_2 scintillator with 10 cm X 10 cm active area followed by a stack of eight plastic cerenkov detectors with 23 cm x 23 cm active area.

The calibration was done at the University of Illinois electron accelerator using their photon tagging spectrometer. Four electron beam energies were used 99, 77, 56 and 35 MeV. These beams provided tagged photons from 74-82 MeV, 53-61 MeV, 37-43 MeV, and 17-23 MeV respectively. The resolution and linearity of

the detector were determined by taking photons from 10 adjacent tag counters corresponding to an energy bite of 2 MeV.

Measuring the absolute efficiency of the detector was more difficult. This was done by comparing the efficiency of our detector relative to a large (30 cm diameter X 36 cm deep) NaI detector provided by the University of Illinois. The NaI detector was then assumed to be 100% efficient. Figure 2 shows a plot of the Cerenkov telescope efficiency as a function of photon energy. It is compared with the efficiency calculated from the pair production cross section and from a calculation using the Stanford electron-gamma shower code EGS4[5]. Both calculations are in reasonable agreement with the measured efficiency.

The gamma ray energy is calculated from the individual detector signals by taking the weighted sum given in Equation 1.

$$E_\gamma = \Sigma_i \ (\Delta E_i X(S_i/S_{0i})) \qquad (1)$$

In Equation 1, the sum extends over the eight detector elements, with ΔE_i being the additional electron energy required to increase the range from stopping in the front to stopping in the back of the i-th detector. S_i ,and S_{0i} are the signals from the i-th detector and the signal for a normally incident electron penetrating the i-th detector. Figure 3 compares the response of the gamma ray telescope for 22, 42, 60 and 80 MeV gamma rays to EGS4 calculations. The energies corresponding to the peak locations in figure 4 are systematically offset from the known gamma ray energy by about 7 MeV. Figure 4 shows this as a plot of peak location versus calibration energy. The calibration points are linear but too low by about 7 MeV. The cause of this offset appears to be due to the neglect of energy loss in the converter. By including the converter in the sum in Equation 1 it is possible to move (as shown in Fig. 4) all the response peaks to their correct locations. The response functions with the converter included are shown in Fig. 5. In this case the peaks are in the correct location and the resolution for lower gamma ray energies is considerably improved.

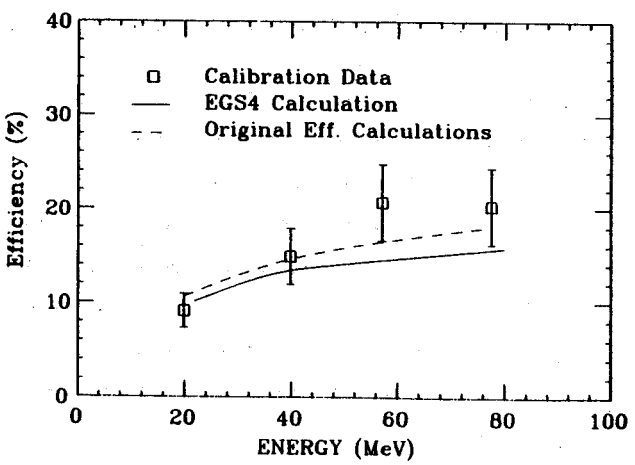

Fig. 2: The data points are the measured detector efficiency. The dashed curve is the calculated detector efficiency used in the cross section calculations of Ref 3. The dashed curve is an efficiency calculation using EGS4.

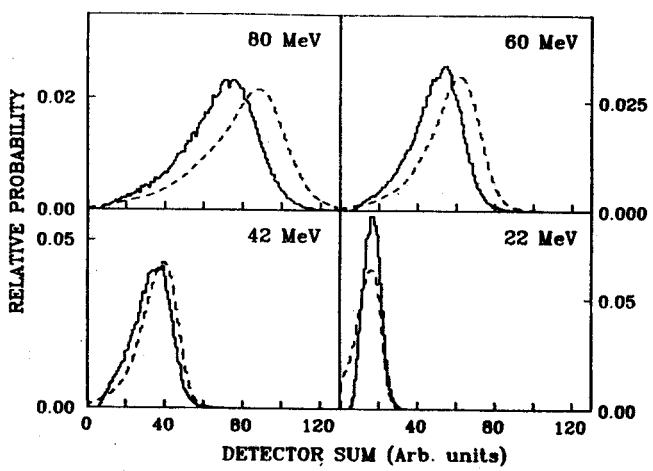

Fig. 3: Comparison of the measured detector response function (solid histogram) to an EGS4 calculation (dashed histogram), for gamma ray energies of 22, 42, 60, and 80 MeV.

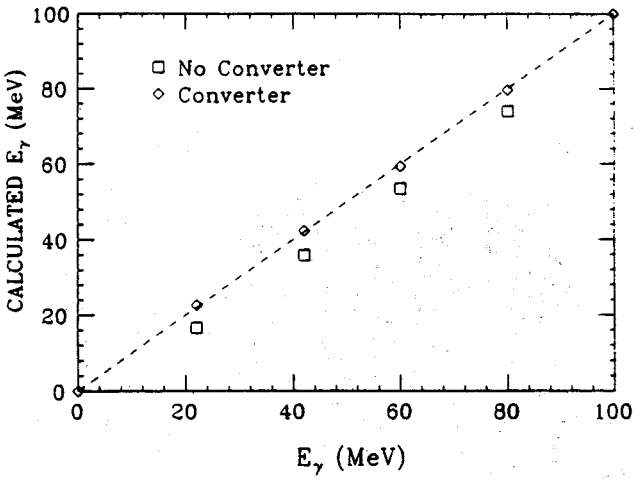

Fig. 4: Plots the peak in the detector response function versus the calibration gamma energy(squares). The dashed line is the ideal response. The diamonds are the peak response when an additional term proportional to the converter signal is added to the calculated energy.

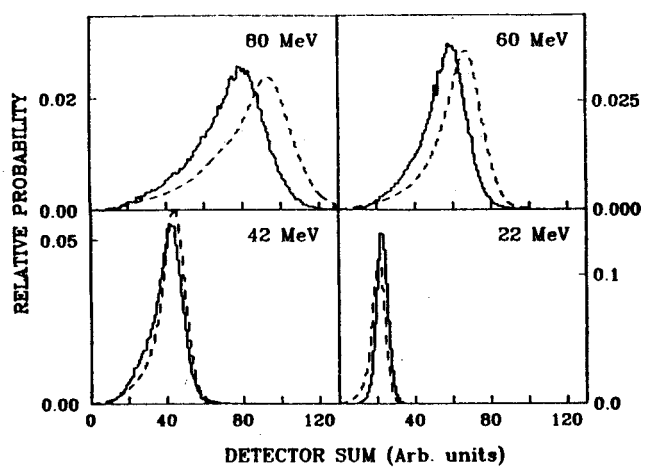

Fig. 5: Shows the measured response functions, solid histograms shown in Fig. 3 except an additional term proportional to the converter signal is added to the calculated energy. The dashed histograms are EGS4 calculations.

The systematic offset in the measured gamma ray energy using the original analysis method resulted in underestimating the gamma ray cross section in the data of Ref. 3. The E/A =40, 30, and 20 MeV data of Ref 3. can be corrected by multiplying the published data by factors of 2., 2.2 and 2.5 respectively.

References

1. E. Grosse, Proceedings of the International Workshop on Gross Properties of Nuclei and Nuclear Excitations XIII, Hirschegg, Austria, 1985.
2. K.B. Beard et al. Phys. Rev. C32, 1111 (1985).
3. J. Stevenson et al. Phys. Rev. Lett. 57, 555 (1986).
4. J. Stevenson et al. Submitted to Nuclear Instruments and Methods (1988).
5. W.R. Nelson et al. SLAC Publication SLAC-265 (1985).

THE 92 INCH SCATTERING CHAMBER

D.P. Sanderson, J. Nolen, R. Swanson, N. Mooney, and R. Blue

The 92 inch scattering chamber is a large piece of experimental equipment designed to house complex detector arrays in vacuum. The chamber contains the usual target mechanism and moveable detector mounts found in any general purpose scattering chamber. At the present, it is located in the interim experimental vault immediately outside the K800 cyclotron vault.[1] By modifying the end of its beamline, beams can be focussed through it into the 4π detector located outside the vault. This report briefly describes the chamber and its subsystems. Anyone wishing to design an apparatus for installation in the chamber should contact D.P. Sanderson for details.

The chamber systems can be divided into six parts: the vacuum vessel, the vacuum pumps, the experimental equipment, the control system, the exit beamline, and the alignment system.

The vacuum vessel is a large 234 cm diameter right circular cylinder on its side with its main flange in the vertical plane (Fig. 1). When installing equipment, 3/4 of the chamber is rolled back on the support frame. There are 17 small ports and 8 large ports for windows and feedthrus. Four large ported flanges in the front of the chamber are used for high vacuum pumps and the cantelevered support rails which extend into the chamber. Two 6-way crosses on the front and rear of the chamber are available for beam diagnostic devices or alternate target mechanisms.

The rough pumping of the chamber is accomplished by a belt driven 90 m^3/hr two stage mechanical vacuum pump coupled to a 500 m^3/hr roots blower. They are used to lower the chamber vacuum to 150 mTorr. At this level, two 2000 l/sec turbo pumps take over. Each turbo has a 60 m^3/hr mechanical pump on its foreline. With an empty chamber, this system

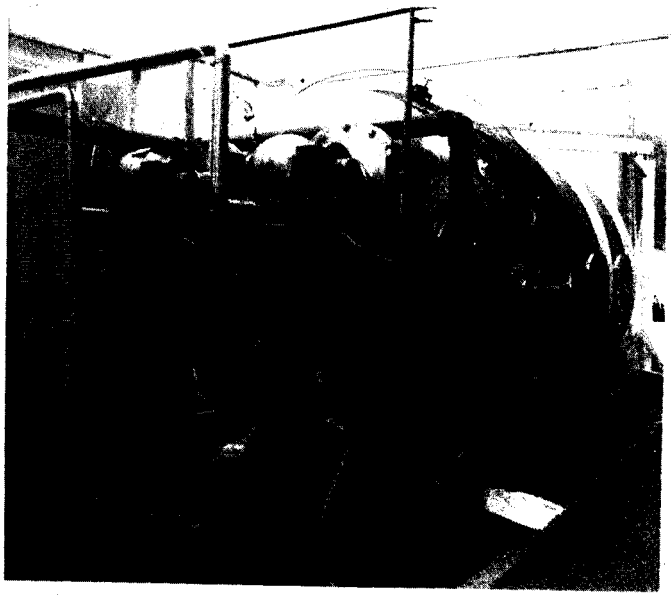

Fig. 1: Photograph of the 92 inch scattering chamber.

can pump the chamber to 150 mTorr in 40 minutes, to 1 x 10^{-5} Torr in 60 additional minutes and to 2 x 10^{-6} Torr overnite. A major problem will be the long pumpdown times expected when the chamber is loaded with multi-detector arrays, but this should be solved when the vacuum system is upgraded to liquid helium cryopumping (in late 1988).

The chamber has vacuum feedthrus for 20 kV target bias, 9 different gas or liquid lines, 60 SHV cables, and 300 BNC signal lines. The detector mounting platform is a square plate, 2.3 m^2 in area, resting on the two cantilevered rails. The target mechanism is mounted in the center and has capacity for 9 of the laboratory's standard targets. A 152 cm diameter turntable rated for 200 kg and a 75 cm arm rated for 20 kg are independently mounted on the base plate for installing moveable detector systems (Fig. 2).

The four motional degrees of freedom, target height, target angle, turntable angle,

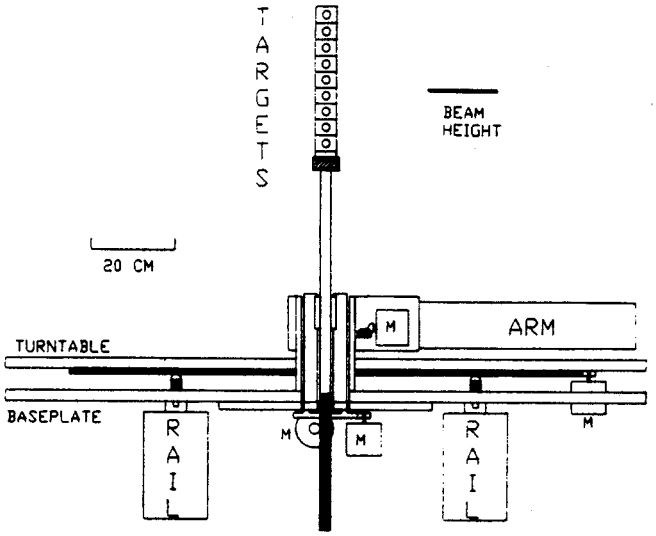

Fig. 2: The baseplate, target mechanism, turntable, and arm.

and arm angle, are varied using high torque 8-phase stepping motors in the vacuum vessel. The positions are monitored using independently geared absolute shaft angle encoders with local displays.

The control system for the stepping motors, encoders, and vacuum systems is outlined in Fig. 3. The stepping motors are controlled locally by a set of switches on the cabinet which holds their control electronics. Both the stepping motor controls and the encoders are interfaced through a camac crate in the distant Data-U to the control system VAX computer. The experimenters can easily change angle settings from the Data-U using any terminal and a simple control program. Through the ETHERNET network, the data aquisition computer has access to the encoder information for storage on the data tapes.

The vacuum systems and the local control switchpanel are wired to a programmable logic controller I/O crate installed next to the chamber. This crate communicates with the "584" controller which is used for all of the other vacuum systems in the area. Since the controller is on the MODBUS system, the vacuum status of the chamber can be monitored anywhere in the laboratory.

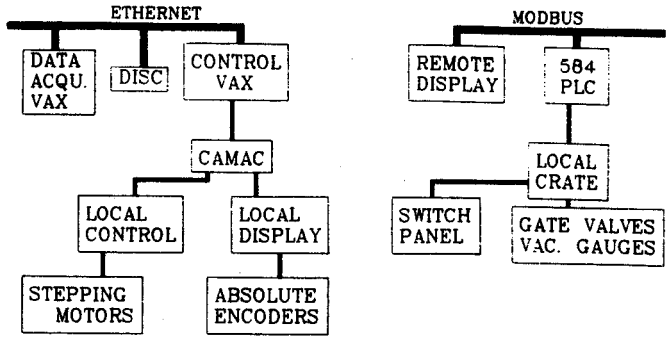

Fig. 3: The control system for the stepping motors and vacuum systems.

The exit beamline contains a diagnostic chamber for mounting either a scintillator or a wire scanner, a turbo pump, and a large classical faraday cup (Fig. 4). Since the chamber opens by rolling backward, the beamline up to the faraday cup is mounted on a wheeled cart resting on a set of angle iron tracks.

The radiation shielding in this area must accomplish two tasks, it must protect the outside of the vault from neutrons produced in the faraday cup and it must shield detectors from neutrons scattered at backward angles toward the chamber. At the same time, the shielding along the beam axis must be removeable so that beam can be focussed into the 4π detector. To protect the detectors in the chamber, the faraday cup is surrounded by 46 cm of steel and further upstream, a stack of concrete blocks surrounds the beampipe to shield against neutrons near the beam axis. At the end of the faraday cup, 100 cm of steel protects the next vault. This cylindrical shield is mounted on a large thrust bearing and a hole drilled through along a diameter allows a beampipe to be installed for using the 4π detector.

For the aligning of detectors and collimators in the chamber, a high precision telescope and mirror system is used. The alignment telescope is set with its optical axis along the beam axis on a removeable mount in front of the faraday cup. A mirror mount on a precision rotary motion stage is placed at the target position. By setting two angles, the

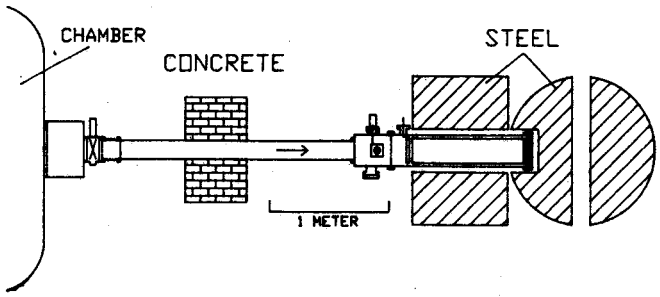

Fig. 4: The exit beamline and neutron shielding between the chamber and the 4π detector vault.

telescope can check the position of any detector.

The 92 inch scattering chamber is a general purpose device designed for large and heavy detector arrays which must operate in vacuum. All of the devices associated with the chamber can be operated remotely from the data taking area. Although its location in the interim vault will make setting up difficult, many useful experiments can be carried out in it with high precision. It will be available in the interim vault for experiments using the K800 cyclotron during the first year of operation and will later be moved to a permanent Phase II vault location.

References

1. B. Sherrill, et. al. contribution to this Annual Report, pg. 183.

IMPROVEMENTS IN THE ENERGY RESOLUTION OF THE S320

B. Sherrill, W.G. Lynch, T. Murakami, J.A. Nolen, R.M. Ronningen, D. Swan,
J.S. Winfield, and J.E. Yurkon

The NSCL users manual states that the energy resolution of the S320 spectrometer is predicted to be 0.1%, which corresponds to an image size of 0.8 mm at the spectrograph focal plane. However, in typical operation the resolution has not been better than 0.17%, or 1.4 mm. There are four possible explanations for the discrepancy. First, the spectrograph optics could be bad. Second, the detector resolution could be worse than 0.8 mm. Third, the beam might not be correctly dispersion matched; and finally, the incoherent spot size might be larger than the 1.0 mm assumed for the calculations. In order to determine which of the above effects (or combination of the above) is responsible for the poor spectrograph resolution, we have performed a series of tests using elastic scattering of ^{12}C and ^{14}N ions.

The first reason could be important if the optics of the spectrometer did not agree with the calculations, e.g. if there were imperfections in the magnetic fields which are not included in the calculations. This effect would primarily dominate the resolution for experiments using the full solid angle of the spectrometer. However, even at small solid angles the resolution is typically not better than 0.17%. Therefore, even though this effect has not been completely studied, it can not be the limiting effect.

Poor detector resolution is one of the more likely causes of the degraded energy resolution. As described in annual report contributions for past years, the S320 uses resistive division of the charge collected on a proportional wire to obtain position. These position sensitive detectors have been studied with alpha sources, and give a resolution of better than 0.4 mm. This is close to the calculated resolution based on the energy loss of the alphas, gas type, electric field, and the detection electronics. Figure 1 shows the position resolution measured for a variety of ions, energies, and total charge collected on the resistive wire. The values in Fig. 1 were determined by placing a second identical wire 1 cm behind the first and taking the difference in position. The FWHM of the resulting distribution for elastic scattering peaks divided by $\sqrt{2}$ gives the FWHM of one of the detectors. Unless otherwise noted, the detector is filled with 50 Torr of isobutane, and the detector voltage is varied to change the integrated charge. As one can see from the figure, the resolution is much worse for higher velocity ions, with the resolution of the low velocity ^{12}C ions equal to the results for the alpha source. Figure 2 shows the difference in peak shapes for the 10 MeV/A and 45 MeV/A ions. In the higher velocity case, there is an effect which gives large Lorenzian-shaped tails. It is also clear from Fig. 1 that at higher ion velocities a large fraction of the discrepancy in the energy resolution of the S320 is due to detector resolution.

There are several possible causes of this degradation in detector resolution at higher ion velocities. The most likely are δ-electron production, UV-photon production, or space charge effects near the wire. Originally, we thought the problem must be due to δ-electrons. In order to study this we have taken the formulas of Sauli[1] for the production probability and energy distribution of δ-electrons. We then make a simulation where the

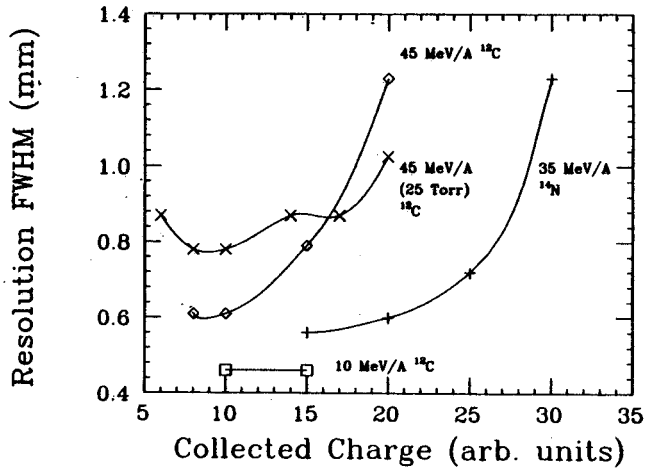

Fig. 1: S320 detector position-resolution versus integrated charge for ^{12}C ions with various energies. The gas is isobutane of pressure 50 Torr, unless otherwise noted.

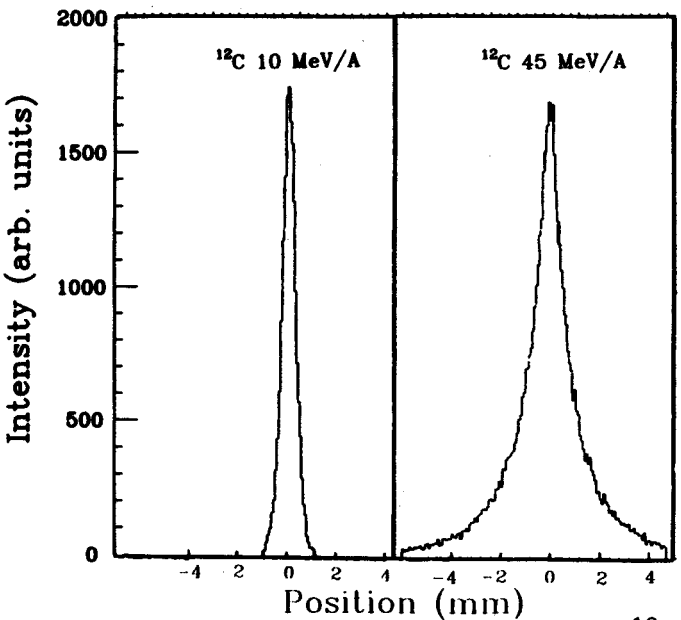

Fig. 2: Peak shapes for elastic scatter ^{12}C ions of 10 MeV/A and 45 MeV/A. At the higher energy the peak is considerably broadened.

centroid of the particle track is shifted by an amount as if the δ-electron deposited all of its energy at the end of its range. This should be an over-estimate of the effect of the δ-electrons. Figure 3 shows the centroid shift in cm for a simulation with 1000 ^{12}C ions of E/A = 50 MeV. From the simulation it is clear that δ-electron production cannot explain the shifts seen in the data. The dashed line in the figure

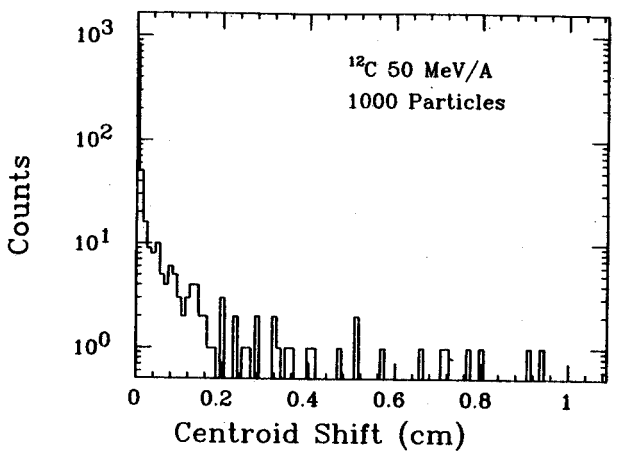

Fig. 3: The calculated effect of δ-electron production on position resolution. The calculation is from a simulation of 1000 ^{12}C ions of E/A = 50 MeV. The simulations show that at these velocities, δ-electron production should have little influence on the measured centroids.

shows the measured peak shape for ^{12}C ions of E/A = 45 MeV. Presently, the problem is under consideration.

Although the detector resolution was confirmed to be better than 0.8 mm, it was found that elastic scattering peaks were still more than 1.5 mm wide. This difference was found to be due to a combination of incorrect dispersion matching in the beam line from the cyclotron to the S320, and a large incoherent beam spot size at the S320 target. In the beam line, the slits at Box 1 are assumed to be the object for the system. By placing an 0.5 mm slit at Box 1, and setting the quadrupole currents based on a prediction by the program TRANSPORT[2], a focal plane spot size of 0.75 mm was measured for a 45 MeV/A ^{12}C elastic scattering peak. This was the first demonstration of 0.1% energy resolution of the S320 spectrometer. Increasing the Box 1 slit size to 2 mm increased the focal plane spot size to 0.85 mm, exactly as expected given a beam line magnification of 0.4, and a detector resolution of 0.65 mm. Therefore, we conclude

that with careful tuning of the beamline it is possible to perform experiments with resolutions of close to 0.1%. A problem with this type of tuning is that the dispersion at Box 1 must be known. Further, the cyclotron must be stable during the run, since changes in the cyclotron could change the box 1 dispersion and reduce the spectrometer resolution. If the dispersion matching is not done correctly at all times, then the spectrometer resolution is limited by the cyclotron beam energy spread.

In conclusion, we believe at present the S320 resolution is limited by detector resolution and beam energy spread from the cyclotron. The source of the poor detector resolution is not understood, and we plan to study this further. However, it appears with careful beamline tuning, resolution in the range of 0.1% is possible, but is sensitive to the tuning of the cyclotron if the full beam intensity is desired.

References

1. F. Sauli, CERN Report 77-09, May 1977.
2. K.L. Brown, D.C. Carey, Ch. Iselin, and F. Rothacker,TRANSPORT computer program, CERN Report CERN 80-04.

NUCLEAR ELECTRONICS DEVELOPMENT

M.R. Maier, K. Niemeyer, M. Robertson, and James Vincent

This year our main work has been concentrated on building special electronics for the different experiments. The exceptions were the quadruple fast-slow shaping amplifiers. These have all been debugged and brought to the same state of performance. The experience of the experimenters with these modules has led to a redesign which is still not finished since new requirements have come up; the requested changes are in the slow channel; shorter peaking times 0.5μs to 3 aμs, and 10V output on 1K, and in the fast channel the possibility to control the timing filter gain from the front panel.

On the special electronics side we have built many modules for the 4π detector. One type of these were the Splitter Boxes, the socket assemblies and the Divider Boxes for the Photomultiplier tubes used on the fast-slow plastic elements of the 4π detector.

These have been built with the following features: the voltage dividers are of the active type (with MOSFET'S as source followers), and the socket assemblies and the splitter boxes were designed so that we need only one coaxial cable to supply the high voltage to the photomultiplier tube and to feed the signal to the different ADC's and discriminators. The splitter boxes have been packaged in single wide NIM modules, with a block connector supplying the high voltage from a commercial (LeCroy) power supply. The high voltage connectors to the photomultiplier tubes are on the back, and the three signals ΔE, E, and time on the front, which allows very efficient packing and connections. We hope to use the same "single cable trick" with the PPAC preamplifiers. There we are going to use commercial RF-amplifier I.C.S. (MAR-6 from mini circuits) where the power supply can be used also as the output signal line.

This year we have built many variants of charge sensitive preamplifiers. The different requirements could all be met with essentially one low power circuit. For the 4π detector we have built 40 preamplifiers for low detector capacitance. For an experiment at the RPMS we built 5 charge sensitive preamplifiers with gain switching by a factor of 10 with a short (< 10 μs) recovery from the gain switch transient.

For the CsJ hodoscope we built 50 small preamplifiers for use with photodiodes to readout CsJ scintillators. As is shown in the figure, this amplifier is compact, and does not use special semiconductor packaging (like eg. SMD). For the silicon ΔE detectors of this hodoscope we have developed a variant of this circuit with faster rise-time (< 20ns) and an onboard calibration pulser. We intend to produce these with different dynamic ranges and calibrations. Since these fit on relatively small boards, we made them modular, so that we can tailor the dynamic ranges and calibrations to different experiments, instead of using high power commercial preamplifiers.

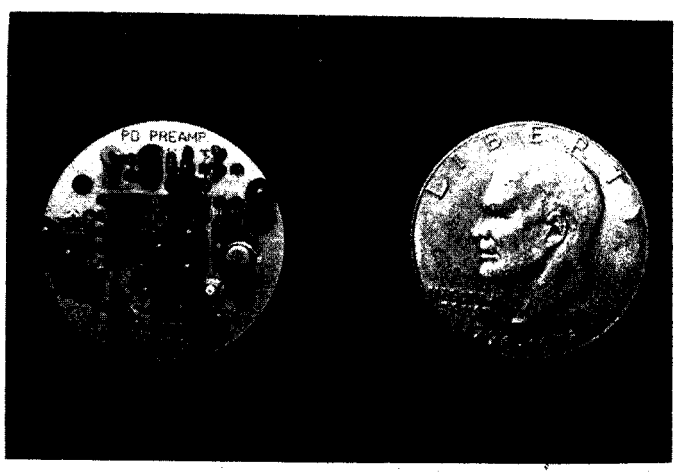

Fig. 1: Photograph of the Photo Diode preamplifier. Notice the small size, even though standard Semiconductor packages were used.

We hope to be able to build these boards for a fraction of the cost of the commercial switchable preamplifiers. Because of their low power consumption they can all be used in vacuum.

We have also built a prototype of a 4 x 6 input, 4 x 6 output fast NIM fan-in fan-out module for use in the 4π detector.

We have started the development of a fast decision module in ECL line technology based on a fast 65K x 1 static RAM. This will be used in experiments with the fully instrumented 4π detector.

A collaboration with David Fossan's group at Stony Brook has built a prototype of a simplified low cost pulse shape discriminator for use with NE213 plastic neutron detectors and inorganic scintillators like BaF_2. Tests at Stony Brook have shown good performance and we foresee the use of this device for the high energy gamma ray detector here, which will use BaF_2, for background suppression from charged particles.

Among our future projects is the development of a fast improved multichannel ADC system, where the zero suppression and readout can be "pipelined", thereby reducing deadtimes. It is planned to use Application Specific I.C.S (ASIC'S) for the digital part of these devices, and have charge integrating, peak sensing, and time measuring versions of this unit.

PROGRESS ON THE LOW ENERGY π^-/π^+ 0° SPECTROGRAPH

Y. Chen, E. Kashy, W. Benenson, N.C. Bhattacharya, and S. Tanaka

Pion production in intermediate energy heavy ion collisions has generated active research both theoretically and experimentally for the past ten years. In one of the earliest experiments (Benenson et al.[1]), an anomaly in the π^-/π^+ ratio at 0° for pions of velocity near the beam velocity was found. Since then, a significant amount of data has been obtained, and similar phenomena have been observed at higher energies[2,3,4]. In contrast, there are not many data at low energies. Such data give information on the source of pions. Experiment 86033 was proposed to extend such measurements down to energies as low as E/A=35 MeV. To accomplish this, a special pion spectrograph is needed.

The spectrograph is designed to separate pions produced at 0° from beam-like particles by means of a nearly 180° deflection and to disperse the pions according to their momenta. The scheme is illustrated in fig. 1. We are modifying a 90°, C shaped magnet known as the 'Michigan Magnet' which was not in use. In order to plan the modifications, we measured the field in the radial direction. The field was found to be flat in the gap, and of magnitude of 8.2 KG with a current 250 A. Such a flat field would only give horizontal focusing, but not the vertical focusing neccessary to bring the focal plane outside the gap of the magnet. In addition, the field has to be raised to about 12 KG to keep the orbit of 16 MeV pions in the field. With those requirements, we designed a vacuum chamber the top and bottom plates of which are wedges of steel. This serves to both give some vertical focusing for the pions and to increase the field. The plates have been made, and with those plates in position we have made more field measurements. Using those measured fields, we did some preliminary calculations of the orbits (see in fig. 2). These calculations were carried out for a gap of only 2 inches. When the plates are in position, a gap of only 0.4 inch is left at the entance, and this would be too small for our purpose. We are presently having iron spacers constructed to increase the gap. The design of the chamber, front flange and beam dump have been completed. The detector is being studied, and we expect the whole system to be ready in July of 1988.

References

1. W. Benenson, et al. Phy. Rev. Lett 43 (1979) 683, Phy. Rev. Lett. 44 (1980) 543.
2. K.A. Frankel, et al. Phy. Rev. C, Vol. 32 (1985) 975.
3. E. Chiavassa, et al. Nucl. Phys. A422 (1984) 621.
4. S. Nagamiya, et al. Phys. Rev. C, Vol. 24 (1981) 971.

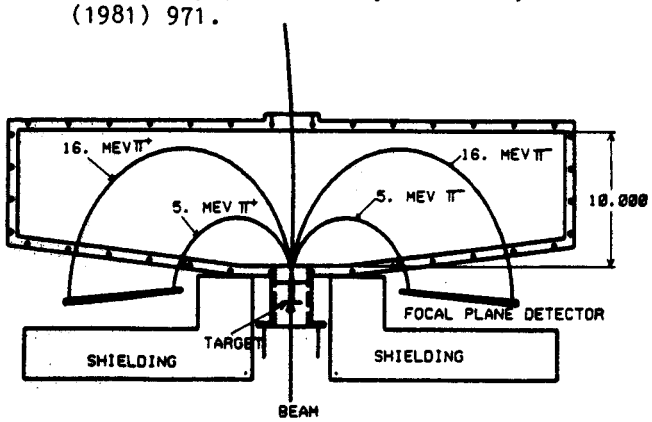

Fig. 1: A schematic drawing of the spectrogragh.

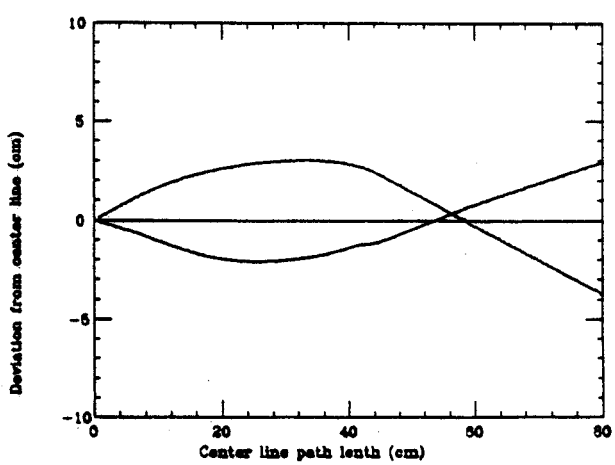

Fig. 2: The envelope of the pion orbit (16 MeV).

CALIBRATION OF PHOSWICH DETECTORS USING THE FRAGMENTATION FROM 50 MEV/N ^{14}N + TA

S. Howden, D. A. Cebra, J. Karn, D. Tristano, K. Wilson, G.D. Westfall

We used the foward angle fragmentation from the reaction 50 MeV/n ^{14}N + Ta to provide a range of energies and particle types to calibrate our phoswich detectors. A Ta target was placed in Box 1 which is located in the beamline just downstream from the K500 cyclotron. It was calculated that a target with a thickness of 37 mill would be sufficient to just stop the beam. The beamline bending magnets, BM1 and BM2, were then used as a rigidity selector for the fully stripped fragmentation particles. The rigidity selector was enhanced by the long flight path between the bending magnets and the 60" scattering chamber. The beamline was tuned to transport only particles with 70% of the rigidity of the original beam. Inside the chamber were 18 fast/slow plastic scintillator telescopes mounted separately on the rotating table. Each telescope was calibrated by moving it directly into the fragmented beam. Fig. 1 shows a raw plot of the slow gate versus the fast gate for the phoswich signals. The labeled isotopes were determined from the Z-bands that had been identified earlier in the experiment. As is apparent in Fig. 1 corrections must be made in order to extract energy calibrations.

The signal from the photomultiplier tube is comprised of the superposition of the signal from the fast scintillator, which has a 10ns rise time and a 20ns decay time, and the signal from the slow scintillator which has a rise time of 50ns and a decay time of 300ns. The first part of the signal is gated for the fast signal with the remaining part gated for the slow signal. Part of the true slow signal will fall within the fast gate while part of the true fast signal will fall within the slow gate. The amount of offset produced in the fast and slow signal histograms is linear; this can be seen

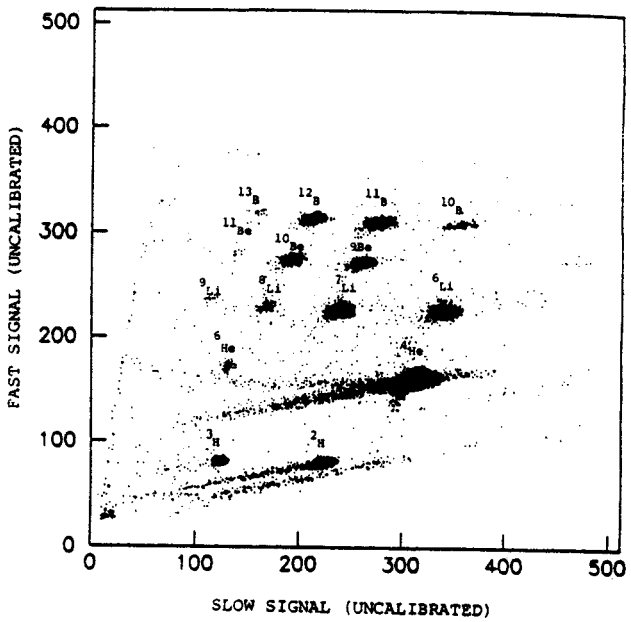

Fig. 1: Raw signal from the fast gate versus the raw signal from the slow gate for the ΔE-E phoswich telescope.

in Fig. 1. Correcting for these offsets produces a plot where the "channel" number for each scintillator will correspond to the pure signal from that scintillator.

The process was repeated with an aluminum degrader ladder placed inside the 60" scattering chamber. The thickness of the degrader varied in incremental steps and was raised into the fragmented beam. Several runs were made with the degrader ladder at different heights. By running an enegy-loss program for the various fragments incident upon each step of the degrader the residual energies could be found. An energy versus "channel" plot was then made for each scintillator and a third order polynomial fit was done on the data. Fig.s 2 and 3 show the calibration curves for the ΔE and E detectors respectively.

To check these results a silicon ΔE-E telescope, which was previously calibrated with pulsers, was placed in the chamber. Several

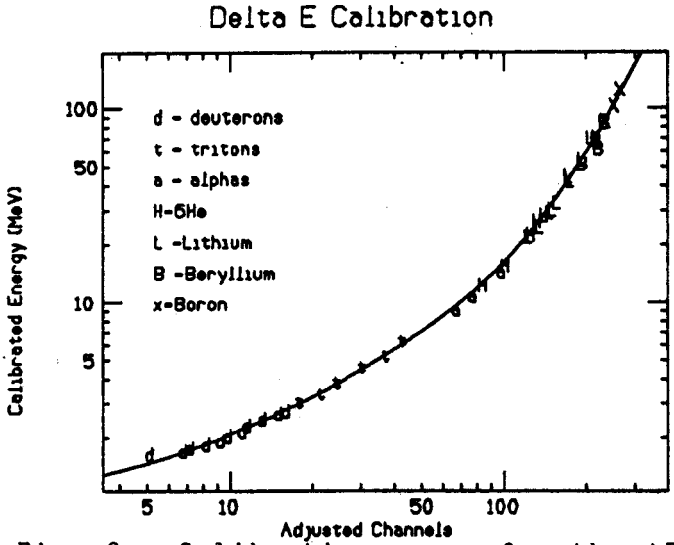

Fig. 2: Calibration curve for the ΔE scintillator.

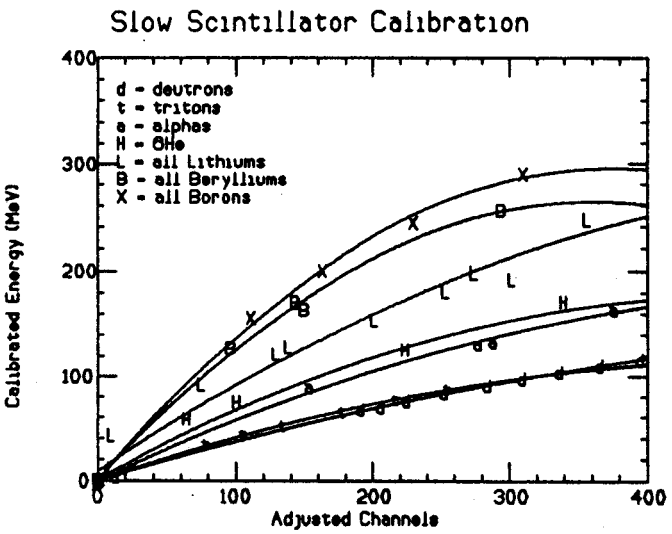

Fig. 3: Calibration curves for the E scintillator.

runs were made with the degrader at various heights. This gave us an independent measurement of the energies of the various istopes and these values agreed with the results of the energy-loss program. The silicon detector also gave us an energy resolution of 7% for the fragmentation beam.

RESOLUTION TESTS OF CsI(Tl) SCINTILLATORS READ OUT BY PIN DIODES

W.G. Gong, Y.D. Kim, G. Poggi[a], Z. Chen, C.K. Gelbke, W.G. Lynch,
M.R. Maier, T. Murakami, M.B. Tsang, H.M. Xu, and K. Kwiatkowski[b]

The study of intermediate energy heavy ion reactions often requires the detection of coincident light particles (p, d, t, α, ...) emitted with energies ranging from the exit channel Coulomb barriers up to several hundred MeV. For moderate resolution requirements, plastic scintillators are adequate. Better resolution can be obtained with inorganic scintillators such as NaI(Tl), for which energy resolutions of the order of one percent have been obtained for light particles of about 100 MeV energy, see for example ref. 1.

Particle detectors using NaI(Tl) scintillators have a number of disadvantages. The crystals are hygroscopic and must be hermetically sealed; the detectors usually employ photomultipliers for photon detection which exhibit rather poor long term stability, particularly when operated in vacuum. Although it is possible to monitor gain drifts with accuracies of the order 1%, the procedures used are rather time consuming and cumbersome.[1,2]

The use of CsI(Tl) scintillators promises to overcome some of these difficulties. The crystals have superior thermal and mechanical properties. Since they are only slightly hygroscopic they do not have to be hermetically sealed. Furthermore, their spectral response is well matched to that of silicon photodiodes which exhibit excellent long term stability when read out with good quality charge sensitive preamplifiers.[3] We have performed detailed resolution tests for a number of larger volume cylindrical CsI(Tl) scintillators of 38 mm diameter and 100 mm length read out by a 400 mm^2 PIN diode. These detectors can stop protons up to energies of about 190 MeV and alpha particles up to energies of about 780 MeV.

A low cost preamplifier of good resolution and low power dissipation was designed by one of us (M.R.M.), see also pg. 233.

Figure 1 shows a scan of a typical detector response obtained by moving the collimated radiation source (scattered protons and α-particles as well as γ-rays) along a diagonal of the circular entrance window of the detector. Plotted is the percentage shift of the peak location measured at position X as compared to the peak position measured at the center, X=0. The exact magnitude of the measured shift depends on the nature of the detected radiation. This can be expected from the different penetration depths of γ-rays, protons and α-particles. For all three measurements, the detector exhibits a response which is distinctly left-right asymmetric with respect to the cylinder axis, X=0. With a collimator of 3 mm diameter, the detector exhibits an excellent energy resolution of the order of one percent for α-particles of 94 MeV. Because of the strong position dependence of the detector response, the energy resolution is considerably worse if a larger collimator is used. With a collimator of 20 mm diameter a double humped peak structure was observed with a full width at half maximum of about 3%.

Figure 2 shows the energy resolution obtained with a ΔE-E telescope consisting of a 400 μm silicon detector and a CsI(Tl) crystal selected for uniformity of reponse to collimated ^{137}Cs γ-rays entering through the front face. Using a collimator of 3 mm diameter, we obtained an energy resolution (FWHM) of 1.0% for 55 MeV protons and 0.8% for 92 MeV α-particles. Due to the rather uniform response of this crystal, the detector resolution is of comparable quality

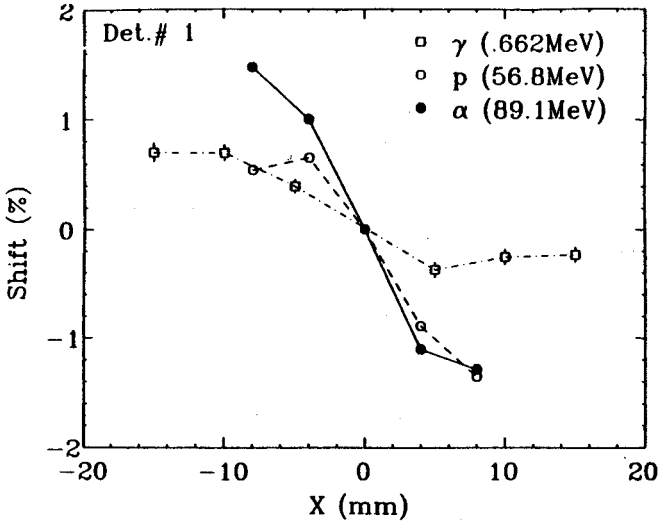

Fig. 1: Left-right asymmetric response of a representative crystal for collimated Υ-rays of 662 keV, protons of 56.8 MeV, and α-particles of 89.1 MeV. Shown is the relative shift of the peak centroid as a function of the X-coordinate of the collimator, keeping Y=0. The data are normalized to the peak position measured for X=Y=0.

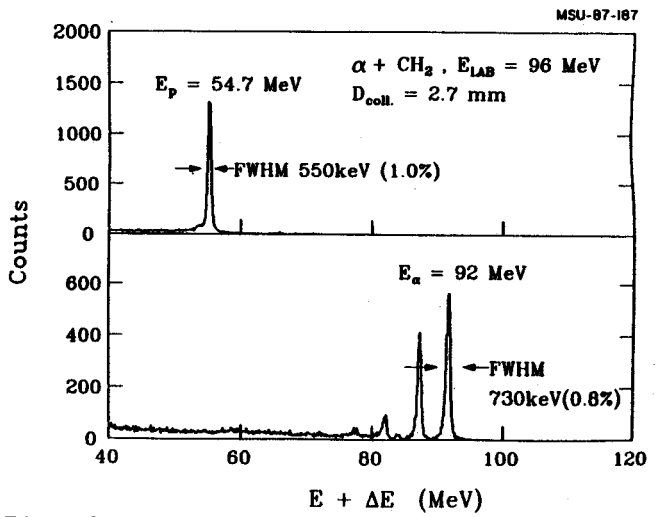

Fig. 2: Energy spectra of protons and α-particles obtained at θ=20° for reactions induced by 96 MeV α-particles on a CH_2 target. The detector collimator was 3 mm in diameter. The detector had been selected for uniform response to Υ-radiation entering the front window.

for larger collimators. For 95 MeV α-particles (obtained from the elastic scattering on Au), a resolution of 0.9% was measured with a collimator of 20 mm diameter. The tests shown in Fig. 2 probe only a small fraction of the crystal. In order to investigate the response to more penetrating radiation, we performed measurements with protons of 178 MeV. Using a collimator of 3 mm in diameter a resolution (FWHM) of 1.4 % was obtained. When a 25 mm diameter collimator was used, the energy resolution was 1.7%. Scans of the detector response revealed non-trivial position sensitivities for protons penetrating to the rear end of the crystal. The nonuniformity of response at the rear end of the crystal was later confirmed with a bench test using collimated Υ-rays which were injected at that side of the crystal.

Our results indicate that the resolution of larger CsI(Tl) crystals is mainly limited by local inhomogeneities of the crystal response. Improved fabrication techniques might overcome these limitations. High quality CsI(Tl) crystals read out by PIN diodes promise to provide excellent particle detectors of good stability and energy resolution.

a. University of Florence, Italy.
b. Indiana University Cyclotron Facility, Bloomington, IN 47405, USA

References

1. J. Pochodzalla, C.K. Gelbke, W.G. Lynch, M. Maier, D. Ardouin, H. Delagrange, H. Doubre, C. Grégoire, A. Kyanowski, W. Mittig, A. Péghaire, J. Péter, F. Saint-Laurent, B. Zwieglinski, G. Bizard, F. Lefèbvres, B. Tamain, and J. Québert, Y.P. Viyogi, W.A. Friedman, and D.H. Boal, Phys. Rev. C35 (1987) 1695.
2. C.B. Chitwood, D.J. Fields, C.K. Gelbke, D.R. Klesch, W.G.Lynch, M.B. Tsang, T.C. Awes, R.L. Ferguson, F.E. Obenshain, F. Plasil, R.L. Robinson, and G.R. Young, Phys. Rev. C34 (1986) 858.
3. E. Blucher, B. Gittelman, B.K. Heltsley, J. Kandaswamy, R. Kowalewski, Y. Kubota, N. Mistry, S. Stone, and A. Bean, Nucl. Instr. and Meth. A249 (1986) 201.

MEASUREMENTS OF ^{131}I AND ^{137}Cs IN EAST LANSING FROM CHERNOBYL REACTOR ACCIDENT

Y.M. Chen, E. Kashy, J. Yurkon, R.M. Ronningen, and R. Lassin

Abstract

Concentrations of ^{131}I and ^{137}Cs in air, rain water, and river water were measured in East Lansing during late April and early May, 1986. The concentration of ^{131}I in air samples showed a four day peak, between 0.5 and 1 picocurie/m^3. In rain water the concentration of ^{131}I was found to be 420 picocurie/liter. In river water ^{131}I was not detected above background.

Introduction

On April 26, 1986, an accident occurred at the Chernobyl nuclear power plant in the Soviet Union. A significant amount of radioactive material, including core fragments, escaped. Prevailing winds spread some of it to the U.S. There was much public confusion about the nature and hazards of the radiation. We were interested in the quantitative aspect of the radioactivity in this area, ie., how serious was it? How do the concentrations of radioactive fallout compare to the maximum permissible concentrations in the regulations of Michigan Department of Health? We performed an experiment to measure radioactivity from the fallout by sampling and collecting water from rain and a river.

First, we had to determine which nuclei to study. The criteria were as follows: i) they must be major fission products, ii) the radionuclides must be long lived to get here, iii) they must have high enough concentrations to be of concern for safety reasons, and iv) the characteristic radiations can be measured by our equipment. The processes that occur in the nuclear reactor are as follows:

$$^{235}U + n \rightarrow \text{fission fragments}$$
$$^{238}U + n \rightarrow {}^{239}U$$
$$^{239}U \rightarrow {}^{239}Np + \beta^-$$
$$^{239}Np \rightarrow {}^{239}Pu + \beta^-$$
$$^{239}Pu + n \rightarrow \text{>73\% fission}$$
$$\rightarrow {}^{240}Pu + n \rightarrow {}^{241}Pu + n \rightarrow \text{>70\% fisson}$$
$$\rightarrow {}^{242}Pu$$

In the fission, ^{131}I and ^{137}Cs are major products. The half-life of ^{131}I is 8 days, that of ^{137}Cs is 30 years. ^{137}Cs tends to distribute throughout the body whereas ^{131}I is readily absorbed by the thyroid gland. The regulations of Michigan Department of Health for the maximum permissible concentrations above natural backgrounds in releases to uncontrolled air and water for ^{131}I in soluble form are: in air, $3x10^2$ pCi/m^3, and in water, $2x10^3$ pCi/liter.[1] In the decay of ^{131}I the most probable gamma ray has an energy of 0.364 MeV (branching ratio 0.81) and in the decay of ^{137}Cs, the γ ray energy is 0.6616 MeV (branching ratio 0.85). These can be efficiently detected by high resolution gamma ray detectors.

The γ rays from ^{131}I and ^{137}Cs were detected by a high purity Ge γ ray detector, having 33% efficiency (relative to a 3 in x 3 in. NaI detector at 25 cm) and 1.90 keV energy resolution at 1.33 MeV. The detector was surrounded by Pb to reduce the background. The electronics were set up to detect gamma rays having energies 40 keV to 1 MeV. The air sampling was done using a high velocity air sampler with paper filters. The efficiency for capturing the radioactivity was estimated from a double filter arrangementnt. We found that 80% of radioactive dust was captured in first filter.

The energy calibration was done using ^{152}Eu source. Using the known strong lines, we

performed a linear least-square fit relating γ energy to channel number. We measured gamma energies to within 0.5 keV. The intensity calibration was done using 0.84 microcurie ^{133}Ba source with the same geometry as the air filter paper sample. This source emits a 356 keV gamma ray (branching ratio 0.621), thus giving the efficiency for detecting the 364 keV ^{131}I gamma ray almost directly. We determined the intensities to within 20%.

We made measurements from April 30 to May 15, 1986. Each day we made a background measurement and a sample measurement, and both were counted for 1 hour. The sample collection time was of one half hour. A typical background run is shown in Fig. 1, where some peaks are identified and the position of the peaks of ^{131}I and ^{137}Cs are indicated. Starting May 10th we saw peaks where ^{131}I and ^{137}Cs should be. ^{137}Cs shows up in both the background as well as in the sample ^{137}Cs is present in the background because of atmospheric nuclear weapon tests during past 40 years). Therefore we used ^{131}I alone as the indication of fallout. A sample measurement is shown in Fig. 2. The peak for ^{131}I is well above background. As shown in Fig. 3, a four day maximum is seen. A sharp drop in radioactivity on May 14 coincided with rain on that day, rain water measurements were also done. The geometry is shown in Fig. 4. And the efficiency calibration was done using known ^{133}Ba source at three different positions within

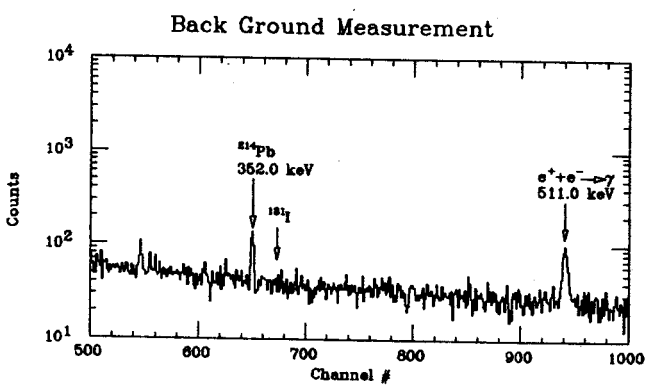

Fig. 1: Result from the measurement of air sample on May 9th (background without fallout).

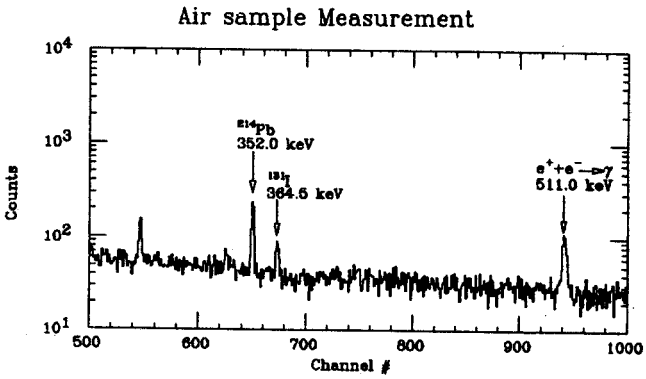

Fig. 2: Result from the measurement of air sample on May 13th.

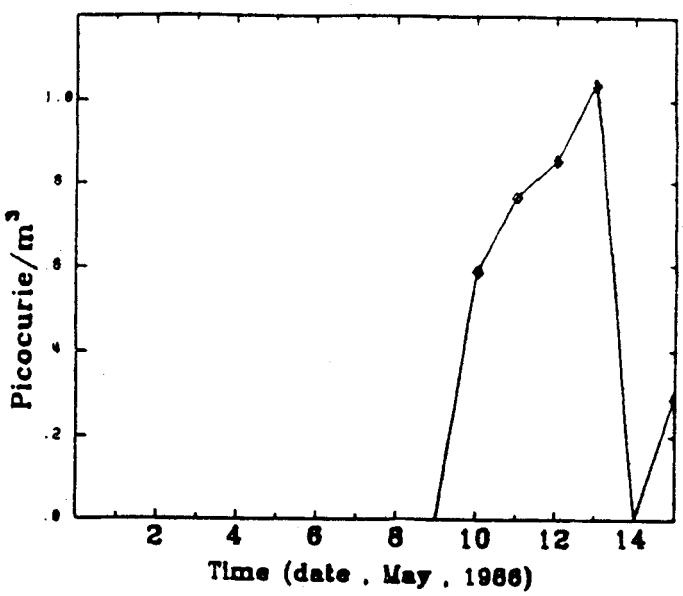

Fig. 3: Plot of radiation level from the air sample measurement v.s. date.

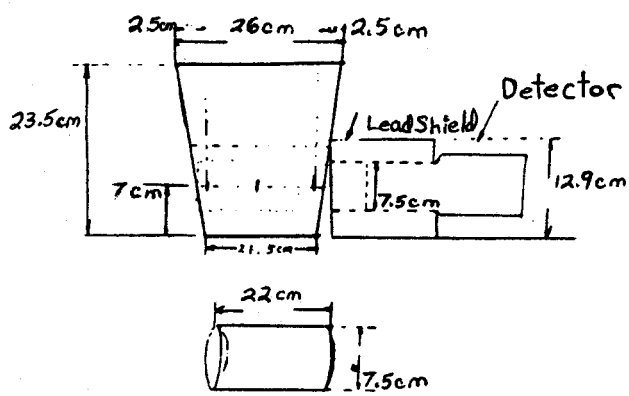

Fig. 4: Geometrical scheme of rain water measurement setup.

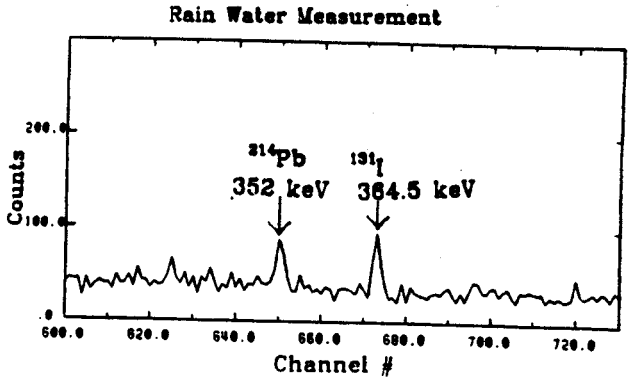

Fig. 5: Result from rain water measurement on May 14th.

the water sample as shown in the Fig. 4. The concentration of ^{131}I in rain water was calculated to be 420 pCi/liter, or about one fifth of the maximum permissible concentration of ^{131}I in water. In a measurement of river water taken the next day, nothing was found above the background.

The concentration of ^{131}I in air in East Lansing due to the Chernobyl accident was measured to be less than 0.5% of maximum permissible concentration. The rain water concentration was one fifth of the maximum permissible concentration for a brief period ie. on May 14, and therefore we concluded that there was insignificant health risk to this area from Chernobyl accident.

References

1. Department of Health.--Occupational health. LSB-P. No. 23. Regulations Governing the Use of Radioactive Isotopes, X-Radiation and All Other Forms of Ionizing Radiation. Appendix B p.23.